Role of the Rac1-P29S driver mutation in tumorigenesis and acquisition of BRAF inhibitor resistance

Dissertation

zur Erlangung des Doktorgrades

Dr. rer. nat.

der Fakultät für Biologie

an der Universität Duisburg-Essen

vorgelegt von

Jana Kathrin Quentin

(geb. Jungkurth)

aus Lüdenscheid

Juni 2020

Die der vorliegenden Arbeit zugrundeliegenden Experimente wurden in der Abteilung für Molekulare Zellbiologie der Universität Duisburg-Essen und in Kooperation mit der Arbeitsgruppe von Prof. Dr. Annette Paschen, Universitätsklinikum Essen, durchgeführt.

1. Gutachter:
Prof. Dr. Perihan Nalbant

2. Gutachter:
Prof. Dr. Stefan Westermann

Vorsitzender des Prüfungsausschusses:
Dr. Doris Hellerschied-Jelinek

Tag der mündlichen Prüfung:
20.10.2020

DuEPublico
Duisburg-Essen Publications online

UNIVERSITÄT DUISBURG ESSEN
Offen im Denken

ub | universitäts bibliothek

Diese Dissertation wird via DuEPublico, dem Dokumenten- und Publikationsserver der Universität Duisburg-Essen, zur Verfügung gestellt und liegt auch als Print-Version vor.

DOI: 10.17185/duepublico/73416
URN: urn:nbn:de:hbz:465-20230726-091508-6

Alle Rechte vorbehalten.

– Für meine beiden Mütter Gabi und Christine –

Table of Content

List of figures

List of tables

Abbreviations

%	Percent (from 100)
(v/v)	volume per volume (1 ml von 100 ml)
(w/v)	weight per volume (1 g von 100 ml)
°C	degrees Celsius
ANOVA	analysis of variance
Arp2/3	Actin-related-protein
bp	base pairs
BSA	Bovine serum albumin
Cdc42	Cell division control protein 42 homolog
CO_2	Carbon dioxide
dd	double-distilled
DMEM	Dulbecco's modified eagle's medium
DMSO	dimethyl sulfoxide
DNA	deoxyribonucleic acid
dNTP	desoxynucleotide-triphosphate
DPBS	Dulbecco's phosphate- buffered saline
ECM	Extra cellular matrix
EDTA	ethylene diamine tetra acetic acid
e.g	exempli gratia
EGF/EGFR	epidermal growth factor / EGF receptor
EGFP	enhanced green fluorescent protein
ERK	Extracellular-signal-regulated kinase
et al.	lat.: and others
FAK	focal adhesion kinase
FCS	fetal calf serum
g	gram
GAP	GTPase activating protein
GDI	GDP-dissociation inhibitor
GDP	guanosine-di-phosphate
GTP	guanosine-tri-phosphate
GEF	guanine nucleotide exchange factors
GTP	guanosin triphosphate
h	hour(s)
kb	Kilobase
kDa	Kilo Dalton
L	liter
LATS	Large-tumor-suppressor-.kinase
LB	Luria-Bertani
LIMK	LIM-kinase
M	Molar
mA	milli ampere
Ma-Mel	Mannheim-Melanoma
MAPK	mitogen-activated protein kinase
MEK	mitogen-activated and extracellular signal-regulated kinase

min	minute
ml	milli liter
MST	Mammalian sterile twenty-like
µg	micro gram
µl	micro liter
NA	numerical aperture
NaN_3	Sodium azide
Nm	nanometer
PAGE	polyacrylamide gel electrophoresis
PAK	p21-activating kinase
PBS	phosphate buffered saline
PDGF/PDGF	Platelet-derived growth factor/-receptor
PI3K	phosphoinositide-3-kinase
PIP3	phosphatidylinositol-(3,4,5)-trisphosphate
PLL	poly-L-lysine
PMT	photo multiplier
PTEN	phosphatase and tensin homolog
PVDF	polyvinylidene difluoride
Rac1	Ras-related C3 botulinum toxin substrate PCR
RAF	rapidly accelerated fibrosarcoma
RhoA/B/C	Ras homolog family member A/B/C
RIPA	radio immunoprecipitation assay buffer
RNA	ribonucleic acid
ROCK	Rho-associated protein kinase
rpm	revolutions per minute
RT	room temperature
RTK	receptor tyrosine kinase
SDS	sodium dodecyl sulphate
SEM	standard error of the mean
Ser	serine
siRNA	Small interfering RNA
TBS, TBS-T	Tris-buffered saline, Tris-buffered saline with Tween
TAE	Tris-acetat-EDTA
TAZ	Transcriptional coactivator with PDZ-binding motif
TEAD	TEA domain
TEMED	tetra-methyl-ethylene-diamine
Tris	Tris (hydroxymethyl) aminomethane
Tyr	tyrosine
UKE-Mel	Universitätsklinikum Essen - Melanoma
V	Volt
WASP	Wiskott–Aldrich syndrome protein
WAVE	WASP family verprolin homologous protein
wt	wild type
YAP	Yes-associated protein 1

Summary

The Rho-GTPase Rac1 is well-known to control the actin cytoskeleton. Recently, the highly active fast-cycling Rac1-P29S mutant was identified as a new driver mutation in melanoma beside the long-characterized mutations in BRAF and NRAS. Initial studies suggest that Rac1-P29S in linked to enhanced melanoma cell proliferation by activation of the MAPK protein ERK 1/2. Moreover, it is proposed that Rac1-P29S promotes early metastatic progression of melanoma and adaption of BRAF inhibitor resistance. However, little is known how this driver mutation regulates these processes. The aim of this study was therefore to characterize the role of Rac1-P29S in cell proliferation, cell survival as well as in BRAF inhibitor resistance and to identify molecular mechanisms that mediate these functions.

For this, we focused on two different patient-derived melanoma cell lines. Both cell lines harbor an activating BRAF mutation but express different Rac1 variants. While Rac1-wild-type (wt) is endogenously expressed in Ma-Mel-86c cells, the Rac1-P29S mutant was found in the UKE-Mel-55b cell line. The characteristic morphology of these cells, including enhanced lamellipodia formation and dynamic membrane ruffling differs substantially from the Rac1-wt expressing Ma-Mel-86c cell line. In the first part of this study, we used RNA interference together with expression of siRNA-resistant constructs to confirm that Rac1-P29S indeed promote this phenotype. In addition, we also established that endogenous expression of Rac1-P29S in UKE-Mel-55b cells is required for accelerated early cell adhesion and spreading as well as for their migratory capacity.

Next, we could show that Rac1-P29S is required for the strongly enhanced proliferation of UKE-Mel-55b cells, while Rac1-wt in Ma-Mel-86c cells does not modulate cell proliferation substantially. In agreement with such prominent role of Rac1-P29S in proliferation in UKE-Mel-55b cells, live-cell imaging revealed a significant decrease of cell division as well as a pronounced mitotic delay upon Rac1 depletion. We next studied the MAPK protein ERK1/2, the cell survival protein AKT and the actin regulated transcriptional coactivators Yap/Taz as potential downstream effectors.

Data suggest that Rac1-P29S expression similarly modulates AKT activity as compared to Rac1-wt expressing cells. In contrast, Rac1-P29S strongly stimulates activities of the proliferation related proteins ERK1/2 and Yap/Taz as compared to Rac1-wt. First, Yap/Taz levels were significantly higher in UKE-Mel-55b cells as compared to Ma-Mel-86c. In addition, Rac1-P29S depletion in UKE-Mel-55b cells distinctly decreased activities

of ERK1/2 and Yaz/Taz, whereas lack of Rac1-wt in Ma-Mel-86c cells did not have any marked effect on these signaling proteins. Our studies also revealed significantly elevated activities of the PAK effector family in UKE-Mel-55b cells as compared to Ma-Mel-86c cells. This implicates the PAK proteins as important effectors in enhanced cell proliferation downstream of Rac1-P29S.

In the second part, we focused on the role of Rac1-P29S in the acquisition of BRAF inhibitor resistance in melanoma cells and studied potential effects on associated signaling pathways. Overall, our proliferation studies suggest that expression of Rac1-P29S in melanoma cells provides an advantage in proliferation as compared to Rac1-wt. In particular, proliferation rates during treatment with the BRAF inhibitor remained low in Rac1-wt cells, while we measured a marked recovery of proliferation in Rac1-P29S expressing cells, despite continuous inhibitor (PLX-4032) treatment. Interestingly, activity of the MAPK protein ERK1/2 in Rac1-wt cells was lost entirely after PLX-4032 treatment, while a substantial residual activity level in the Rac1-P29S cell line was measured.

Depletion of Rac1-P29S significantly decrease the residual ERK1/2 activity, further indicating that endogenous expression of this Rac1 variant in melanoma stimulates ERK1/2 activation during BRAF inhibitor treatment. In addition, BRAF inhibition lead to increased nuclear Yap/Taz localization in both cell lines. Depletion of Rac1-P29S reduced this effect significantly, suggesting that the driver mutant promotes activity of these transcriptional coactivators upon BRAF inhibition. Enhanced stress fiber formation upon PLX-4032 treatment in both melanoma cell lines suggested that contractility regulatory Rho-GTPase might be also involved in acquisition of drug resistance in addition to Rac1-P29S. While stress fiber formation is typically associated with RhoA, our preliminary results with RNAi and the C3 inhibitor suggest that activities of RhoB and RhoC might be functionally more relevant in this cellular context.

Taken together, our findings have established a stimulatory role of the Rac1-P29S driver mutation in tumor-related cell proliferation and advanced our understanding of how this mutation might promote BRAF inhibitor resistance in melanoma patients. Thus, the targeted inhibition of downstream signaling pathways of the Rac1-P29S mutation could therefore enable the development of new pharmacological treatment strategies for melanoma patients.

Zusammenfassung

Die Rho-GTPase Rac1 kontrolliert das Aktin-Zytoskelett und reguliert so die Zelldynamik. Kürzlich wurde in Melanomzellen die hoch-aktive „fast-cycling“ Mutante Rac1-P29S entdeckt, welche neben den lang bekannten Mutationen in BRAF und NRAS eine neue Hot-Spot-Mutation im Melanom darstellt. Erste Studien legen nahe, dass die endogene Expression von Rac1-P29S eine verstärkte Zellproliferation verursacht und hierfür die Aktivierung des MAPK-Signalwegs verstärkt. Darüber hinaus wird vorgeschlagen, dass Rac1-P29S die frühe Metastasierung beim Melanom fördert und zur Bildung einer Resistenz gegen BRAF Inhibitoren beiträgt. Es ist jedoch wenig bekannt, wie diese Treibermutation diese Prozesse reguliert.

Das Ziel dieser Studie war es daher, die Rolle von Rac1-P29S bei der Zellproliferation, dem Zellüberleben sowie bei der Resistenz gegen BRAF-Inhibitoren zu charakterisieren und molekulare Mechanismen zu identifizieren, die diese Funktionen vermitteln.

Zu diesem Zweck konzentrierten wir uns auf zwei verschiedene vom Patienten stammende Melanomzelllinien. Beide Zelllinien weisen eine aktivierende BRAF-Mutation auf, exprimieren jedoch unterschiedliche Rac1-Varianten. Während in den Ma-Mel-86c Zellen der Rac1-wildtyp (wt) endogen exprimiert wird, wurde die Rac1-P29S-Mutante in der UKE-Mel-55b Zelllinie gefunden. Die Morphologie der UKE-Mel-55b Zellen unterscheidet sich deutlich von den Ma-Mel-86c Zellen und zeichnet durch eine erhöhte Lamellipodien- und Membran „ruffling“ Bildung aus. Im ersten Teil dieser Studie verwendeten wir RNA-Interferenz zusammen mit der Expression von siRNA-resistenten Konstrukten, um zu bestätigen, dass Rac1-P29S diesen Phänotyp tatsächlich induziert. Darüber hinaus haben wir festgestellt, dass die endogene Expression von Rac1-P29S in UKE-Mel-55b Zellen für eine effiziente frühe Zelladhäsion und Zellausbreitung sowie für deren Migrationsfähigkeit erforderlich ist.

Als nächstes konnten wir zeigen, dass Rac1-P29S für die stark erhöhte Proliferation von UKE-Mel-55b-Zellen erforderlich ist, während Rac1-wt in Ma-Mel-86c-Zellen die Zellproliferation nicht beeinflusst. Die prominente Rolle von Rac1-P29S in der Zellproliferation von UKE-Mel-55b Zellen wurde ebenfalls daraus ersichtlich, dass wir in videomikroskopischen Lebendzellaufnahmen eine signifikante Abnahme der Zellteilung, sowie eine ausgeprägte mitotische Verzögerung nach Rac1-Depletion feststellten. Als nächstes untersuchten wir das MAPK-Protein ERK1/2, das Zellüberlebensprotein AKT und die Aktin-regulierten Transkriptions-koaktivatoren Yap/Taz als potenzielle Signalwege stromabwärts von Rac1-P29S. Wir konnten zeigen, dass Rac1-P29S und Rac1-wt die AKT-Aktivität ähnlich beeinflussen. Im Gegensatz dazu stimuliert Rac1-P29S die Aktivitäten der proliferationsbezogenen Proteine ERK1/2 und Yap/Taz im Vergleich zu Rac1-wt deutlich stärker. So war zum einen die nukleare Lokalisation von Yap/Taz in UKE Mel 55b Zellen signifikant höher als in den Rac1-wt Ma Mel-86c Zellen. Des Weiteren verringerte die Depletion von Rac1-P29S in UKE-Mel-55b Zellen die Aktivitäten von ERK1/2 und Yaz/Taz deutlich,

wohingegen das Fehlen von Rac1-wt in Ma-Mel-86c-Zellen keinen merklichen Effekt auf diese Signalproteine hatte. Unsere Studien zeigten ebenfalls eine signifikant erhöhte Aktivitäten der PAK-Familie in UKE-Mel-55b-Zellen im Vergleich zu Ma-Mel-86c-Zellen. Dies impliziert das die PAK-Proteine als wichtige Effektoren bei der verstärkten Zellproliferation stromabwärts von Rac1-P29S fungieren könnten.

Im zweiten Teil konzentrierten wir uns auf die Rolle von Rac1-P29S beim Erwerb der BRAF-Inhibitorresistenz in Melanomzellen und untersuchten mögliche Auswirkungen auf die damit verbundenen Signalwege. Insgesamt legen unsere Proliferationsstudien nahe, dass die Expression von Rac1-P29S in Melanomzellen einen Vorteil bei der Proliferation im Vergleich zu Rac1-wt bietet. Während die Proliferationsrate in Rac1-wt Zellen während der Behandlung mit dem BRAF-Inhibitor (PLX-4032) stark verringert blieb, konnten wir in Rac1-P29S exprimierenden Zellen eine deutliche Erholung der Proliferation in Rac1 messen. Interessanterweise ging die Aktivität des MAPK-Proteins ERK1/2 in Rac1-wt Zellen nach PLX-4032-Behandlung vollständig verloren, während ein erhebliches Restaktivitätsniveau in der Rac1-P29S-Zelllinie gemessen wurde. Darüber hinaus führte die Depletion von Rac1-P29S zu einer weiteren Verringerung der verbleibende ERK1/2-Aktivität, was ebenfalls darauf hinweist, dass die endogene Expression dieser Rac1-Variante im Melanomzellen die ERK1/2-Aktivierung während der Behandlung mit BRAF-Inhibitoren stimuliert. Zusätzlich führte die BRAF-Hemmung zu einer erhöhten nuklearen Yap/Taz-Lokalisierung in beiden Zelllinien. Die Depletion von Rac1-P29S reduzierte diesen Effekt jedoch signifikant, was darauf hindeutet, dass die Mutante die Aktivität dieser Transkriptions-koaktivatoren bei BRAF-Hemmung fördert. Eine verstärkte Bildung von Stressfasern nach PLX-4032-Behandlung in beiden Melanomzelllinien deutete darauf hin, dass neben Rac1-P29S auch weitere Rho-GTPases, welche die Kontraktilität regulieren, an dem Erwerb der Arzneimittelresistenz beteiligt sein könnten. Während die Bildung von Stressfasern typischerweise mit RhoA assoziiert ist, legen unsere vorläufigen Ergebnisse unter Verwendung von RNAi und dem C3-Inhibitor nahe, dass die Aktivitäten von RhoB und RhoC in diesem zellulären Kontext funktionell relevanter sein könnten.

Zusammengenommen haben unsere Ergebnisse eine stimulierende Rolle der Rac1-P29S Mutation bei der tumorbedingten Zellproliferation festgestellt und unser Verständnis erweitert, wie diese Mutation die Resistenz gegen BRAF-Inhibitoren bei Melanompatienten fördern könnte. Die gezielte Hemmung der nachgeschalteten Signalwege der Rac1-P29S-Mutation könnte daher die Entwicklung neuer pharmakologischer Behandlungsstrategien für Melanompatienten ermöglichen.

1. Introduction

The human body is made up of trillions of individual cells. In a healthy human, all cells undergo a cycle of growth, division and apoptosis, known as the programmed cell death. In physiological conditions, these cell behaviors are tightly controlled by complex signal networks. In pathological context e.g. upon DNA-damage induced by environmental factors such as chemicals or UV-radiation, gene mutations can occur and lead to abnormal cell proliferation and tumorigenesis (Feitelson et al., 2015; Hanahan and Weinberg, 2011; Narayanan et al., 2010). While some solid-tumors can be removed e.g. by surgery, malignant tumors often invade other tissues and form metastasis (Roy and Saikia, 2016). Today, more than 100 types of cancers are known. However, we are far away from understanding signaling pathways that underlie the malignancy of this multifaceted disease. In this thesis, we focus on malignant melanoma, a UV-induced skin cancer type, which carries mutations in the oncogenes BRAF and Rac1 (Krauthammer et al., 2012). Recent studies identified a new driver mutation in the Rho-GTPase Rac1, which is a well-known regulator of the actin cytoskeleton in malignant melanoma (Krauthammer et al., 2012).

1.1 Melanoma

Cutaneous malignant melanoma is a common type of skin cancer in adults and is the most fatal form with a particularly low survival rate (Hawryluk and Tsao, 2014; Jenkins and Fisher, 2020). The human skin is made of various cell types, including keratinocytes and melanocytes, which have different functions. The primary function of keratinocytes and melanocytes is the protection against damage by environmental components such as heat or UV-radiation. Melanocytes produce melanin, a dark pigment to protect the skin (Hoogduijn et al., 2004) and DNA-damage due to UV–radiation leads to their malignant transformation resulting in increased melanoma formation (Gray-Schopfer et al., 2007). UV-radiation can trigger DNA base transitions from C (cytosine) to T (thymine), resulting in mutations in various genes (Krauthammer et al., 2012). These mutations have significant impact on cancer-associated signaling pathways and tumor formation (Hawryluk and Tsao, 2014). In particular, UV-light induced gene alterations have been found to cause dysregulations in cell proliferation and survival signals, including PTEN,

PI3K and AKT activities as well as the hippo-Yap/Taz and MAPK pathways (Fecher et al., 2008; Hennessy et al., 2005; Nallet-Staub et al., 2014; Wu et al., 2003).

1.1.1 Signaling pathways in melanoma

Around 50 % of all melanoma patients harbor a constitutively activating mutation in the serine/threonine kinase BRAF (Ascierto et al., 2012), with approx. 90 % being V600E (valine to glutamic acid) and the remaining 10 % V600K (valine to lysine) (Ascierto et al., 2012). In non-cancerous cells, stimulation with various types of growth factors such as EGF (epidermal growth factor) or PDGF (Platelet-derived growth factor) induces signal transmission by receptor tyrosine kinases (RTKs) to the small G-protein Ras (rapidly accelerated fibro sarcoma), which then activates RAF (Liu et al., 2018). The RAF kinase family consist of three proteins – ARAF, BRAF and CRAF, all of them can activate the MAPK pathway, a protein cascade of multiple serine/threonine kinases including RAF, MEK1/2 and ERK1/2 (Dhillon et al., 2007) (Fig. 1). Phosphorylation and activation of MEK1/2 by RAF activates the kinase, which in turn phosphorylates and activates ERK1/2. Active ERK1/2 stimulates downstream targets in the cytosol or translocated into the nucleus (Daum et al., 1994; Liu et al., 2018). In the nucleus, the kinase regulates proliferation and cell survival via transcriptional control of multiple target genes such as cyclin D1 (Chambard et al., 2007; Lavoie et al., 1996; Ramos, 2008). Thus, oncogenic BRAF mutants in melanoma have been shown to strongly stimulate activation of MAPK signaling inducing enhanced proliferation and cell survival (Holderfield et al., 2014).

The PI3K/AKT pathway can be activated by receptor-tyrosine kinases (RTKs) or G-protein coupled receptors (GPCRs) (Davies, 2012) (Fig. 1). Both receptor types activate phosphatidylinositol-3-kinase (PI3K), which phosphorylates phosphatidylinositol-4,5-bisphosphate (PIP2) (Maehama and Dixon, 1998). The resulting phosphatidylinositol-3, 4, 5-triphophate (PIP3) activates downstream effectors such as PDK1 (Phosphoinositide-dependent kinase-1), AKT (protein kinase B) or the Rho-GTPases Rac1 and Cdc42, which control the actin cytoskeleton (Carnero et al., 2008). The PI3K/AKT pathway is upregulated in many tumors and lead to enhanced cell survival and is also associated with drug resistance behavior of tumor cells (Manzano et al., 2016). The phosphatase and tension homolog (PTEN) antagonizes the activity of PI3K by de-phosphorylation of PIP3 and thereby suppressing AKT activity (Davies, 2012) (Fig. 1). In

agreement with this role, loss of PTEN has been shown to promote melanoma formation due to strong PIP3 elevation and enhanced downstream activity (Stahl et al., 2003; Whang et al., 1998).

The transcriptional coactivators Yap (Yes-associated protein 1) and Taz (WW-domain-containing transcription regulator 1, commonly referred to as Yap/Taz) promote cell proliferation, organ growth and cell survival downstream of the hippo signaling cascade (Fisher et al., 2017; Kanai et al., 2000; Sudol et al., 1995). In particular, the hippo signaling kinases, MST1/2 (Mammalian sterile twenty-like 1/2) and LATS1/2 (Large tumor suppressor kinase 1/2) control activation of Yap/Taz (Moroishi et al., 2015) (Fig. 1). Activation of LATS1/2 promotes phosphorylation of Yap/Taz and thereby preventing their translocation into the nucleus. Thus, this inactivating phosphorylation of Yap/Taz leads to accumulation in the cytoplasm, where it is largely degraded (Zhao et al., 2010). Upon inactivation of the hippo signaling, un-phosphorylated Yap/Taz shuttle into the nucleus and interact with DNA-binding factors such as TEAD (transcriptional enhanced associate domain) to induce transcription of target genes such as cyclin D1 (Cao et al., 2008; Fisher et al., 2017; Kim et al., 2013). Protein levels and activity of Yap/Taz have been identified in various cancer types and several studies suggest that active Yap/Taz cause enhanced cell proliferation and tumor growth (Zanconato et al., 2016). Moreover, Yap/Taz has been shown to be involved in malignancy and drug resistance in cancer cells (Kim et al., 2016; Nguyen and Yi, 2019). Furthermore, Yap/Taz activity is also regulated by ECM (extra cellular matrix) components and Rho-GTPase activity (Dupont et al., 2011; Moroishi et al., 2015; Seo and Kim, 2018). ECM, cell-matrix adhesions and the actin cytoskeleton can activate Yap/Taz. High ECM stiffness facilitates integrin-mediated cell-matrix adhesion formation, which in turn is associated with the activity of Rho-GTPases such as Rac1 and RhoA (Seo and Kim, 2018). Both GTPases promote actin polymerization and cell spreading. The resulting flat cell shape enables the transport of active Yap/Taz into the nuclei (Dupont, 2016) (Fig. 1). However, mechanistic details of these regulatory mechanisms are only emerging and their relevance in tumorigenesis and adapting drug resistance is not well-understood.

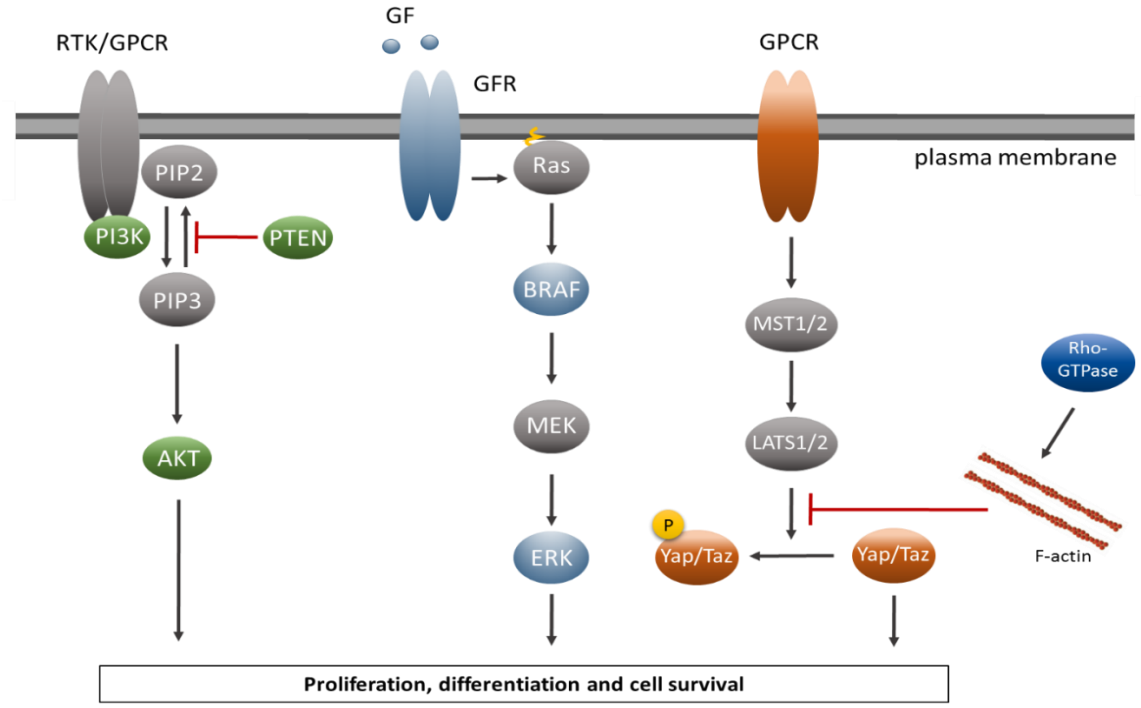

Figure 1: Proliferation and survival signaling pathways in melanoma. Gene alternations such as in BRAF can result in aberrant signaling activity and promote formation of melanoma e.g. by stimulation of proliferation signaling. **(left)** The PI3K/AKT signaling is often activated in melanoma As the tumor suppressor PTEN antagonizes PI3K function, loss of the phosphatase as found in many cancers prominently increases the survival signaling activity. **(middle)** MAPK pathway: Growth factors (GF) stimulate signal transmission via activation of the small GTPase Ras and a downstream protein kinase cascade including, RAF, MEK and ERK. **(right)** Yap/Taz activity is regulated by GPCR signaling as well as Rho-GTPase mediated actin polymerization. F-actin and acto-myosin structures have been associated with de-phosphorylation of Yap/Taz which facilitates its translocation into the nucleus and increase gene transcription of proliferation and survival related genes. Modified from (Davies, 2012; Liu et al., 2018; Seo and Kim, 2018).

1.1.2 Drug resistance against BRAF inhibitors in melanoma therapy

Physiological BRAF activity is regulated by phosphorylation that induces conformational changes in the kinase and promotes activation of the downstream kinase MEK1/2 by phosphorylation. BRAF mutations such as V600E and V600K have long been characterized in melanoma and it was found that these mutations mimic the phosphorylated state, resulting in a permanently active conformation (Wan et al., 2004; Wellbrock and Hurlstone, 2010). A structure-guided discovery approach (Tsai et al., 2008) identified one of the first selective BRAF V600E inhibitors called PLX-4720, which served as basis for the development of advanced BRAF inhibitors such as vemurafenib (PLX-4032) (Yang et al., 2010). PLX-4032 selectively inhibits BRAF V600E/K but not the wild-type form and decreases both ERK1/2 activation and expression of the cyclin D1, which controls cell cycle progression (Yang et al., 2010). In 2011,PLX-4032 was approved

by the FDA (Chapman et al., 2011; Flaherty et al., 2010; Shtivelman et al., 2014; Yang et al., 2010).

Unfortunately, a substantial portion of approx. 20 % of melanoma patients with an activating BRAF mutation develop resistance to BRAF inhibitors such as vemurafenib (PLX-4032) within six months (Griffin et al., 2017; Villanueva et al., 2011). Today, several mechanisms that mediate drug resistance in melanoma have been identified (Griffin et al., 2017). First, general loss of PTEN which occurs in 35 % of all melanoma patients, results in upregulated AKT activity and promotes cell proliferation and survival, also when the MAPK pathway is downregulated by using BRAF-inhibitors (Griffin et al., 2017; Paraiso et al., 2011; Stahl et al., 2003). To circumvent the compensatory effect of PTEN, AKT inhibitors are currently in early phases of clinical trials. Secondly, growth factor receptors, such as EGFR (epidermal growth factor receptor) and PDGFR (Platelet-derived growth factor-receptor), have been reported to be upregulated in melanoma cells and it was shown that increased receptor signaling enhanced activity of multiple downstream pathways such as MAPK to promote tumor progression (Lee et al., 2016; Lee et al., 2020; Sun et al., 2014). Moreover, activating mutations in the BRAF effector MEK1 can promote MAPK signaling activity and lead to ERK1/2 activation (Griffin et al., 2017). Currently, patients with mutations in both, BRAF and MEK1, are treated with a combination of two inhibitors in clinical trials, which facilitates to target the mutated proteins simultaneously (Arozarena and Wellbrock, 2017; Winder and Viros, 2018). Unexpectedly, even the combined treatment of BRAF and MEK inhibitors seems not sufficient to permanently suppress tumor relapse in some melanoma patients. Watson *et al.* reported that patients that had developed resistance to the commonly prescribed BRAF inhibitors often expressed the newly identified driver mutant Rac1-P29S in addition to the BRAF mutation in melanoma (Watson et al., 2014). This mutation, biochemical characterized as so-called fast-cycling mutation, increases Rac1 signaling and will be discussed in detail in chapter 1.6 (Davis et al., 2013; Hodis et al., 2012; Krauthammer et al., 2012). They hypothesized that Rac1-P29S can promote ERK1/2 activity independent of BRAF signaling (Hodis et al., 2012).

1.2 Rho-GTPases

Rho-GTPases are important key players in actin cytoskeleton regulation and therefore involved in essential cellular processes such as cell migration and cell division (Ridley, 2015; Villalonga and Ridley, 2006). Approximately 20 members of human Rho-GTPases with a molecular weight of 20-30 kDa are known to this day (Hodge and Ridley, 2016; Van Aelst and D'Souza-Schorey, 1997). The most well characterized Rho-GTPases are Rac1, Cdc42 and RhoA.

1.2.1 Rho-GTPases act as molecular switches

Proteins of the Rho-GTPase family can act as so-called molecular switches and cycle between an inactive and active state. In their inactive state, Rho-GTPases are bound to GDP (guanosine-di-phosphate), whereas the active form binds GTP (guanosine-tri-phosphate) (Bishop and Hall, 2000). Only in the active form, Rho-GTPases can interact with their downstream effectors. Today, three different protein families are known to regulate the transitioning between the two states (Boguski and McCormick, 1993; Tybulewicz and Henderson, 2009) (Fig. 2). GEFs (guanine-nucleotide-exchange-factors) are necessary for Rho-GTPase activation by catalyzing the GDP-to-GTP exchange, whereas GAPs (GTPase-activating-protein) increase the intrinsic GTP hydrolysis activity of Rho-GTPases, resulting in inactivation (Moon, 2003; Rossman et al., 2005; Tybulewicz and Henderson, 2009). The third group, called GDIs (guanine-nucleotide-dissociation inhibitors), sequesters Rho-GTPases in the cytosol and inhibits their activation (DerMardirossian and Bokoch, 2005). In addition to their regulation by GEFs and GAPs, Rho-GTPase activity is also controlled by post-translational-modifications (PTMs), which allow specific localization to certain membrane compartments and thus determine the sub-cellular localization of Rho-GTPases (Hodge and Ridley, 2016). Here, the irreversible prenylation within the CAAX-motif (C: cysteine; A: aliphatic amino acid; X: can be any amino acid) at the C-terminus is the most frequent PTM in Rho-GTPases, followed by reversible palmitoylation (Clarke, 1992; Hodge and Ridley, 2016; Roberts et al., 2008). Furthermore, phosphorylation at different amino acid positions also influences the localization and affects GDP/GTP cycling and consequently the activity of Rho-GTPases (Hodge and Ridley, 2016). Thus, the combination of different regulatory mechanisms enables the spatio-temporal coordination and activation of Rho-GTPases to orchestrate cellular processes such as cytoskeleton dynamics, cell polarity and proliferation.

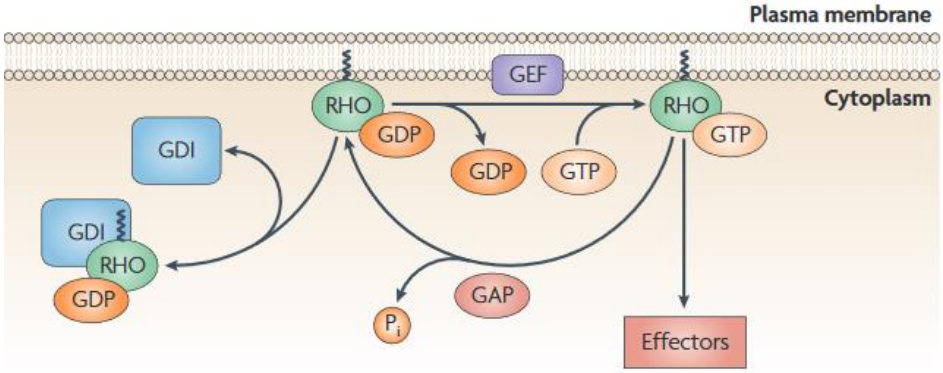

Figure 2: Regulation of Rho-GTPases by GEFs, GAPS and GDIs. GDP-bound and prenylated Rho-GTPase sequestered by GDI in the cytosol (left). After release form GDI, Rho-GTPase anchored to the plasma membrane and interact with GEFs for GDP-GTP exchange. The active GTP-bound Rho-GTPase can now promote downstream signaling by binding effector proteins before intrinsic GTP-hydrolysis is maintained by GAP protein to inactivate the Rho-GTPase. Modified from (Tybulewicz and Henderson, 2009).

1.2.2 Rac1 regulates actin dynamics, proliferation and cell survival

The small Rho-GTPase Rac1 (Ras-related C3 botulinum toxin substrate) was first characterized by Didsbury *et al.* (Didsbury et al., 1989). While three Rac isoforms are known, only Rac1 is ubiquitously expressed (Guo et al., 2008; Ridley et al., 1992). Rac1 consists of different domains with specific functions: While the C-terminal region is important for modification and regulation by PTMs, the switch I domain (amino acid 26-45) is involved in the interaction with downstream effectors such as PAK1/2 (p21-activating kinase). Switch II (amino acid 59-74) is responsible for binding to GEFs and enables Rac1 activation (Kumar et al., 2013). Rac1 primary regulates the actin cytoskeleton at the cell front, where it promotes lamellipodia and membrane ruffle formation but is also known to control proliferation and cell survival (Bid et al., 2013; Chhabra and Higgs, 2007; Hall, 1998; Ridley et al., 1992) (Fig. 3). To control the actin cytoskeleton, Rac1 activates two different downstream pathways. First, Rac1 activates proteins of the PAK protein family, which promote activation of the LIM-kinase (LIMK). LIMK phosphorylates and inactivate an actin-destabilizing protein, named Cofilin. Inhibition of Cofilin promotes then actin polymerization. Next, Rac1 activates the nucleating protein Arp2/3 (actin-related-protein) and thus induce lamellipodia formation (Bid et al., 2013). Moreover, Rac1 is involved in adhesion dynamics and the regulation of signaling pathways to control proliferation and cell survival (Moore et al., 1997; Murga et al., 2002; Parsons et al., 2010) (Fig. 3). PAK activation downstream of Rac1

also promote proliferation signaling through activation of the kinase ERK1/2 (Bid et al., 2013; Krauthammer et al., 2012). Moreover, Murga *et al.* showed that Rac1 is involved in cell survival signaling through activation of the PI3K/AKT pathway (Murga et al., 2002).

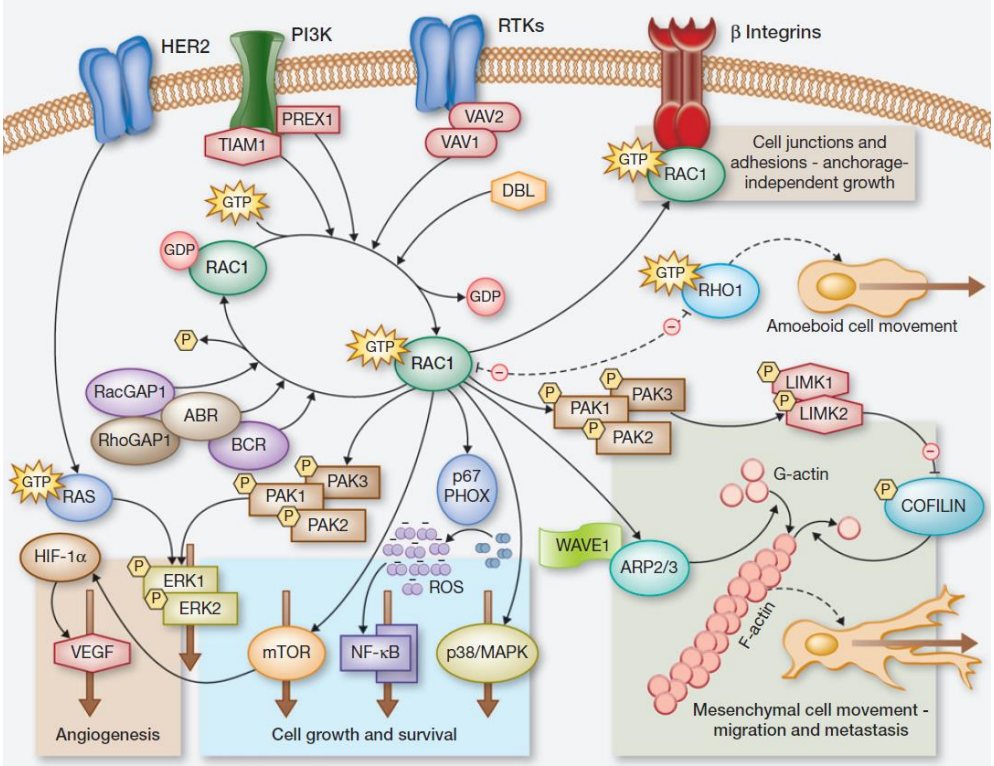

Figure 3: Illustration of Rac1 signaling pathways. The small GTPases Rac1 is involved in various signaling pathways, which control migration, proliferation and cell survival. Activation of various receptors promote activation of Rac1-specific GEFs. Active Rac1 interacts with several effector proteins to further stimulate different pathways (Bid et al., 2013).

1.3 Actin cytoskeleton

In general, G-actin (globular actin) assembly for filament formation is kinetically unfavorable and actin-nucleators are necessary to initiate polymerization (Fig. 4A). One such nucleator is Arp2/3 (actin-related-protein), a complex that mimics an actin dimer and thus serves as template to enable the elongation of the new filament by binding to the side of an existing filament with a 70° angle (Chhabra and Higgs, 2007; Goley and Welch, 2006). Formins, facilitate actin polymerization of longer filaments (Otomo et al., 2005; Rottner et al., 2017; Schulze et al., 2014). Other nucleators, such as spire, bind and stabilize actin trimers to promote actin elongation (Rottner et al., 2017). Activation of different Rho-GTPases results in various high-order actin structures with specific

functions (Fig. 4B). Rac1 activation promotes the formation of lamellipodia, a branched dendrite-like network of actin filaments located at the leading edge of motile cells (Chhabra and Higgs, 2007; Hall, 1998; Ridley, 2015). Filopodia are formed by bundling of several protruding actin filaments that project out of the branched network and are initiated by Cdc42 activity (Hall, 1998; Rottner et al., 2017). In contrast, RhoA generates contractile stress fibers (Bishop and Hall, 2000; Hall, 1998).

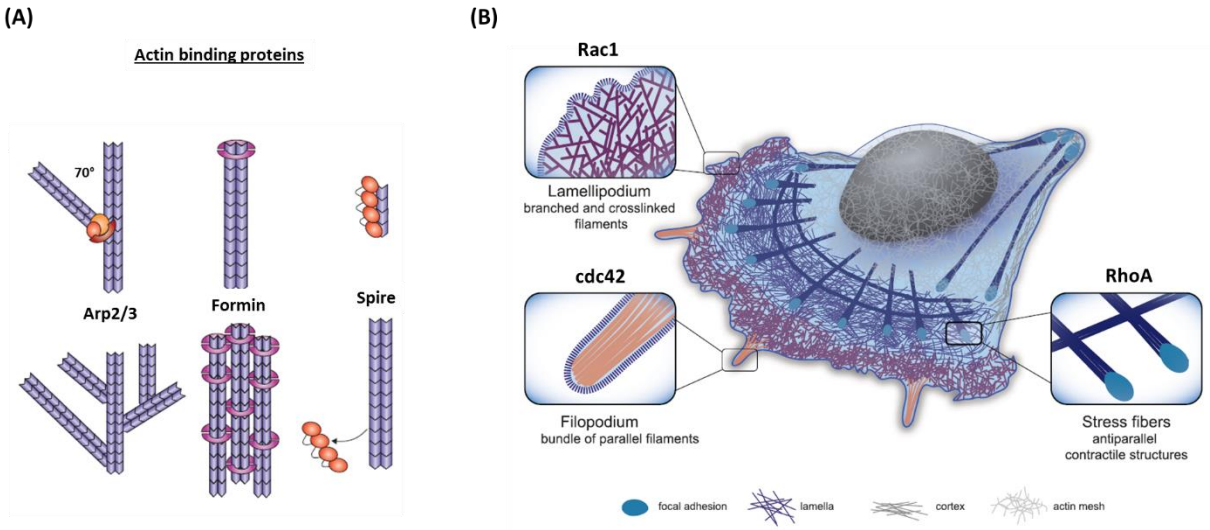

Figure 4: Highly organized actin structures regulated by the Rho-GTPases Rac1, Cdc42 and RhoA. (A) Actin nucleators promote actin polymerization. Arp2/3 binds on existing filaments and promote the formation of a branched actin network. Formins and spire stabilize actin dimers and trimers and thus induce actin polymerization. **(B)** The Rac1-induced branched actin network, called lamellipodia is generated at the leading edge of cells. Here, Cdc42 activity promotes the formation of the finger-like actin bundled filopodia. These structures allow sensing of the microenvironment. Anti-parallel actin bundles are promote by RhoA activity and are required for cell contraction during cell migration. Modified from (Chhabra and Higgs, 2007; Letort et al., 2015).

1.3.1 Rac1 promotes lamellipodia and membrane ruffling

Rac1 activates Arp2/3 via its effector WAVE (WASP-family verprolin homologous protein 1) and promotes lamellipodia formation in the cell front (Miki et al., 1998; Takenawa and Miki, 2001) (Fig. 5(1a)). Moreover, Rac1 also regulates membrane ruffle formation (Ridley et al., 1992) (Fig. 5(2a,b)). Membrane ruffles are actin induced sheet-like protrusions and are formed downstream of Rac1 signaling (Small et al., 2002; Suetsugu et al., 2003). Abercrombie *et al.* described two types of membrane ruffles, termed peripheral and dorsal. Peripheral ruffles are generated at the leading edge of a motile cell and move rearward, while dorsal ruffles are circular membrane protrusions related to receptor internalization and micropinocytosis (Abercrombie et al., 1970;

Buccione et al., 2004). Generation of membrane ruffles is linked to the high turnover rates of nascent adhesions as disassembly of these adhesions leads to detachment of the lamellipodia, which then fold back and move rearward as a membrane ruffle (Abercrombie et al., 1971; Chhabra and Higgs, 2007) (Fig. 5(2a,b)). It has been previously well-documented that overexpression of the constitutively active Rac1-Q61L variant strongly enhances membrane ruffle formation as compared to Rac1-wt. (Davis et al., 2013).

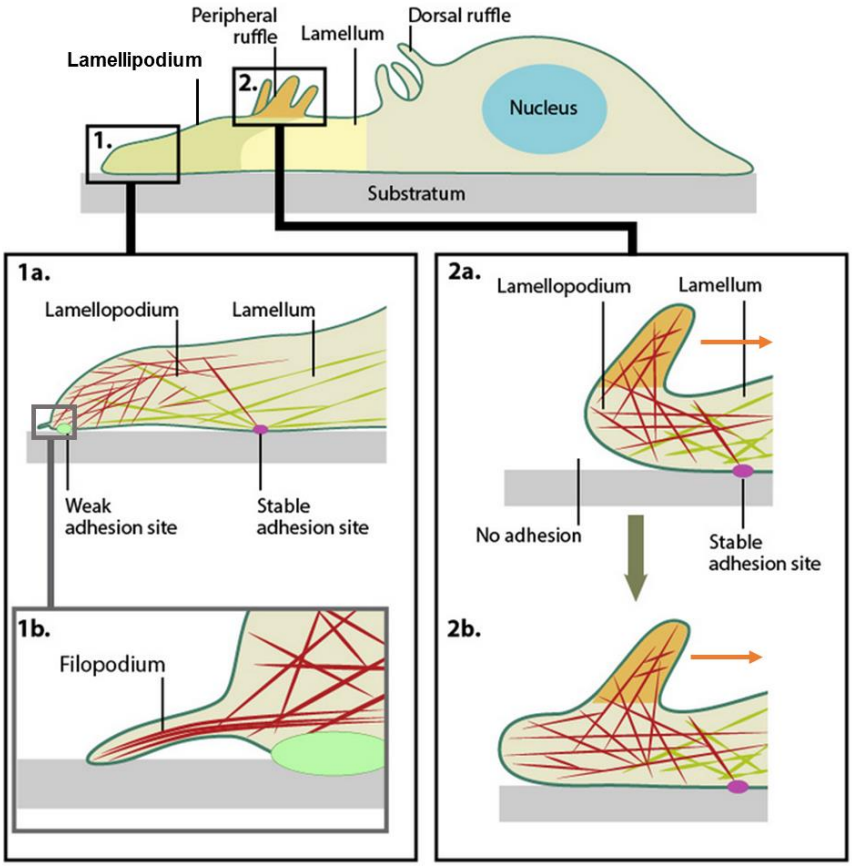

Figure 5: Rac1 promotes lamellipodia formation and membrane ruffling. Rac1 promotes lamellipodia formation in the leading edge of motile cells (lamellipodia) and sheet-like protrusions on the dorsal cell side. **(1/1a)** Branched actin filaments in the lamellipodia and actin-bundled filopodia form the leading edge. Cells form weak adhesions (green) with high turnover rates in the cell front. **(2a/b)** Loss of adhesions in the lamellipodium enables folding of the leading edge and generates peripheral membrane ruffles, which can move rearward. Modified from MBI, National University of Singapore.

1.4 The role of Rac1 in cell migration and adhesion dynamics

Cell migration is a fundamental process, which is not only relevant during embryonic development but also in the adult immune responses and wound healing. While cell migration also occurs in three-dimensions and can be divided into several subtypes, we focus in this study on 2D mesenchymal cell migration. This migration type is a complex and tightly regulated mechanism that involves adhesion dynamics and actin remodeling. It is controlled by spatial-temporal coordinated interactions of cell adhesion proteins and Rho-GTPases (Huveneers and Danen, 2009; Lawson and Burridge, 2014). The spatially regulated activity of Rho-GTPases results in the formation of different actin structures, which determine the polarity of the cell. This polarity is essential for cell motility (Schaks et al., 2019) (Fig. 6A). The leading edge of a motile cell is formed due to Rac1 and Cdc42 activity at the cell front. Cdc42 promotes the formation of filopodia, which are required for sensing the surrounding microenvironment (Hall, 1998). Defined activity of the Rho-GTPase Rac1 promotes the formation of membrane protrusions such as lamellipodia, which can push the cell forward (Goicoechea et al., 2014; Ridley, 2015) (Fig. 6A). In contrast, cell contraction is modulated via RhoA and stress fiber formation in the cell rear (Parsons et al., 2010) (Fig. 6A).

Cell adhesions with the surrounding matrix are one of the most important key players to control the cell polarity. The extra-cellular matrix (ECM) is a three-dimensional network that contains various proteins such as collagen I, fibronectin and proteoglycans (Frantz et al., 2010). The composition of the ECM influences its stiffness, which has a direct impact on cell behavior. To sense the tension of the ECM, cells form cell-matrix adhesions. The integrin protein family is the most important protein family to form these adhesions. Integrins are transmembrane proteins that promote signal transmission from ECM to signaling pathways within the cell (Hynes, 2002). To activate downstream signaling, integrins form heterodimers consisting of an α- and β-chain. Today, 18 different isoforms of the α-chain and 8 β-chains are known (Hynes, 2002). The expression of different integrins is associated with the spatial activation of Rho-GTPases. Integrin-mediated signaling leads to activation of specific Rac1 GEFs such as Tiam1 or β-PIX in the leading edge, whereas other integrin dimers cause activation of RhoA in the cell rear (Huveneers and Danen, 2009) (Fig. 6B). Moreover, Rac1 activates RhoA GAPs to reduce RhoA activity in the cell front (Huveneers and Danen, 2009) (Fig. 6B).

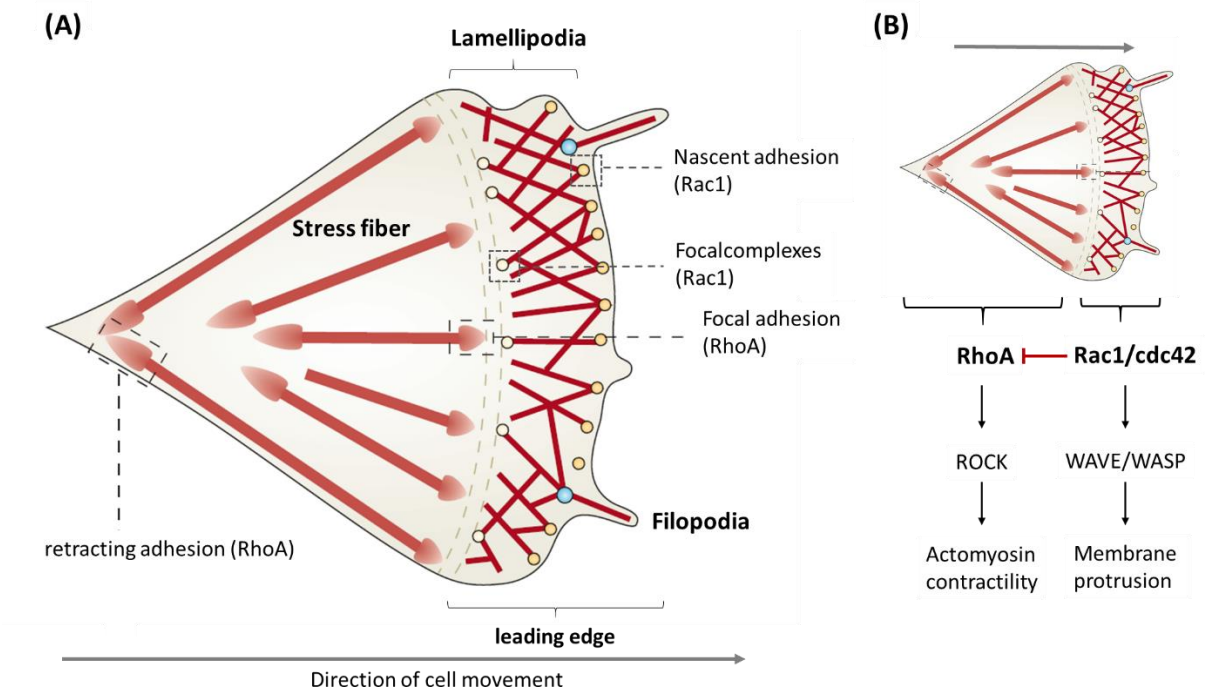

Figure 6: Rho-GTPases control cell polarity in migration cells. Spatial-temporal activity of the Rho-GTPases Rac1, RhoA and Cdc42 control cell polarity and migration by forming high-ordered actin structures. **(A)** Activity of Rac1 and Cdc42 induces lamellipodia and filopodia formation at the leading edge of a migratory cell, respectively. These membrane protrusions push the cell forward, while active RhoA promote stress fiber formation and acto-myosin contraction in the cell rear. **(B)** High Rac1 and Cdc42 activity is found in the cell front of the cells and promote membrane protrusions by activation of the WAVE/WASP and Arp2/3 complexed, which increase actin polymerization. To reduce RhoA activity in the leading edge Rac1 activates RhoA specific GAPs to inhibit this GTPases. In contrast, higher RhoA activity and low Rac1 levels are found in the cell rear. There RhoA activate the ROCK pathway and leads to acto-myosin contraction to pull the cell. Modified from (Parsons et al., 2010).

The activity of Rho-GTPases is mainly responsible to induce and sustain cell polarity by controlling the actin and adhesion dynamics. To obtain different activity patterns of a single Rho-GTPases, a fine tuned-signaling cascade is involved. First, integrins can directly modulate the activity of Rho-GTPases-controlling proteins such as GEFs or GAPs (Huveneers and Danen, 2009). Furthermore, the activity of a single Rho-GTPase has also direct effects on the activity status of other Rho-GTPases by regulating their respective GEFs and GAPs (Guilluy et al., 2011). Thus, integrins and the crosstalk between Rho-GTPases are important to coordinate adhesion dynamics and cell migration.

The adhesion formation and maturation can be classified in three phases (Fig. 6+7): Nascent adhesion formation, maturation and dissociation (Parsons et al., 2010). Nascent adhesions are formed in the early state of adhesion and are associated with Rac1 activity in the lamellipodia, have short life-times and are RhoA and Myosin II independent

(Fig. 6+7) (Choi et al., 2008; Lawson and Burridge, 2014; Vicente-Manzanares and Horwitz, 2011). In the beginning, integrin heterodimers recruit the scaffold protein Paxillin. This protein has no enzymatic activity, but has multiple protein binding domains, which activate downstream signaling depending on which protein kinases or phosphatases are recruited over time (Lopez-Colome et al., 2017). Today, four Paxillin isoforms are known, while the α-isoform is the most widely expressed one (Lopez-Colome et al., 2017). Paxillin contains several tyrosine/serine phosphorylation sites to regulate the interactions with other proteins (Webb et al., 2005). Paxillin interactions with protein kinases such as FAK (focal adhesion kinase) or Src, recruit Rac1 specific GEFs like β-PIX (Huveneers and Danen, 2009; Kiyokawa et al., 1998; Lopez-Colome et al., 2017; Nayal et al., 2006). Next, Paxillin phosphorylation leads to complex formation with GIT1 (G-protein-coupled receptor kinase-interacting protein 1) and the Rac1 downstream effector PAK1 (Nayal et al., 2006). Both integrin-mediated Rac1 activation mechanisms facilitate the recruitment of Rac1 to the leading edge and promote the formation of membrane protrusions and early cell-matrix adhesions (Huveneers and Danen, 2009; Parsons et al., 2010). In parallel, RhoA activity is reduced by the recruitment of RhoA-specific GAPs, such as the p190RhoGAP, to the cell-matrix adhesions in the leading edge (Huveneers and Danen, 2009; Tomar and Schlaepfer, 2009).

The first larger adhesions are found in the interspace between lamellipodium and lamellumg and called focal complexes. These adhesions also require Rac1 activity but also α-actinin and Myosin II activity (Choi et al., 2008; Guo et al., 2006; Nobes and Hall, 1995) (Fig. 6+7).

Further adhesion maturation is facilitated by both, increased RhoA activity and reduced Rac1 activity in the rear of the cell (Parsons et al., 2010). These adhesions are called focal adhesions and are generated through the RhoA/ROCK/Myosin II pathway (Fig. 6+7) (Narumiya et al., 2009; Parsons et al., 2010). RhoA-specific GEFs are recruited to focal adhesions in response to mechanical tension downstream of FAK signaling (Huveneers and Danen, 2009). RhoA activates ROCK and this causes Myosin II phosphorylation that promotes focal adhesion maturation (Parsons et al., 2010). To reduce Rac1 activity in the cell back, several pathways activate either Rac1-specific GAPs or downregulate the activity of Rac1 GEFs.

Adhesion disassembly is also tightly regulated through integrin-mediated downstream signaling. Upon Rac1 activation, signaling cascades such as MAPK are activated. Activated ERK1/2 localizes to Paxillin/FAK complexes, where it phosphorylates Paxillin at multiple

serine residues, resulting in Paxillin disassembly (Ishibe et al., 2004; Lopez-Colome et al., 2017). Next, Paxillin can activate RhoA-specific GAPs to suppress focal adhesion maturation and thereby promotes adhesion disassembly (Tsubouchi et al., 2002).

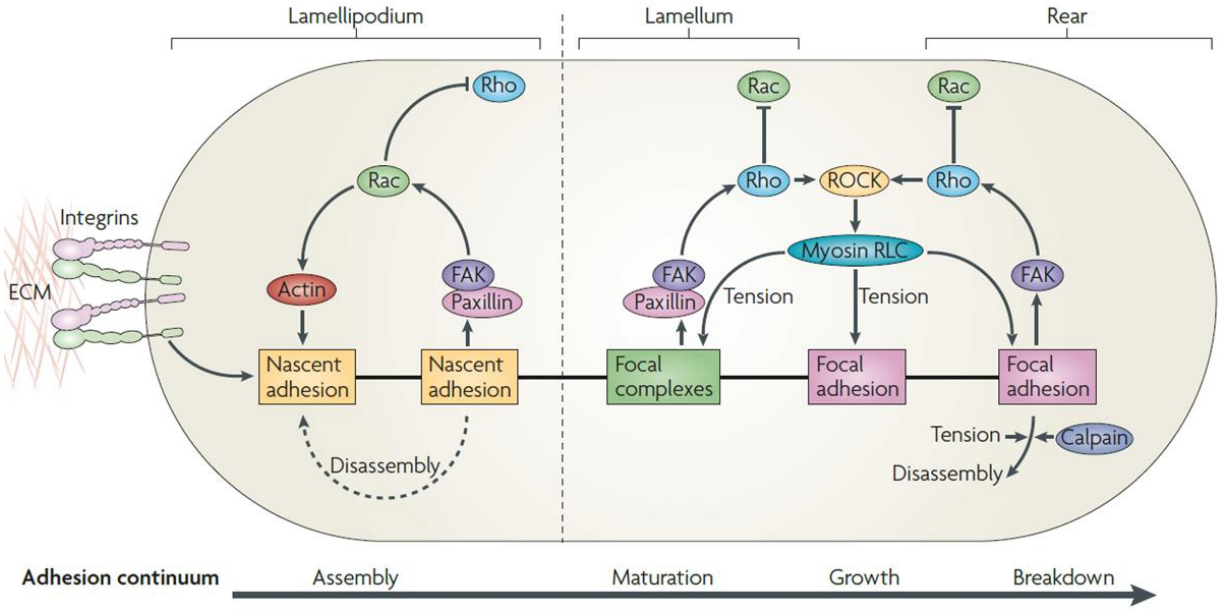

Figure 7: Maturation of focal adhesions is regulated by spatial-activity patterns of Rho-GTPases. Integrin-mediated recruitment of the scaffold protein Paxillin and the protein kinase FAK promotes Rac1 activation in the leading edge, where the small GTPases regulate the formation and disassembly of nascent adhesions. Local RhoA activity is present in the lamellum, which is induced through FAK-mediated GEF activation and mediates adhesion maturation. RhoA sustains Myosin II phosphorylation through activation of ROCK. The generated tension facilitates the binding of actin filaments to the adhesions and therefore sustains adhesion maturation. Modified from (Parsons et al., 2010).

1.5 Rac1 controls cell cycle progression

The cell cycle or cell division is a series of events, which cells undergo to grow and divide. Replication of DNA and organelles occurs during the interphase, followed by the separation into two daughter cells during mitosis. Cyclins, Cdks (cyclin-dependent kinase) and various cell cycle checkpoints thereby control correct cell division.

While cyclins and Cdks (cyclin-dependent kinases) are the best-characterized cell cycle regulators, Rho-GTPases play major roles in cell division control as well (Villalonga and Ridley, 2006). In particular, Rho-GTPases have been shown to control the cell cycle progression in multiple ways. The actin cytoskeleton undergoes drastic changes during cell division (Heng and Koh, 2010). In interphase, cells exhibit an extensive actin network due to lamellipodia and stress fiber formation. These actin structures need to be reorganized to enter mitosis and are responsible for the characteristic roundish shape of

the cell (Heng and Koh, 2010). Several groups have shown that perturbation of actin results in multinuclear cells or cell cycle arrest in the G1-phase (Moulding et al., 2007; Reshetnikova et al., 2000). Recently, Molinie *et al.* showed that the Rac1-induced cortical branched actin network (lamellipodia) integrates growth factor and mechano-transduction signals and thus determines S-phase entry (Molinie et al., 2019). Rac1 and RhoA do not only control actin organization, but also the formation of cell-matrix adhesions. These adhesions detach during mitosis to enable cell rounding (Heng and Koh, 2010). Additional important contributors to cell cycle control are integrins and the ECM stiffness. High ECM stiffness promotes FAK activation through integrin signaling (Koohestani et al., 2013). Downstream of FAK, Rac1 is activated and promote cyclin D1 expression to drive cell division (Fournier et al., 2008). Interestingly, a dual role for FAK and Paxillin is has been observed. Normally, these proteins are recruited to cell-matrix adhesion, but during cell division they are also associated with the mitotic spindle (Heng and Koh, 2010).

Rac1 and RhoA are linked to elevated cyclin D1 levels and therefore control the G1/S transition (Villalonga and Ridley, 2006; Watts et al., 2006; Yoshida et al., 2010; Zhang et al., 2009). Zhu *et al.* observed in various cancer types that upregulated EGFR signaling promotes increased cyclin D1 expression through PI3K/AKT/Rac1 signaling (Zhu et al., 2015). Other groups reported high activity of the Rac1 effector PAK1 during G1/S-phase (Nheu et al., 2014). In addition, they also observed a correlation of PAK1 and cyclin D1 expression (Balasenthil et al., 2004). Interestingly, PAK1 is also located to centrosomes via the β-PIX/GIT1 complex (Cernohorska et al., 2016; Zhao et al., 2005). These findings together with the observations from Michaelson *et al*. that Rac1 accumulates in the nucleus during late G2-phase, suggest an important regulatory role for Rac1 in cell cycle progression (Michaelson et al., 2008).

1.6 The newly identified driver mutation Rac1 P29S in melanoma

Dysregulation of Rac1 activity can lead to tumorigenesis and overexpression of Rac1 has already been linked to testicular, gastric and breast cancer formation (Karlsson et al., 2009). In addition to overexpression of Rac1-wt protein, also single-point mutations can influence Rac1 activity and thus cause cancer formation. After whole exome-sequencing of 147 melanoma patients, the Rac1-P29S variant was identified as a hot spot mutation in 5-9 % of cases (Krauthammer et al., 2012). It was shown that this mutation can be induced by UV-B radiation and that it causes a C to T transition, which results in an exchange of the amino acid proline to serine at position 29 (P29S). Biochemical studies by Davis *et al.* and Hodis *et al.,* using *in vitro* nucleotide-exchange-pulldown assays and protein crystallization revealed that the Rac1-P29S mutation is self-activating. The mutation destabilizes the GDP-bound inactive state and causes a higher binding affinity to GTP when compared to the Rac1 wild-type form (Davis et al., 2013; Hodis et al., 2012). Thus, the exchange rate of GDP to GTP in this Rac1-mutant is increased, resulting in faster cycling between the inactive and the active state and overall elevated activity. In agreement with this, overexpression of Rac1-P29S in Cos-7 cells and mouse melanocytes causes upregulated membrane ruffling and lamellipodia formation (Davis et al., 2013; Krauthammer et al., 2012). Furthermore, Krauthammer *et al.* observed increased PAK1-binding affinity and elevated ERK1/2 activity in cells expressing the Rac1-P29S mutant as compared to Rac1-wt (Krauthammer et al., 2012). Moreover, Van Allen *et al*. performed whole-exome sequencing studies on melanoma patients, which harbor a BRAF-V600K/E mutation. The patients were initially treated with BRAF inhibitors such as vemurafenib (PLX-4032) or dabrafenib, but developed BRAF inhibitor resistance. Since some of these patients with BRAF-inhibitor resistance also expressed the Rac1-P29S mutant, this mutation has been suggested to be a marker for tumor cells with genetically resistance against single BRAF inhibitor treatment (Van Allen et al., 2014). The group of Watson *et al*. was then further interested in analyzing whether the Rac1-P29S is not only a marker for BRAF inhibitor resistance, but if this mutation is also responsible for this resistance behavior (Watson et al., 2014). They observed that overexpression of Rac1-P29S in BRAF inhibitor treated melanoma cell lines correlates with increased cell viability and tumor growth. Higher viability was also observed in the endogenously Rac1-P29S expressing melanoma cell line IRG1 (Watson et al., 2014). More recently, Lionarons *et al.* showed that overexpression of Rac1-P29S activates PAK and AKT in mouse melanocytes and epithelial

cell. This induce a melanocytic to mesenchymal transition, resulting in increased cell survival and promote resistance to BRAF inhibitor treatment (Lionarons et al., 2019). Thus, several studies shown that Rac1-P29S might be critical to overcome BRAF inhibition by activating various signaling pathways (De et al., 2019; Mohan et al., 2019). However, detailed mechanism how Rac1 mediate the single pathways and thus control cell behavior and tumorigenesis is not yet understood.

1.7 Aim of the study

The aim of this study is to characterize the role of Rac1-P29S in tumor-associated cell behavior in patient-derived melanoma cells. We will focus on two model-systems that either endogenously express Rac1-P29S (UKE-Mel-55b) or Rac1-wt (Ma-Mel-86c) to better understand differences in Rac1-mediated signal pathways.

Rac1-P29S mediated morphodynamic changes might be linked to tumor progression such as enhanced tumor cell migration and invasiveness. Thus, we will first using fluorescent microscopy and RNAi depletion to study the characteristic phenotype changes induced by the fast cycling Rac1-P29S mutant. As critical components of tumor progression into acquisition of invasive cell state, we will focus on how Rac1-P29S might alter cell migration efficiency, cell adhesion and cell spreading.

Rac1-P29S was also shown to be involved in signaling pathways to control cell proliferation and survival. Thus, we aim to dissect potential signaling pathways that might mediate these findings using western blot analysis and siRNA depletion of Rac1 in both melanoma cell lines. In particular, we will investigate the role of Rac1 in signaling pathways, which are associated with cell proliferation and survival including ERK1/2, AKT and the actin regulated hippo signaling transcriptional coactivator Yap/Taz.

Finally, we will study the potential contribution of Rac1-P29S to the acquisition of BRAF inhibitor resistance in melanoma cells. For this, we will use a combinatorial approach including inhibitor treatment and Rac1 RNAi and measure effects on individual signal pathways related to proliferation and cell survival.

Overall, our study will reveal novel insight how Rac1-P29S promote tumor-related cellular processes and might provide a basis for further studies to overcome Rac1-induced drug resistance behavior in melanoma patients.

2. Materials and Methods

2.1 Materials

2.1.1 Eukaryotic cell lines and bacterial strains

Table 1: Eukaryotic cell lines.

Cell line	Species	Type	Organ/ Tissue	Morphology	Company	Mutations
U2-OS	*homo sapiens*	osteo-sarcoma	bone	epithelial	ATCC HTB-96	--
UKE-Mel-55b	*homo sapiens*	melanoma	skin	epithelial	Universitätsklinikum Essen, Prof. Dr. Anette Paschen	BRAF-V600K Rac1-P29S
Ma-Mel-86c	*homo sapiens*	melanoma	skin	epithelial	Universitätsklinikum Essen, Prof. Dr. Anette Paschen	BRAF - V600E

Table 2: Bacterial strains.

Cell line	Species	Type	Company
DH5α	*E.coli*	F-, supE44, ΔlacU169, [Φ80lacZΔM15], hsdR17,recA1, endA1, gyrA96, thi-1, (res-, mod+), deoR	Invitrogen

2.1.2 Media for cell lines and bacterial culture

Table 3: Media and supplements used for cell culture.

Cell line	Components
UKE-Mel-55b growth media	DMEM, high glucose, HEPES, L-Glutamine 10 % (v/v) FBS
U2-OS growth media	DMEM GlutaMAX™ 10 % (v/v) FCS
Ma-Mel-86c growth media	RPMI 1640 10 % (v/v) FCS
imaging media	HBSS (Hank`s balanced salt solution) 1 mM Calcium chloride 10 % (v/v) FCS 10 mM L-Glutamine 10 mM HEPES 1 mM Magnesium chloride

Table 4: Bacterial growth media and supplements.

Medium	Components
Luria-Bertani (LB)-Medium	1 % (w/v) Sodium chloride 1 % (w/v) Tryptone 0.5 % (w/v) Sodium hydroxide 0.25 % (w/v) Yeast Extract pH 7.4
LB Agar	1 % (w/v) Sodium chloride 1 % (w/v) Tryptone 0.5 % (w/v) Sodium hydroxide 0.25 % (w/v) Yeast Extract 1.5 % (w/v) Agar pH 7.4
Antibiotics	Ampicillin 100 µg/ mL Kanamycin 30 µg/mL

2.1.3 Reagents and buffers

Table 5: Buffers for DNA agarose gel electrophoreses.

Buffer	Components
TAE buffer	40 mM Tris-Acetate, pH 8,0 5 mM EDTA
DNA Loading dye 6x	0.25 % (w/v) Bromo phenol bleu 0.325 % (w/v) Xylencyanol 30 % (v/v) Glycerol

Table 6: Buffers for SDS-gel electrophorese and western blot.

Buffer	Components
Cathode buffer	25 mM Tris-HCl, pH 9,4 40 mM 6-Amino-hexanoic acid 10 % (v/v) Methanol
Anode buffer I	300 mM Tris-HCl, pH 10,4 10 % (v/v) Methanol
Anode buffer II	25 mM Tris-HCl, pH 10,4 10 % (v/v) Methanol
TBS buffer	20 mM Tris-HCl, pH 7,6 137 mM NaCl
TBS-T buffer	20 mM Tris-HCl, pH 7,6 137 mM NaCl 0.1 % (v/v) Tween-20

RIPA Lyse buffer	50 mM Tris-HCl, pH 7,4 150 mM NaCl 1 % (v/v) NP-40 0.25 % (v/v) Sodium-deoxycholate 1 mM EDTA **add fresh** 1x Protease-Inhibitor NaF 1mM (Stock 200 mM) Na_3VO_4 1mM (Stock 200 mM) 1x Phospho-Stop
SDS running buffer	12,5 mM Tris-HCl 0.05 % (w/v) SDS 125 mM Glycine
SDS loading buffer	500 mM Tris-HCl, pH 6,8 50 % (v/v) Glycerol 10 % (w/v) SDS 0.025 % (w/v) Bromophenol bleu 300 mM DTE
PBS buffer	2.7 mM KCl 1.5 mM K_2HPO_4 137 mM NaCl 10 mM Na_2HPO_4 pH 7.4

Table 7: Reagents and buffers used in cell culture.

Cell culture reagents	Supplier
DPBS	Life Technologies (Gibco)
DMEM high glucose (+) HEPES; (+) L-Glu; (-) Pyruvate	Life Technologies (Gibco)
DMEM (Dulbecco's modified eagle medium) GlutaMAX™	Life Technologies (Gibco)
Fetal calf serum (FCS)	Life Technologies (Gibco)
HBBS (Hank`s balanced salt solution)	Life Technologies (Gibco)
HEPES (4-(2-hydroxyethyl)-1- piperazineethanesulfonic acid)	Life Technologies (Gibco)
jetPrime	VWR
L-Glutamine 200 mM	Life Technologies (Gibco)
Lipofectamine 2000	Life Technologies (Gibco)
Lipofectamine 3000	Life Technologies (Gibco)
Poly-L-Lysine	Sigma-Aldrich
RNAiMax	Life Technologies (Gibco)
RPMI 1640	Life Technologies (Gibco)
OPTI-MEM® I Reduced Serum Medium [+] L-Glutamine [+] HEPES [-] Phenol Red	Life Technologies (Gibco)
Trypsin-EDTA	PAN Biotech

Table 8: Cell culture drugs.

Drug	Description	Concentration & incubation time	Solvent	Company
C3 (Rho-Inhibitor I)	RhoA, RhoB, and RhoC	1 µg/ml, 5 h	H_2O	Cytoskeleton
FRAX597	PAK 1/2/3 inhibitor	1 µM, 1 h	DMSO	Selleckchem
LY294002 (PI3K inhibitor)	PI3Kα/δ/β inhibitor	10 µM, 1 h	DMSO	Selleckchem
Phosphatase-Inhibitor cocktail Phospho-STOP	Phosphatase inhibitor	1x	H2O	Roche
Protease inhibitor cocktail complete Mini-EDTA free	Protease inhibitor	1x	H2O	Roche
Vemurafenib (PLX4032)	BRAFV600E/K inhibitor	1 µM, permanent	DMSO	Selleckchem

Table 9: Coating reagents for cell culture dishes.

Coating reagents	Supplier
Poly-L-lysine	Sigma-Aldrich
Collagen from calf skin (0.1% solution in 0.1 M acetic acid)	Sigma-Aldrich

2.1.4 DNA plasmids, siRNAs and primers

Table 10: Kits.

Kits	Supplier
RNeasy Mini Kit (250)	Qiagen
GenElute™ HP Plasmid Miniprep Kit	Sigma-Aldrich
QIAshredder	Qiagen
Total protein staining kit	Li-cor

Table 11: Enzymes.

Enzymes	Supplier
Pfu ultra II Fusion HS DNA Polymerase	Agilent
*Dpn*I, recombinant	NEB
RNase-Free DNase Set (50)	Qiagen
RNaseOUT™	Invitrogen
SuperScript II Reverse Transcriptase	Invitrogen
Taq Polymerase	NEB

Table 12: Plasmids used in this study.

Name	Description	Source
pcDNA3.1 EGFP-Rac1wt	Wild-type Rac1	Dr. Melanie Gräßl
pcDNA3.1 EGFP- Rac1Q61L	constitutive active Rac1	Dr. Melanie Gräßl
pcDNA3.1 EGFP	empty control vector for EGFP	Dr. Nina Schulze
pcDNA3.1 EGFP-Rac1P29S	fast-cycling Rac1 P29S mutation	Jana Quentin
pcDNA3.1-EGFP-Rac1-wt res. D8	Rac1P29S siRNA resistant dharmacon Rac1 siRNA # 8	Jana Quentin
cDNA3.1-EGFP-Rac1-P29S res. D8	Rac1P29S siRNA resistant dharmacon Rac1 siRNA # 8	Jana Quentin
PAK1 wt-EGFP (in pEGFP-N1)	PAK1-WT cloned in pEGFP-N1 using Gibson cloning- RP	Dr. Rutuja Patwardhan
PAK2 wt-EGFP (in pEGFP-N1)	PAK2-WT cloned in pEGFP-N1 using Gibson cloning- RP	Dr. Rutuja Patwardhan

Table 13: SiRNA for protein depletion in eukaryotic cell lines.

Name	Sequence (5´→ 3´)	Source
ON-TARGET plus non-Targeting #2	UGGUUUACAUGUUGUGUGA	Dharmacon
ON-TARGET plus siRNA Rac1 #8	TAAAGACACGATCGAGAAA	Dharmacon
ON-TARGET plus siRNA Cdc42 #5	CGGAAUAUGUACCGACUGU	Dharmacon
ON-TARGET plus siRNA Cdc42 #6	GCAGUCACAGUUAUGAUUG	Dharmacon
ON-TARGET plus siRNA PAK1 (αPAK)	ACCCAAACAUUGUGAAUUA GGAGAAAUUACGAAGCAUA UCAAAUAACGGCCUAGACA CAUCAAAUAUCACUAAGUC	Dharmacon
ON-TARGET plus siRNA PAK2 (ɣPAK)	GAAACUGGCCAAACCGUUA GAGCAGAGCAAACGCAGUA ACAGUGGGCUCGAUUACUA GAACUGAUCAUUAACGAGA	Dharmacon
ON-TARGET plus siRNA RhoA #11	GACCAAAGAUGGAGUGAGA	Dharmacon
Qiagen non-Targeting siRNA	unknown	Qiagen
AllStars siRNA Rac1 #6	ATGCATTTCCTGGAGAATATA	Qiagen

Table 14: Primers for PCR mutagenesis and Sanger-sequencing. Point mutations highlighted in red.

Name	Sequence (5´→ 3´)	Source
Primer forward sequencing Rac1 plasmids	CTGTACAAGGAATTCATGCAGGCC	Sigma-Aldrich
Primer reverse sequencing Rac1 plasmids	CTCGAGTTACAACAGCAGGCATTT	Sigma-Aldrich
Primer forward sequencing cDNA human cell lines	CTGATGCAGGCCATCAAGTGTGTGG	Metabion
Primer reverse sequencing cDNA human cell lines	CCAAGAACGAGGGGCTGAGACATTTAC	Metabion
Primer forward Rac1 P29S point mutagenesis	CTGATCAGTTACACAACCAATGCA TTT**T**CTGGAGAATATATCCC	Sigma-Aldrich
Primer reverse Rac1 P29S point mutagenesis	GGGATATATTCTCCAG**A**AAA TAGCATTGGTTGTGTAACTGATCAG	Sigma-Aldrich
Primer forward siRNA resistant EGFP-Rac1-wt/P29S dharmacon #8	GGGATGATAAAGA**T**ACGATCG**A**AAAA CTGAAGGAGAAGAAGC	Sigma-Aldrich
Primer reverse siRNA resistant EGFP-Rac1-wt/P29S dharmacon #8	GCTTCTTCTCCTTCAGTTT **T**TCGATCGT**A**TCTTTATCATCCC	Sigma-Aldrich

2.1.5 Antibodies and dyes

Table 15: Primary antibodies used for western blot and immune-detection.

Antibody	Type	Dilution	Western blot	Company
AKT (40D4)	mouse monoclonal	1:500	15% gel 17 min blotting	Cell signaling
pAKT (Ser473) (D9E)	rabbit monoclonal	1:500	15% gel 17 min blotting	Cell signaling
β-PIX	rabbit	1:500	12% gel 35 min blotting	Cell signaling
Cdc42 (B8)	mouse monoclonal	1:100	15% gel 15 min blotting	Santa Cruz
EGFP	rabbit polyclonal	1:500	15% gel 17 min blotting	Abcam
ERK 1/2	rabbit monoclonal	1:500	15% gel 17 min blotting	Cell signaling
pERK1/2 (T202/Y204)	mouse monoclonal	1:500	15% gel 17 min blotting	Santa Cruz
FAK	mouse monoclonal	1:500	10% gel 45 min blotting	Millipore
pFAK (Y397)	rabbit monoclonal	1:500	10% gel 45 min blotting	Invitrogen
ki-67	rabbit polyclonal	1:500	--	Novus
NFkβ p65 (C-20)	rabbit polyclonal	1:500	12% gel 35 min blotting	Santa Cruz
PAK α/β/ɣ	mouse monoclonal	1:300	12% gel 26 min blotting	Santa Cruz
pPAK1 (Ser199/204) pPAK2 (Ser192/197)	rabbit polyclonal	1:200	12% gel 26 min blotting	Cell signaling
Paxillin (clone 349)	mouse monoclonal	1:500	--	BD bioscience
PTEN	rabbit monoclonal	1:500	12% gel 17 min blotting	Santa Cruz
Rac1	mouse monoclonal	1:500	15% gel 17 min blotting	Millipore
RhoA	mouse monoclonal	1:200	15% gel 17 min blotting	Santa Cruz
RhoB	mouse monoclonal	1:500	15% gel 17 min blotting	Santa Cruz
RhoC	rabbit monoclonal	1:500	15% gel 17 min blotting	Cell signaling
Yap	mouse monoclonal	1:1000	12% gel 20 min blotting	Santa Cruz
pYap (Ser397) (D1E7Y)	rabbit monoclonal	1:1000	12% gel 20 min blotting	Cell signaling
Yap/Taz	rabbit monoclonal	1:500	--	Cell signaling

Table 16: Secondary antibodies and dyes for western blot and immune-detection.

Antibody/dye	Conjugation	Dilution	Company
Hoechst 33342	DNA	1:2000	Sigma-Aldrich
rhodamin-phalloidin	F-actin	1:500	Invitrogen
Goat-anti-mouse	Alexa-Fluor® 488	1:500	Invitrogen
Goat-anti-rabbit	Alexa-Fluor® 633	1:500	Invitrogen
Goat-anti-mouse	IRDye 680RD	1:20 000	Li-Cor
Goat-anti-mouse	IRDye 800CW	1:20 000	Li-Cor
Goat-anti-rabbit	IRDye 680RD	1:20 000	Li-Cor
Goat-anti-rabbit	IRDye 800CW	1:20 000	Li-Cor

2.1.6 Consumables

Table 17: Consumables. All non-mentioned consumables were in accordance with laboratory standards.

Consumables	Supplier
6-well IBIDI glass bottom PH+	Oehmen
6-well plates Flat Bottom with Lid	IBIDI
Cell culture dish 100x20 mm	Sartstedt
coverslip Ø 10 mm	Hecht/fisher scientific
Cryokontainer, Mr. Frosty	Nalgene
Cryo-tube, PP, 2 ml	Carl Roth
Drigalskispatel	Hartenstein
falcon tubes (15-ml)	Sarstedt
falcon tubes (50-ml)	Sarstedt
Filter tips 0,5-20 µl,	Sarstedt
Filter tips 2-200 µl	Sarstedt
Filter tips 1000 µl	Sarstedt
Haemacytometer, 20x26x0,4mm	Hartenstein
Neubauer improved counting chamber	Hartenstein
Nitrile gloves	Starlab
Parafilm	Hartenstein
Pasteur pipette	Hartenstein
Pipette tips 0.1-2.5 µl	Sarstedt
Pipette tips 1000 µl	Sarstedt
Pipette tips 250 µl	Sarstedt
PS semi-micro cuvettes	Sarstedt
PVDF-Membrane	Merck Millipore
safe seal 0.2 ml	Thermo Scientific
safe seal 0.5 ml	VWR
safe seal 1.5 ml	VWR
safe seal 2 ml	Sarstedt

serological pipette 10 ml	Sarstedt
serological pipette 25 ml	Sarstedt
serological pipette 5 ml	Sarstedt
Sterile culture tubes, PP, 12 mL	Carl Roth
Sterile filter: Filtropur; 0,2 µm	Sarstedt
Syring without needle, 50 mL	VWR
Type F immersion liquid	Leica
Whatman 2mm blotting paper	Hartenstein

Table 18: Chemicals used for molecular biological experiments.

Chemical reagent	Supplier
Acetic acid	Roth
Acrylamide-Mix (Rotiphorese Gel 30)	Roth
Agar	Roth
Agarose	Biozym
Antibiotics, Ampicillin	Roth
Antibiotics, Kanamycin	Roth
Ammonuim peroxydisulfate	Roth
Bradford Protein Assay	BioRad
Bromophenol bleu	Serva
BSA, powder pH 6.5-7.5	Sigma-Aldrich
CutSmart Buffer	New England Biolabs
Calcium chloride	Roth
ddH_2O RNase free	Invitrogen
DMSO	Roth
dNTPs	Roth
DPBS	Pan Biotech
EDTA	AppliChem
Formaldehyde solution, 37 %	Sigma-Aldrich
Glycerine	AppliChem
Glycine	AppliChem
HD green	Intas
Isopropanol	Roth
Potassium chloride (KaCl)	Roth
Potassium hydrogen phosphate (KH_2PO_4)	Roth
Magnesium chloride ($MgCl_2$)	Roth
Methanol	VWR
MES	Sigma-Aldrich
Oligo(dT) 12-18, 25UG	Life Technologies
Sodium chloride (NaCl)	Roth
Sodium deoxycholate	Sigma-Aldrich
Sodium fluoride	Sigma-Aldrich
Sodium hydrogen phosphate (Na_2HPO_4)	Roth

Sodium hydroxide (NaOH)	Roth
Sodium ortho vanadate	Sigma-Aldrich
NP-40	Life technologies
Nucleotide-Mix (Roti Mix PCR3)	Roth
Odyssey Blocking buffer (TBS)	Li-cor
PEG 8000	Merck
PEG 6000	Merck
SDS	Roth
TEMED	Roth
Tris	AppliChem
Trition-x-100	Sigma-Aldrich
Trypton	Serva
Tween 20	Roth
Yeast extract	Serva

2.1.7 Equipment, microscopes and software

Table 19: Devices. All non-mentioned devices were in accordance with laboratory standards.

Device	Supplier
Analytical balance	Kern
Bacterial incubator	Function Line Heraeus
Centrifuge 5415D, 5804	Eppendorf
CO2-incubator HEPA Class 100	Thermo Scientific
cooling micro centrifuge	Hettich
DNA agarose chamber	Roth
Energy supply	VWR
Heating block BioTech TH26	HLC
Laminar flow cabinet HERAsafe	Thermo Scientific
micro centrifuge	Roth
Micro scales	Kern
Nanodrop	PeqLab
PCR MultiGene Gradient	Labnet
pH-meter seven easy pH	Mettler-Toledo
SDS-gel electrophoreses chamber	BioRad
Semi-dry blotting chamber	Invitrogen
Shaker	Thermo Scientific
Spectral photometer Genesis 6	PeqLab
Suction pump Vacusafe comfort ISB	INTEGRA Bioscience
UV-Transilluminator	BioRad
vertical SDS-electrophoreses, TetraCell	BioRad
Voltage source	VWR
Vortexer	Grant-Bio
Water bath Aqualine AL 18	Lauda
Western blot fluorescence detection system	Li-Cor

Table 20: Inverted transmitted light microscope for cell culture analysis.

VWR 400	transmitted light microscope
illumination source	Halogen lamp 6V/30W
objective	10x PHP2

Table 21: Epi-fluorescence microscopy for immune-detection of fixed cell samples.

Zeiss Axio observer 7	Epi-fluorescence microscopy
fluorescence illumination source	Colibri multi-color LED
reflector	Cy5, Dapi, HEGFP, YFP, CFP, TR
camera	Zeiss AxioCam 506 mono CCD camera, 2752 x 2208 imaging array, 4.54 µm x 4.54 µm pixels, 14-bit digitization
objective	Plan-Neofluar 20x/0.50; NA 0.5
filter	Set 01 UV: Ex BP 365/12, FT 395, Em LP 397 Set 38 HE: Ex BP 470/40, FT 495, Em BP 525/50 Set 46: Ex BP 500/20, FT 515, Em BP 535/30 Set 15: Ex BP 546/12, FT 580, Em LP 590 Set 50: Ex BP 640/30, FT 660, Em BP 690/50
software	ZEN 2.3, Zeiss

Table 22: Epi-fluorescence and phase-contrast microscopy for fixed and live-cell imaging.

Nikon Ti-Eclipse Epi	Epi-fluorescence & phase-contrast microscopy
illumination source	Halogen lamp
fluorescence illumination source	mercury burner (100 W)
filter wheel changer	Lambda 10-2 RS232 (Sutter Instruments)
camera	Roper Scientific CoolSNAP HQ2 interline-transfer CCD camera, 1392 x 1040 imaging array, 6.45 x 6.45-µm pixels, 14-bit digitization
objective	CFI S Plan Fluor ELWD 20x/0.45 DIC; NA 0.45
filter	EGFP/mCherry Dualband sbxm ET Filterset EGFP/mCherry Dualband sbxm ET Filterset CFP/YFP Dualband sbxm ET Filterset
software	Nikon NIS Elements AR

Table 23: Confocal fluorescence microscopy for immune-detection of fixed cell samples.

Leica TCS SP5	Confocal fluorescence microscopy
Laser	Diode Laser: 405 nm (50 mW) Argon Laser: 458 nm (5 mW), 476 nm (5 mW), 488 nm (20 mW), 496 nm (5 mW), 514 nm (20 mW) HeNe Laser: 594 nm (2.5 mW) and 633 nm (10 mW)
detectors	3 PMTs, 2 HyD
objective	HCX PL APO 63x/1.40-0.60 Lbd. BL; N.A 1.4; oil
software	LAS AF (Leica Microsystems)

Table 24: Used software.

software	
Fiji (Just Image J) 1.51n	imaging analysis
GraphPad Prism 5	Graphs and statistical analysis
IBIDI chemotaxis tool	migration analysis
ApE	PCR mutagenesis
Image Studio Lite Version 5.2	western blot analysis
Endnote	reference management
Microsoft office	

2.2 Methods

2.2.1 Molecular biology

2.2.1.1 Site-directed PCR-mutagenesis

Site-directed PCR-mutagenesis is a common technique to introduce single-point mutations in plasmids using primers, which contain the desired mutation (Tab. 14). This method was used to introduce the Rac1-P29S mutations and to generate siRNA resistant plasmids (Tab. 12).

Table 25: Overview of new generated and used plasmids together with the used melting temperatures (T_m).

Original plasmid	New plasmid	T_m [°C]
pcDNA3.1 EGFP-Rac1wt	pcDNA3.1 EGFP-Rac1-P29S	73°C
pcDNA3.1 EGFP-Rac1wt	pcDNA3.1 EGFP-Rac1-wt res. siRac1 D#8	68°C
pcDNA3.1 EGFP-Rac1-P29S	pcDNA3.1 EGFP-Rac1-P29S res. siRac1 D#8	65.9°C

For preparing the different PCR amplifications, the following standard PCR mixture (Tab. 26) were used.

Table 26: Components for site-directed PCR-mutagenesis mixture. Primers see table 14.

Reagents	Final quantity
ddH_2O	add to final volume
10x Buffer	5 µl
DNA	5-25 ng
dNTPs	1 µl
primer forward	125 ng
primer reverse	125 ng
Pfu Ultra II HS Polymerase	1 U
final volume	50 µl

For introducing the single-point mutations, PCR was performed using conditions described in Table 27. The melting temperature (T_m, Tab. 25) various depending on the used primers.

Table 27: PCR amplification cycles for single point mutation of the Rac1-plasmids.

Temperature [°C]	Time	Cycle	Process
95 °C	2 min	1	initial denaturation
95 °C	20 sec	30	denaturation
T_m °C	20 sec		annealing
72 °C	2 min		elongation
72 °C	3 min	1	
4 °C	storage		

After PCR amplification, the parent template was removed by *Dpn*I restriction digestion and first analyzed with agarose gel electrophoreses to examined the correct plasmid size (chapter 2.2.1.2/3). Next, the new plasmid was transformed into bacteria such as *E. coli* and was selected by adding antibiotics, depending on the vector-containing resistant gene. Subsequently, plasmids were purified form single colonies and analyzed by sanger-sequencing (eurofins, GATC) for the modified DNA sequence.

2.2.1.2 Agarose gel electrophoresis

With agarose gel electrophoresis, DNA fragments can be separated based on their size which allows further quantification studies. In general, the gels contain 0.5-2 % agarose depending on the expected size of the DNA fragments. Here, 1 % agarose gels were used to measure plasmid size after PCR-mutagenesis. For that, the agarose was dissolved in 1x TAE-buffer and heated until the solution was clear. When the solution cooled to around 60 °C, 2-4 µl HDgreen was added. The complete mix was then poured into an agarose gel chamber followed by comb insertion for generating of loading wells. After the gel solidified , the chamber was filled with 1x TAE-buffer and the samples were loaded. For loading, the DNA samples were mixed 1:5 with 6x loading dye. The NEB Quick load 1 kb marker was used to determine the DNA fragment size. The gel was then run at 100 V for one hour. The DNA was then visualized under UV-light. Detection of performed by mobile phone camera or UV-Transilluminator system from BioRad.

2.2.1.3 Restriction digestion

*Dpn*I is a restriction enzyme, which allows the specific degradation of methylated DNA. This enables removal of parental plasmid DNA after introducing single point mutations. For this, 5 µl of *Dpn*I was directly added to the full PCR product and incubated at 37°C for one hour. After incubation, the mixture was directly used for transformation into bacterial strains.

2.2.1.4 Preparation of heat-shock competent *E.coli* cells

All working steps were prepared under flame for sterility and the LB-media was in general without any antibiotics.
On day one 4 ml LB-media were inoculate with 10 µl of *DH5α E.coli* cells and incubated at 37 °C and 180 rpm overnight. The next day, the 4 ml overnight culture were used to inoculate 400 ml LB-media and incubated using the same parameters until the culture reached an OD_{600} between 0.3-0.5. After that, the cell suspension was transferred in 50 ml falcon tubes and incubated for 20 min on ice, followed by centrifugation at 4 °C, 4000 rpm for 10 minutes. The supernatant was discard and the pellets were suspended in 15 ml ice-cold TSS-buffer (total volume). 200 µl of this suspension was transferred in 1.5 ml tubes and directly frozen in liquid nitrogen before keeping at -80 °C for long-term storage.

2.2.1.5 Transformation of competent *E.coli* cells

Competent *E.coli* cells stored at -80 °C were incubated on ice for at least 20 minutes. After that, 1 µl DNA was added and the mix was incubated on ice for another 30 minutes. To open the bacterial membrane a short heat shock was performed at 42 °C for 60-90 seconds. This was stopped by incubation on ice of 2 min. Next, 1 ml LB-media without any antibiotic was added and the cells were incubated at 37 °C, 180 rpm for one hour. The cells were collected via centrifugation at 13000 rpm for 2 minutes, 850 µl supernatant was discarded while the rest was used to suspend the cell pellet. This *E.coli* cell suspension was plated on an LB-plate containing the respective antibiotic and incubated overnight at 37 °C.

2.2.1.6 Bacterial overnight cultures and preparation of bacterial glycerol stocks

Bacterial overnight cultures were used to amplify plasmid-containing *E.coli* for DNA purification and for long-term storage. To do so, a single colony from the DNA containing *E.coli* plate was used to inoculate 4-5 ml LB-media containing the respective antibiotic. The suspension was incubate overnight at 37 °C and 180 rpm. For glycerol stocks, 500 µl of the suspension was then mixed with 500 µl glycerol (50 % v/v) in a cryo-tube and stored at -80°C. The leftover could be used for plasmid purification.

2.2.1.7 Isolation and purification of plasmid DNA from *E.coli* cells

Here, plasmid DNA form *E. coli* overnight cultures was purified with the GenElute Plasmid Miniprep Kit (Sigma-Aldrich), following the manufacturer's instructions. The concentrations of eluted plasmids was measured by using the Nanodrop™ and then stored at -20/-80°C.

2.2.2 Biochemical methods

2.2.2.1 Protein lysis from adherent cells

At the beginning of cell lysis, cells which were cultured on 6-well plates, were placed on ice and washed once with ice-cold PBS. After removal of PBS, the cells were incubated for several minutes with ice-cold RIPA lysis buffer (50 µl/well) on ice. Thereafter, the cells were detached from the surface with a cell scraper and transferred into a pre-cooled tube (1.5 ml) and centrifuged at 4 °C for 30 minutes at 14.000 rpm. The supernatant was transferred to a new cooled tube, concentration of total protein was determined (chapter 2.2.2.2), followed by SDS-Page gel electrophoresis and western blot (chapter 2.2.2.3).

2.2.2.2 Determination of protein concentration via Bradford

To determine the protein concentration, the so-called Bradford test was used (Bradford 1976). It is a photometric method to determine the protein concentration. The method uses the Coomassi Brilliant Blue G250 dye, which binds to the side chains of the amino acids. This binding leads to a shift of the absorption maximum from 465 nm to 595 nm and enables photometric detection of the protein concentration.

For calibration, a standard BSA calibration curve with the concentrations 0.2/0.5/1 and 2 µg/µl was prepared. For this purpose, 5 µl of each BSA solution were mixed with 1 ml Bradford reagent respectively. The Bradford reagent was previously diluted 1:5 with ddH_2O. Using the calculated linear regression equation, based on the known BSA concentrations, the protein concentration of the unknown samples could later be determined over the absorption value. The unknown protein samples were prepared analogously to the BSA samples.

2.2.2.3 SDS-PAGE and Western Blot for immune-detection

SDS-PAGE is a well-known method in protein analysis and is used primarily for the separation of protein mixtures. Proteins are denatured by incubation with SDS (sodium dodecylsulphate). The SDS treatment leads to an approximately equal negative charge density, so that the proteins can now be separated in the gel based on their molecular weight.

In this work, discontinuous polyacrylamide gels were used. The gels for this method consist of two different areas, the stacking and resolving part. The upper stacking gel is used to collect the protein samples before the separation based on the molecular weight takes place in the lower separation gel. To generate different SDS-gels, which differ in their pore size, to analyze proteins more specific based on their size, polymerization of the acrylamide was modified by varying the ratios of acrylamide to APS and TEMED.

Table 28: Components of stacking and separation SDS-gels for gel electrophoresis. See Tab. 15 for gel and blotting conditions of the individual analyzed proteins.

Reagent	15 % Gel (10 ml)	12 % Gel (10 ml)	10 % Gel (10 ml)	5 % Stacking Gel (4 ml)
ddH_2O	2.3 ml	3.3 ml	4 ml	2,7 ml
Acryl-Bisacrylamid-Mix (30 %)	5 ml	4 ml	3,3 ml	670 µl
SDS (10 %)	100 µl	100 µl	100 µl	40 µl
Stacking gel buffer Tris pH 6,8	--	--	--	500 µl
Resolving gel buffer Tris pH 8,8	2.5 ml	2.5 ml	2.5 ml	--
APS (10 %)	100 µl	100 µl	100 µl	40 µl
TEMED	4 µl	4 µl	4 µl	4 µl

The protein mixtures were initially mixed 5:1 with 5x SDS sample buffer and denatured for 5 minutes at 95 °C. 15-30 µg of the protein mixture were loaded on the gel. To determine the molecular weight, a protein marker was used. Empty pockets were filled with 1-2 µl 5x SDS sample buffer. The separation of the proteins was then carried out for one hour at 250 V, 40 mA, 8 watts (1 gel) and for one hour at 300 V, 60 mA, 10 watts for two gels.

Western blotting is a method to transfer proteins, which were first separated by SDS-PAGE, to a membrane and further allowing immune-detection of target proteins.

In this work, a PVDF membrane and the semi-dry transfer method were used. For this purpose, the stacking gel was removed and the separating gel was pivoted for 15 min in a cathode buffer at RT. During this time, the membrane was cut, activated in methanol for 20 seconds, washed with ddH_2O and then incubated for 5 minutes in anode buffer II. In addition, Whatman™ papers were cut and incubated for a few minutes in the respective buffer (see below). Thereafter, the components were stacked on the plate anode of the western blot chamber as follows:

1. two Whatman™ filter papers in anode buffer I
2. one Whatman™ filter paper in anode buffer II
3. membrane in anode buffer II
4. the SDS gel incubated in cathode buffer
5. three Whatman™ filter papers in cathode buffer

The transfer was carried at 20 V, 160 mA and 8 W for one gel. The time duration varied according to the molecular weight of the target protein (Tab. 15).To assess the protein transfer, the applied total protein was stained (staining solution from Li-Cor). For this, the membrane was washed briefly with ddH_2O and then swirled in the dyeing solution in the dark for five minutes, followed by two short washes with the washing solution from Li-Cor. The total protein was then detected at 680 nm with the Li-Cor Odyssey scanner. The staining solution was removed by incubating the membrane with the removal solution (Li-Cor) for five minutes at RT. Subsequently, the membrane was incubated for one hour in the blocking solution (Li-Cor). The incubation with the primary antibodies (Tab. 15) was performed overnight at 4 °C. 0.05 % NaN_3 was added to the primary antibody solutions, which allows to use the solutions several times by avoiding contamination. The next day, the membrane was washed three times with 1× TBS-T and then incubated for one hour with the secondary antibodies (Tab. 16). To improve fluorophore signals, 0.1 % SDS and 0.1 % Tween-20 were added to the antibody solutions. The membrane was then washed twice with 1x TBS-T and finally once with 1x TBS. The detection was carried out on the Li-Cor Odyssey scanner at 680 nm and 800 nm.

2.2.3 Cell biological methods

All buffers, media and reagents used in this work were sterile filtered and heated to 37 °C in a water bath, unless otherwise stated. Culturing of the eukaryotic cells were carried out at 37 °C, 5 % CO_2 and 95 % humidity. In order to avoid contamination, all work for culturing and experimental implementation were performed under sterile benches.

2.2.3.1 Thawing and subculture of adherent cell lines

The cryo-cultures were briefly thawed in a water bath and diluted with 9 ml of medium. The suspension was centrifuged for 5 min at 1000 rpm, the supernatant was discarded and the pellet suspended in 10 ml medium. The cells were seeded in 10 ml fresh growth medium on a 10 cm cell culture dish and incubated as described above. After reaching the required confluence (> 80 %), the cells were passaged and could be used to perform the respective experiments. For this purpose, the old medium was removed, cells were washed once with 5 ml DPBS and incubated with 2 ml of a trypsin/EDTA solution

(0.05 %) for several minutes in the incubator (Tab. 29). Subsequently, cells were suspended with fresh media and transferred to a falcon (15 ml). Depending on how long the cells should be cultured, different amount of cells were plated on a new culture dish (Tab. 29).

Table 29: Quantities used to obtain the respective cell line.

Cell line	incubation time trypsin	resuspension volume	72 h culturing	96 h culturing
U2-OS	6 min	6 ml	$3 \cdot 10^4$ cells	$4 \cdot 10^4$ cells
UKE-Mel-55b	6 min	3 ml	1.5 ml cell suspension	1-1.2 ml cell suspension
Ma-Mel-86c	3 min	3 ml	1 ml cell suspension	800 µl cell suspension

The Neubauer counting chamber was used to determine the number of cells. For this, the four corner squares per chamber were counted, and the mean value was calculated and the result multiplied by 10^4, whereby the number of cells / ml was obtained.

2.2.3.2 Cryopreservation of eukaryotic cells

Cells were detached from the surface using the trypsin/EDTA solution and suspended with new medium and transferred to a 15 ml falcon tube. The cells were then centrifuged for 5 min at 1000 rpm. In parallel, the freezing medium was produced by adding 10 % (v/v) DMSO to the normal growth medium. After centrifugation, the supernatant was discarded and the cell pellet suspended in 1 ml freezing medium, transferred to a suitable cryogenic tube and frozen in the isopropanol-filled cryo-container (Mr. Frosty, Nalgene) at -80 °C overnight. Subsequently, the cells were stored permanently at -150 °C.

2.2.3.3 Sequencing of Rac1 cDNA in eukaryotic cell lines

Cells were plated on a 6-well or 10 cm dish until they reach a confluence of approx. 80%. mRNA isolation and lysate homogenization were then performed with the RNeasy Mini Kit and QIAshredder-columns from Qiagen, as indicated by the manufacturer. To remove genomic DNA, RNase-free DNase (Qiagen) was added as described in the manufacturer's

protocol. The isolated and purified mRNA could then be stored at -80°C and concentration could be measured with the Nanodrop™.

For further studies, mRNA was translated in cDNA by using the SuperScript II reverse transcriptase form Invitrogen. Mix 1 and 2 were prepared separately and mixed after cycle 1 (Tab. 30). After cycle 2, 1 µl of the SuperScript II reverse transcriptase was added and followed by cycle 3 and 4.

Table 30: Sample mixture and incubation for cDNA synthesis.

Mix 1		**Cycle 1**	**Mix 2**		**Cycle 2**	**add**	**Cycle 3**	**Cycle 4**
RNA	0.1-1 µg		5x FS buffer	4 µ		Super		
dNTP Mix	1 µl	65°C	0.1 M DTT	2 µl	42°C	Script II	42°C	70°C
Oligo-dT	1 µl	5 min	RNase out	1 µ	2 min		50 min	15 min
ddH_2O	fill up		$\sum_{Mix2}$	7 µl		1 µl		
$\sum_{Mix1}$	12 µl		$\sum_{Mix1+2}$	50 µl				

After cDNA synthesis, PCR was performed to amplify the endogenous Rac1 sequencing (579 bp). Table 31 and 32 show the used PCR mixtures and PCR amplification programs.

Table 31: Components for site-directed PCR-mutagenesis mixture. Primers see table 14 (Primer forward/reverse sequencing cDNA human cell lines).

Reagents	**Final quantity**
ddH_2O	add to final volume
10x Buffer	5 µl
cDNA	1 µl
dNTPs mix	1 µl
primer forward 10 µM	1 µl
primer reverse 10 µM	1 µl
Taq Polymerase	0.25 µl
final volume	50 µl

Table 32: PCR amplification cycles for single point mutation of the Rac1-plasmids.

Temperature [°C]	**Time**	**Cycle**	**Process**
95 °C	1 min	1	initial denaturation
95 °C	30 sec	30	denaturation
57 °C	30 sec		annealing
68 °C	1 min		elongation
68 °C	5 min	1	
4 °C	storage		

2.2.3.4 Transient plasmid transfection of UKE-Mel-55b and U2-OS cells

Lipofectamine 3000 was used for transient plasmid transfection in UKE-Mel-55b cells and for U2-OS cells Lipofectamine 2000 was used. For both cell lines the following protocol was followed:
For each well of a 6-well plate 3 µl Lipofectamine 3000/2000 were mixed with 100 µl OptiMEM and incubated for 5 minutes at RT. In parallel 100 µl OptiMEM was mixed with DNA. Next, the DNA-OptiMEM was mixed with the Lipofectamine-OptiMEM solution and incubated for 15 min at RT. The mixed solution was added dropwise to the cells. Before adding the transfection mix, the cell culture growth media was replaced with fresh one. For other sample dishes, the necessary amount of Lipofectamine 3000/2000, OptiMEM and DNA were re-calculated based on growth-area of the dish.

2.2.3.5 Transient plasmid transfection of Ma-Mel-86c cell lines

For transient plasmid transfection in the Ma-Mel-86c cell line, the transfection reagent jetPrime (VWR) was used. To do so, 200 µl of the buffer solution was mixed directly with 3 µl jetPrime and DNA (for one well of a 6-well plate). This was incubated for 15 min at RT and then added dropwise to the cells.

2.2.3.6 Transient siRNA transfection of melanoma cell lines

To transfect the melanoma cells with small-interfering RNA, the Lipofectamine RNAiMax reagent was used, following the fast forward transfection protocol. For each well of a 6-well plate, 2.4 µl RNAiMax was mixed with 100 µl OptiMEM and incubated for 5 min at RT. Next, 100 µl OptiMEM was mixed with siRNA (final concentration after adding to the cell suspension: 10 nM). The siRNA solution was mixed with the RNAiMax-OptiMEM and incubated for 10-15 min at RT. In this time, $6 \cdot 10^4$ cells/well on a 6-well plate were seeded in 1.8 ml medium (for 72 h knock-down). After incubation, 200 µl of the siRNA-RNAiMax mix were added dropwise to the cell suspension. The cells were incubated for 24 h and transfection was then stopped by media change. After 72 h, the cells were used for further experiments such as western blot or microscope studies. For rescue experiments, the transient transfection of siRNA resistant plasmids takes place 24 h after siRNA treatment.

2.2.3.7 Coating of cell culture dishes for microscopy experiments

Based on the experimental question, the used cell dishes were coated in advance with various components of the extracellular matrix. If glass coverslips were used for microscopy experiments, the coverslips were first sterilized in 70% ethanol for minimal 24 h and were then washed with 1x DPBS before coating reagents were added. The various reagents were diluted in 1x DPBS. In this work, a 0.001% (v / v) collagen type I solution or poly-L-lysine with similar concentration were used. Coated dishes were incubated for one hour at 37°C, followed by three times washing with 1x DPBS.

2.2.3.8 Sample preparation and drug treatment

Cells were cultured on 6-well plates for 24 h before drug treatment was started (Tab. 8). The respective solvent of the individual drugs was used in equal concentration as control condition. For long-term treatment with PLX-4032, growth media was replaced after three days and fresh inhibitor was added.

2.2.4 Microscopy

2.2.4.1 Live-cell phase-contrast microscopy

Live-cell phase-contrast microscopy was performed on the Nikon Ti-Eclipse with the 20x air objective (Tab. 22). Cells were plated on 4-well IBIDI glass bottom Ph^+ dishes ($0.2 \cdot 10^5$ cells/well) and imaged all 20 min for 10 h. If necessary, the IBIDI dish was coated with collagen I or poly-L-lysine before. After seeding, cells were first incubated for 2 hours in normal cell culture media under 37°C and 5 % CO_2 atmosphere. Then the media was change to imaging medium (Tab. 3), cells were transferred to the microscope incubation chamber (pre-warmed to 37°C) and let settled again for 30 min prior imaging. Live-cell movies were then used to analyze cell migration and cell division behavior with Fiji (just Image J). Single cell tracking for cell migration studies was performed with the manual tracking plugin form Fiji. Parameters in the tracking tool were set as described in the following table 33.

Table 33: Parameters for the manual tracking with the Fiji plugin in.

Parameters	Settings
time interval	20 min
x/y calibration	0.3245 µm
line width	4

Different color lines were used to show migration of individual cells in the live-cell movie. Results for single cell migration were collected in an excel sheet and uploaded in the IBID chemotaxis tool to analyze migration velocity and accumulated distance. Moreover, the graphs for the accumulated distances were also generate with this program.
For analyzing cell division events, total cell number of the first frame was counted as well as the number of cell division events for those cells. Both numbers were used to calculate the percentage of mitotic events in n.t siRNA and siRac1-treated cells. Additionally, the number of cells with cell-matrix adhesions during mitosis was counted and the time for cell division was measured. For this, we set the start point (t_0) as the frame before cell rounding and end point (t_{end}) was set when the daughter cells reattached. If cell division takes longer than the calculated mean time for the n.t siRNA-treated cells, it was depicted as `mitotic delay`.

2.2.4.2 Indirect fluorescence staining – sample preparation for fixed cells

Depending on the primary antibodies the cells were fixed in pre-warmed 4 % formaldehyde (FA) in 1x PBS for at 37 °C for 20 min or with ice-cold methanol at -20 °C also for 20 min. The FA and methanol fixed samples were washed three times with 1x PBS. For the methanol fixed samples, the first PBS washing step was incubated for 5 min at RT before proceeding for other washing steps. The samples were transferred in a wet chamber in dark to avoid photo-bleaching and to reduce the total amount of reagents. After washing the FA-fixed samples were permeabilized with 0.2 % Trition-X-100 solution in 1x PBS for 15 min at RT followed by three times washing with 1x PBS. To overcome the problem of unspecific binding sites, all samples were incubated for 30 min at RT with a blocking solution containing 10 % (w/v) BSA in 1x PBS. Afterwards, the blocking solution was removed and the primary antibody solution (antibody in 2 % (w/v) BSA in 1x PBS; Tab. 15) were added and incubated for one hour at RT in the dark. Next, the samples were washed again three times before the secondary antibody solution

(antibody in 2 % (w/v) BSA in 1x PBS; Tab. 16) was added and incubated also for one hour at RT in the dark. After three more washing steps the samples were incubated with 1 % formaldehyde in 1x PBS for 10 minutes at RT, this was followed by three final washing steps with 1x PBS and one with ddH_2O before the cells were mounted with 3 µl Prolong gold mounting medium on glass slides and stored overnight at RT in the dark.

2.2.4.3 Epi-fluorescent microscopy of fixed cell samples

Epi-fluorescence microscopy was performed on two different microscopes. For detailed analysis, background was measured and subtracted from the images.
The Nikon-Ti inverted epifluorescence microscope was used with the 20x air objective for nuclei (Hoechst 33342), actin (rhodamin-phalloidin) and EGFP-plasmid visualization in some experiments.

Table 34: Filter combinations of the Epi-fluorescence microscope Nikon Ti-Eclipse.

Fluorophore	excitation [nm]	emission [nm]	dichroic beam splitter
Hoechst 33342	370/36 Bright line HC	435-485	HC Triple beam splitter 395/495/610
Rhodamin-phalloidin	572/35 ET Band pass	608-683	ET dual band beam splitter GFP/mCherry
EGFP, Alexa-Fluor 488	470/40 ET Band pass	510-560	ET dual band beam splitter GFP/mCherry

Most experiments were performed on the epi-fluorescence microscope from Zeiss. Here, we also used the 20x air objective for imaging with normally 2x2 binning (0.23µ/pixel) for ki-67 and 3x3 (0.68 µm/pixel) binning for Yap/Taz imaging. For counting ki-67 and Yap/Taz positive cells, a threshold was set for all conditions to determine positive cells. Nuclei counting was then used to calculate the percentage of positive cells.

Table 35: Filter combinations of the epi-fluorescence microscope Zeiss Axio observer 7.

Fluorophore	Excitation [nm]	Emission [nm]	Dichroic beam splitter
Hoechst 33342	BP 359-371	397	BS 395
EGFP, Alexa-Fluor 488	BP 459-490	500-550	BS 495
Rhodamin-phalloidin	BP 540-580	593-668	BS 585
Cy5, Alexa Fluor 633	BP 625-655	665-715	BS 660

2.2.4.4 Confocal microscopy of fixed cells

Fluorescent confocal microscopy can be used to increase optical resolution by using a spatial pinhole. This pin-hole can block out-of-focus light and therefore increase signal-to-noise ratio, resulting in a higher contrast. Emission of fluorophore-labelled samples is performed by a laser beam with defined wavelength. In this study, the confocal microscope TCS sp5 from Leica was used to analyze F-actin modelling of the melanoma cell lines in 3D spatial organization. For this, the 63x oil objective (Tab. 23) was used and z-stacks was measured with 0.25 µm height. Hoechst 33342 and rhodamin-phalloidin were used to stain nuclei and F-actin, respectively. The installed plugin `temporal color-code` was used for illustrating the 3D F-actin organization based on a defined color code. Here, we used the color code – rainbowsmooth-2-3 (generated by Dr. Nina Schulze, ICCE, Essen). The first 29 frames of each z-stack were used (7.25 µm in total) for both cell lines, to measure the height of cells and membrane ruffles.

2.2.4.5 Statistical analyses

Statistical analysis was only performed if three or more individual experiments were performed. Then, the mean values and SEM (standard error of the mean) of each experiments were calculated and plotted in GraphPad Prism to use the statistical tools. For experiments with two different conditions (e.g. n.t siRNA vs siRac1), unpaired two-tailed t-test was performed. For comparing more than two conditions with one as a control, One-way Anova with Dunnett`s post-test was used (RNAi and drug treatment). (P-values are indicated by stars *: $P<0.05$; **: $P<0.01$; ***: $P<0.001$; ns: non-significant).

3. Results

3.1 Endogenous Rac1-P29S stimulates dynamic of the cell morphology in melanoma cells

Rac1 is primarily known as a master regulator of the actin cytoskeleton and cellular morphogenesis. However, it has also been linked to proliferation and survival pathways (Prudnikova et al., 2015; Villalonga and Ridley, 2006).

Individual mutations in the *rac1*-gene cause abnormal cell behavior. This is not only associated with various types of cancer, but also with other diseases such as neurodegenerative disorders (Marei and Malliri, 2017). Recent studies have identified the fast-cycling Rac1-P29S mutation as the third most common mutation in malignant melanoma (Davis et al., 2013; Li and Machesky, 2013). Overexpression of Rac1-P29S in melanoma cell lines resulted in enhanced tumor growth and survival rate, and it is suggested that this Rac1 mutation plays a potential role in drug resistance under standard therapeutic BRAF inhibitor treatment (Watson et al., 2014). However, the mechanisms by which Rac1-P29S mediates distinct cell responses remain poorly characterized.

In this work, we have studied two different melanoma cell lines with an activating BRAF mutation as model systems (Paschen et al., unpublished data). While Ma-Mel-86c cells express the Rac1-wild-type (Rac1-wt) variant, the UKE-Mel-55b cells express the fast-cycling Rac1-P29S mutant endogenously. The use of melanoma cell lines with different Rac1 variants enables us to better understand the role of Rac1-P29S in tumor-relevant cell processes.

We analyzed the genetic locus of Rac1 to confirm the existence of the fast-cycling Rac1-P29S mutation, using commercial Sanger-sequencing (Eurofins, GATC). Sequence alignment with a common DNA database (NCBI, AF498964) revealed in UKE-Mel-55b cells a single point mutation (nucleotide replacement C to T) which results in the exchange of proline to serine at the corresponding amino acid position 29 (Fig. 8B). Similarly, sequencing results of Ma-Mel-86c cells confirmed that these cells harbor the Rac1-wt form (Fig. 8D).

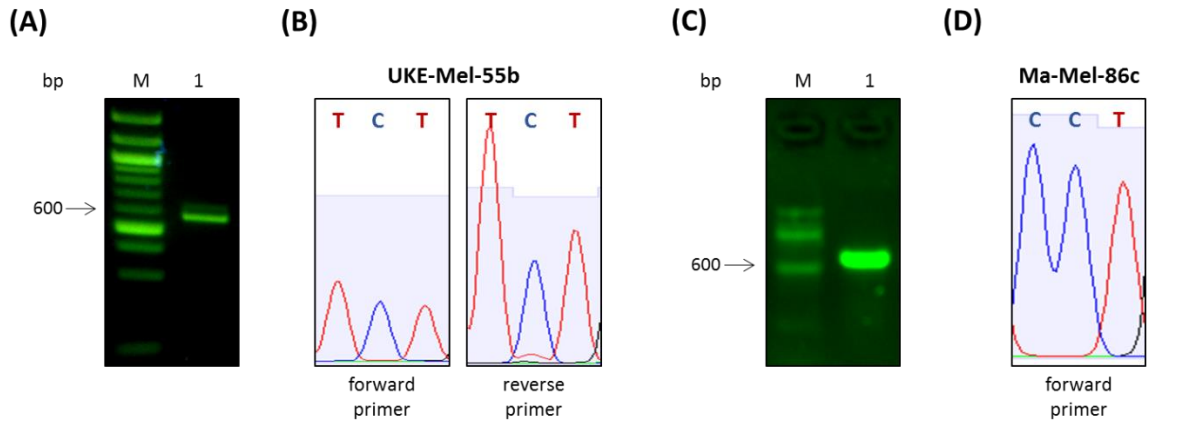

Figure 8: Validation of the endogenously expressed Rac1 variants in melanoma cell lines. (A) HDgreen stained agarose gel after cDNA synthesis for UKE-Mel-55b cell line. M: marker. Lane 1: cDNA sample. Expected band for Rac1 at 579 bp. **(B)** Sanger-sequencing results for the nucleotide triplet TCT (C → T transition at base c.85) encoding the amino acid serine at position 29 in Rac1 protein. **(C)** HDgreen stained agarose gel after cDNA synthesis for Ma-Mel-86c cell line. M: marker. Lane 1: cDNA sample. Expected band for Rac1 at 579 bp. **(D)** Sanger-sequencing results of the CCT triplet, which is encoding a proline at pos. 29.

3.1.2 Melanoma cells endogenously expressing the fast-cycling Rac1-P29S generate excessive membrane ruffles and lamellipodia

Rac1 has been well-established to regulate cellular morphogenesis via control of the actin cytoskeleton (Hall, 1998; Ridley et al., 1992). We hypothesize that the fast-cycling Rac1-P29S mutant might alter the actin phenotype and cellular dynamics of melanoma cells. Thus, we characterized the effects of Rac1-P29S on the actin cytoskeleton. In a first step, we compared the cell morphology of the two melanoma cell lines using rhodamine-phalloidin staining of filamentous actin (F-actin) in fixed cells and confocal microscopy. In Ma-Mel-86c cells, we found a diverse range of actin structures, including prominent bundled actin filaments reminiscent of contractile stress fibers (Fig. 9, orange arrows) and occasional formation of peripheral lamellipodia (Fig. 9, magenta arrows). In UKE-Mel-55b cells, that endogenously express the Rac1-P29S mutant, we found excessive formation of membrane ruffles (Fig. 9, green arrows) and lamellipodia regions suggesting strong stimulation of molecular mechanisms that control actin protrusions (Fig. 9, magenta arrows).

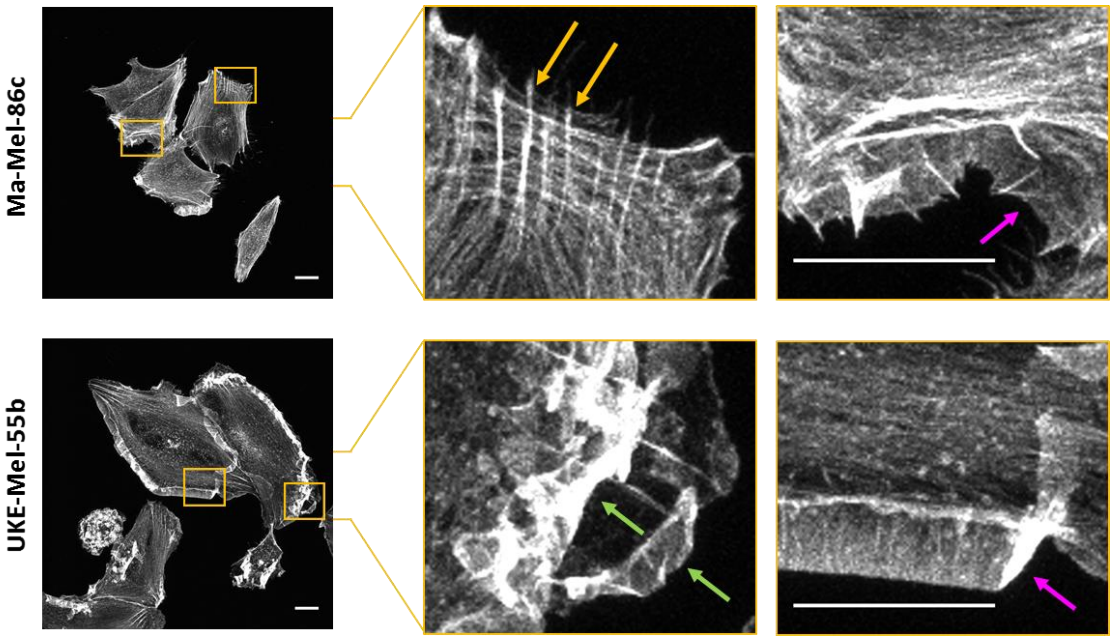

Figure 9: Melanoma cells endogenously expressing Rac1-P29S generate more lamellipodia and membrane ruffles as compared to melanoma cells with wild-type Rac1. Cells were plated on glass coverslips for 24 h and F-actin was visualized with rhodamin-phalloidin staining. Representative maximum projections of confocal z-stacks of Ma-Mel-86c (top panel, 46 cells of 1 experiment) and UKE-Mel-55b cells (bottom panel, 20 cells of one experiment). Enlargment (orange boxes) showing the F-actin organisation in stress fiber (orange arrows), membrane ruffles (green arrows) and lamellipodia formation (magenta arrows). Scale bar 20 µm.

We next investigated the three-dimensional F-actin organization within the cell using the Temporal color-code plugin from Fiji and the 3D LUT was provided by Dr. Nina Schulze (ICCE, Essen) (Fig. 10A). Based on the color code, we were able to distinguish between ventral (magenta, dark blue) and dorsal (yellow, red) F-actin structures. In melanoma cells with endogenous Rac1-P29S, we observed prominent membrane ruffles located on the dorsal surface in peripheral regions (Fig. 10A, enlarged). Rac1-wt cells, in contrast, did not show the same extent of membrane ruffling. Instead, these cells were characterized by an increased formation of stress fibers and small filamentous extensions. X,Z-profiles of reconstituted cell volumes allowed us to estimate the height of peripheral membrane ruffles that were generated in UKE-Mel-55b cells with the highly active Rac1-29S mutant(Fig. 10B). With up to several micrometer height ruffles were almost as high as the entire cell body (Fig. 10B, yellow arrows). In addition to this highly distinct F-actin phenotype, we also observed that cell bodies of Rac1-P29S cells were in general higher (z-height) as compared to cells with endogenous Rac1-wt.

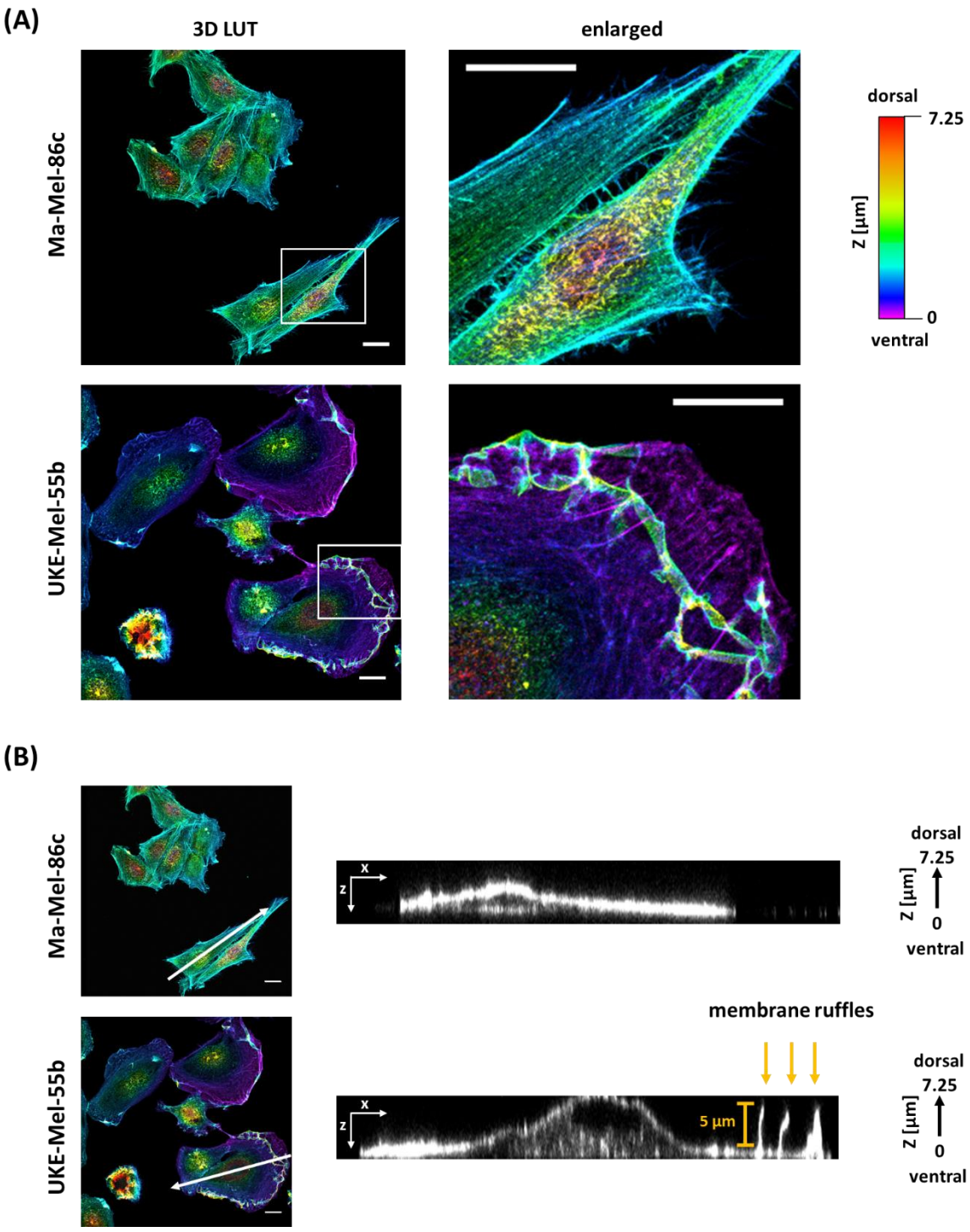

Figure 10: 3D-cell morphology of melanoma cells endogenously expressing Rac1-P29S. Representative confocal images of melanoma cells on glass coverslips after fixation and staining with rhodamin-phalloidin (F-actin). **(A)** 3D organization of actin cytoskeleton in Ma-Me-86c cells (top panel) and UKE-Mel-55b (bottom panel). Depicted is the maximum projection of a confocal z-stack for F-actin. Z-coordinates are indicated by the color bar. Scale bar 20 µm. **(B)** Confocal stacks were used to generate z-sections (right panel) along the indicated white arrows in the maximum projections (left panel). Scale bar 20 µm. Yellow arrows: Membrane ruffles.

Overall, these observed morphological differences between the two cell lines suggest that the fast-cycling Rac1-P29S mutant induces a highly altered phenotype with enhanced membrane ruffling in UKE-Mel-55b cells. To confirm this role in cell morphogenesis, we next analyzed the actin organization after Rac1 depletion.

3.1.3 Depletion of endogenous Rac1-P29S in melanoma cells decreases membrane ruffling, promotes increased stress fiber and modulate cell adhesion formation

Although the general role of Rac1 in actin organization has been studied extensively, the effect of the fast-cycling Rac1-P29S mutation on melanoma cell behavior is still elusive. To thoroughly study how Rac1 regulates the architecture of the F-actin network in melanoma cells, we established a Rac1 knock-down protocol using RNA interference which lead to significantly reduced Rac1 protein levels of approximately 20 % (supplementary data). After Rac1 depletion, F-actin organization, cell area and roundness were analyzed to characterize the cell morphology (Fig. 11B, C). For the Rac1-wt melanoma cell line (Ma-Mel-86c), we only observed slight changes in the actin cytoskeleton after Rac1 depletion (Fig. 11D).

More dramatic effects were observed in the Rac1-P29S expressing UKE-Mel-55b cell line. Under control conditions (n.t siRNA) the UKE-Mel-55b cells showed the typical phenotype, characterized by a round cell shape and a higher amount of membrane ruffles and lamellipodia regions. Upon reduction of Rac1 level (siRac1), these cells did not only show a remodeling of their F-actin network, but also exhibited an elongated cell shape. In addition, we observed an increased formation of actin stress fibers and less membrane ruffles (Fig. 11D).

In order to quantify the effect on the global cell morphology, the shape descriptor parameters, cell area and roundness were measured using Fiji (Fig. 11B, C). Because of the high degree of membrane ruffling in UKE-Mel-55b cells, automatic membrane segmentation using Cell profiler pipelines failed. Therefore, cell boundaries were segmented manually using the free hand selection tool in Fiji.

Depletion of endogenous Rac1-wt in Ma-Mel-86c cells did not significantly alter the cell area (n.t siRNA 1945 μm^2 ± 138.4 SEM; siRac1 1638 μm^2 ± 83.09 SEM, Fig. 11B). Similarly,

the effect of Rac1 depletion on cell roundness was not statistically significant (n.t siRNA 0.53 ± 0.06 SEM; siRac1 0.4 ± 0.05SEM; Fig. 11C).

In contrast to the Rac1-wt cell line, depletion of Rac1-P29S in UKE-Mel-55b cells significantly reduced the cell area (n.t siRNA 7255 µm² ± 1012 SEM; siRac1 3890 µm² ± 437.2 SEM, Fig. 11B) and roundness (n.t siRNA 0.6 µm ± 0.03 SEM; siRac1 0.4 µm ± 0.04 SEM, Fig. 11C).

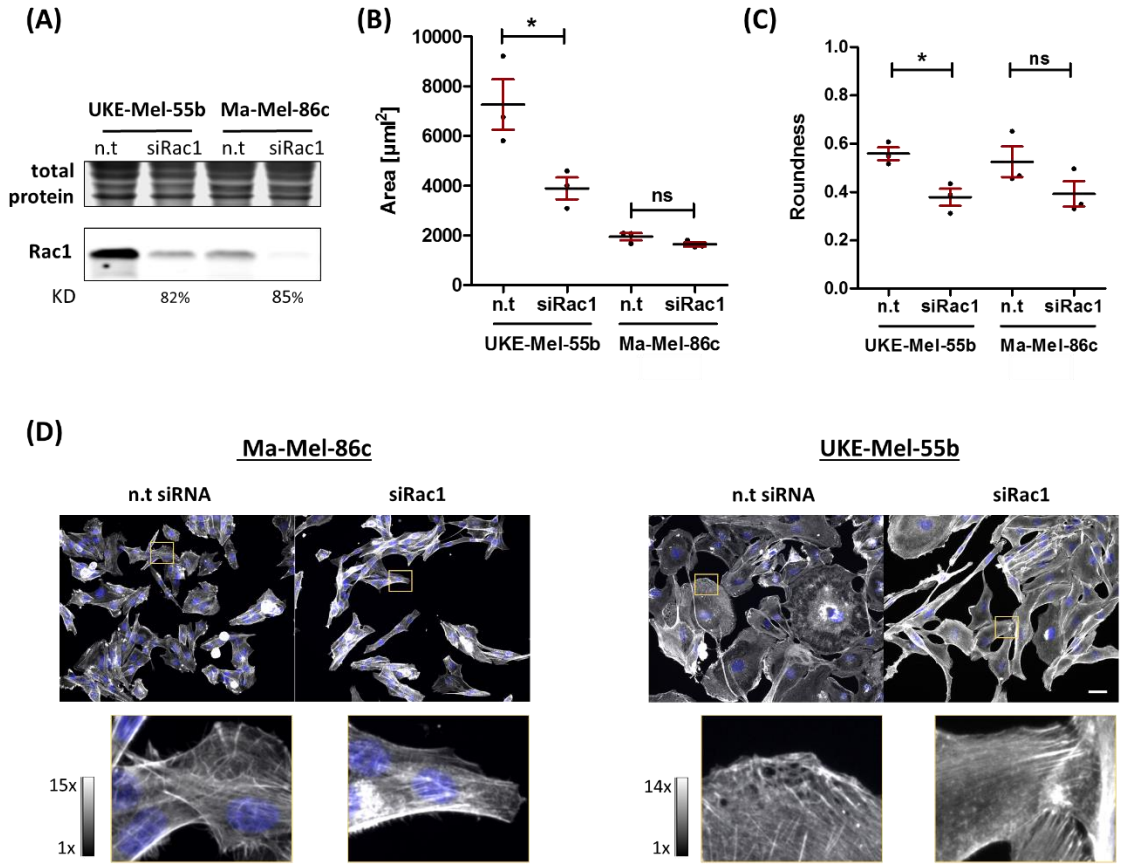

Figure 11: Rac1 depletion caused morphological changes and stress fiber formation in melanoma cells. Cells were treated with n.t siRNA and siRac1 for 72 h. **(A)** Representative western blot with total protein staining and Rac1 signal for both cell lines. **(B)** Cell area measurements [µm²] for control cells (n.t siRNA) and Rac1 depleted (siRac1) melanoma cells. **(C)** Graph shown shape descriptor roundness for both melanoma cell lines after Rac1-knock down. **(D)** Representative F-actin (rhodamin-phalloidin, grey) and nuclei (Hoechst 33342, blue) microscope images for Ma-Mel-86c cells (left) and the Rac1-P29S expressing UKE-Mel-55b cell line (right). Scale bar 20 µm. All graphs showed mean values of three independent experiments. Statistical analysis was performed with a two-tailed t-test unpaired P<0.05:*, ns=non-significant. Error bars indicate SEM.

In addition to the control of actin organization, Rac1 activity is also required for the dynamic turnover of focal adhesions. In particular, Rac1 is has been associated with the formation of nascent focal complexes, which are found in the lamellipodia in the leading edge of cells (Huveneers and Danen, 2009; Parsons et al., 2010).

We therefore analyzed the effect of Rac1 depletion on cell adhesion formation in melanoma cells. As the morphological effects of Rac1 depletion were profound in UKE-Mel-55b cells with endogenous Rac1 P29S, we focused on these cells.

Rac1-depleted cells were stained with rhodamin-phalloidin and anti-FAK (focal adhesion kinase) antibody to visualize F-actin and focal adhesions, respectively, followed by fluorescence imaging. (Fig. 12). Similar to prior experiments in UKE-Mel-55b cells, Rac1 depletion resulted in enhanced stress fiber formation (Fig. 11). In addition, we found that cell adhesions upon Rac1 depletion were substantially enlarged and less variable in size as compared to the control group (n.t siRNA) (Fig. 12). While in control cells, both small adhesions (orange arrows) and larger adhesions (green arrows) were enriched, a large number of cell-substrate adhesions was observed after Rac1-depletion.

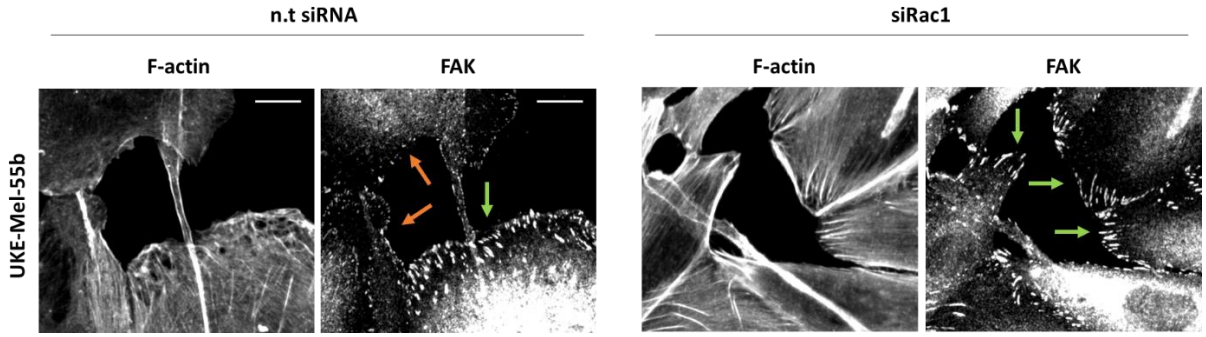

Figure 12: Rac1 depletion in UKE-Mel-55b cells causes enhanced FAK requirement to cell adhesions. Images depict F-actin (rhodamin-phalloidin) and focal adhesion kinase (anti-FAK antibody) after Rac1-P29S depletion. Cells with predominantly small focal adhesions marked with an orange arrow. Green arrows indicate cells with strong formation of large focal adhesions. Scale bar 20 µm.

As the focal adhesion kinase (FAK) is one of the main regulators of focal adhesion dynamics (Tapial Martinez et al., 2020), together with a master student under my supervision (Mrug, 2020), we further measured the activation state of this protein with western blot analysis after Rac1 depletion (Fig. 13A) (. This allowed us both, to estimate total FAK protein levels (FAK) as well as the amount of the active phosphorylated form (pFAK). FAK activity level was measured in both, UKE-Mel-55b and Ma-Mel-86c cells to better assess the differential effect of Rac1 depletion in cells with Rac1 activity background. Overall, global FAK protein levels were not affected by Rac1 depletion in either cell line (Fig 13B). In contrast, FAK phosphorylation was significantly altered upon Rac1 depletion in both cell lines (Fig. 13C). Interestingly, the effects were reciprocal.

Whereas, depletion of endogenous Rac1-P29S in UKE-Mel-55b cells significantly increase FAK phosphorylation (pFAK) as compared to non-targeted siRNA (n.t siRNA 100 %, siRac1 122.8 ± 9.3 % SEM), pFAK level was significantly reduced upon depletion of endogenous Rac1-wt in Ma-Mel-86c cells (n.t siRNA 100 %; siRac1 79.4 ± 6.4 % SEM). As a result, the pFAK/FAK ratio (Fig. 13D), which is a measure for FAK signaling activity, was significantly increased in UKE-Mel-55b after Rac1 knock-down (n.t siRNA 100 %; siRac1 123.6 ± 6.7 % SEM), whereas depletion of Rac1-wt in Ma-Mel-886c cells lead to a slight but significant decrease of this marker signal as compared to n.t cells (n.t siRNA100 %; siRac1 84.1 ± 2.6 % SEM).

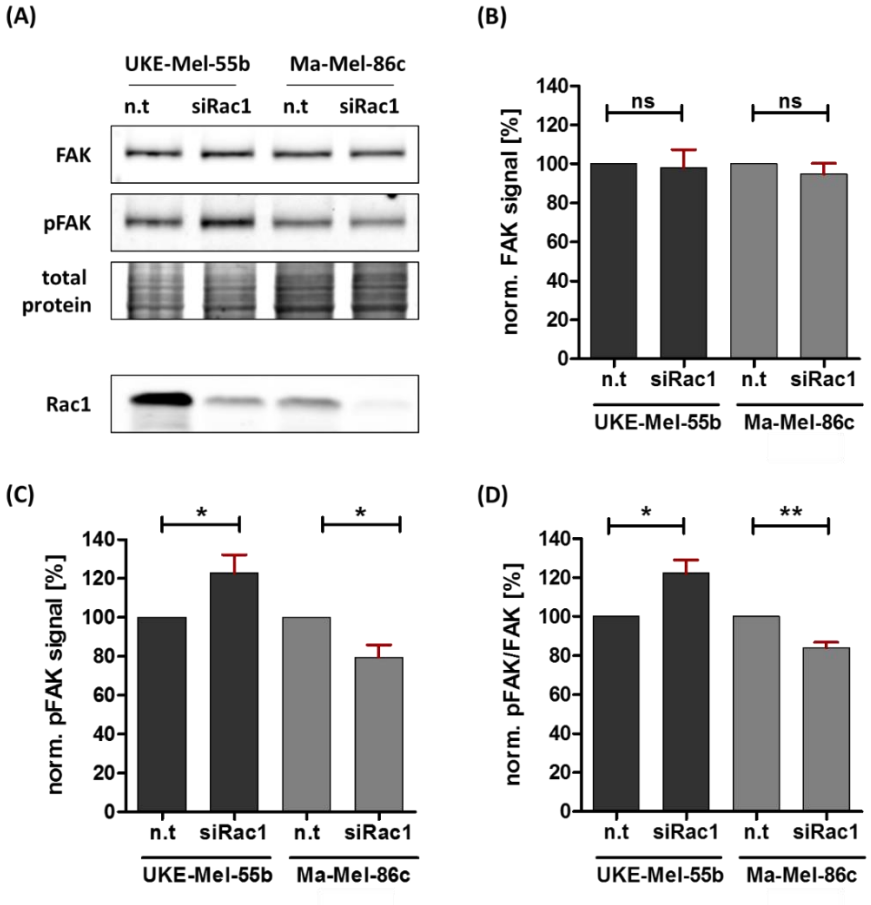

Figure 13: Depletion of endogenous Rac1-P29S in UKE-Mel-55b melanoma cells caused increased FAK activity whereas depletion of endogenous Rac1-wt in Ma-Mel-86c cells reduces FAK activity. Cells were plated on glass coverslips and treated with n.t siRNA and siRac1 for 72h. **(A)** Representative western blot for Rac1 depletion and FAK signaling. Protein levels for FAK and pFAK were normalized with a section of the total protein signal (loading control) and plotted relative to the control (n.t siRNA 100%). Graphs show signals for FAK, pFAK and signaling ratio pFAK/FAK. N=10 independent experiments for UKE-Mel-55b; N=6 experiments for Ma-Mels-86c. Statistical analysis was performed by column statistics with a one-sample t-test against 100. P<0.05:*, p<0.001:**, ns=non-significant. Error bars indicate SEM.

3.1.4 Expression of siRNA resistant Rac1-P29S in Rac1-depleted UKE-Mel-55b melanoma cells promotes a recovery of ruffling and lamellipodia

To confirm that Rac1-P29S is indeed responsible for the observed morphology in the melanoma cell line UKE-Mel-55b, we performed rescue experiments in Rac1 depleted cells. For this purpose, we generated siRNA-resistant Rac1 plasmids by introducing silent point mutations into the EGFP-Rac1-wt and EGFP-Rac1-P29S constructs using site-directed PCR-mutagenesis (c.372 bp: exchange C to T; g.381 bp: exchange G to A). The siRNA-resistant plasmids were analyzed via agarose gel electrophoresis and sanger-sequencing (Fig. 14A). As expected, we obtained bands at approx. 6000 bp on the agarose gels after PCR for both plasmids and the sanger-sequencing results confirmed the introduction of the two silent point mutations at the indicated positions in Fig. 14A (red arrows). 24 h after treatment with the Rac1 siRNA was started, cells were transfected with siRNA-resistant plasmids encoding for EGFP-Rac1-wt and EGFP-Rac1-P29S as well as an EGFP-control vector. Western blot analysis 72 h after siRNA treatment confirmed successful knock-down of endogenous Rac1 and sufficient expression of EGFP-constructs (Fig. 14B). Endogenous Rac1 was detected at 21 kDa (lower green bands), the empty EGFP-control vector at 27 kDa (red bands) and the EGFP-Rac1 plasmids at 50 kDa (upper bands).

Next, wide field microscopy was performed to assess the effect of Rac1 depletion and expression of siRNA resistant Rac1 constructs on F-actin organization (Fig. 14C). The control group (n.t siRNA + EGFP-control) exhibited the typical membrane ruffling phenotype and lamellipodia formation as previously shown (Fig. 14C). This protrusive actin phenotype was lost after Rac1 depletion (Rac1 siRNA + EGFP-control; Fig. 14C). Instead, cells were found to generate moderate levels of stress fibers (Fig. 14C, red arrow) similar to UKE-Mel-55b cells shown in the previous chapter that were depleted of endogenous Rac1 (Fig. 11). Expression of siRNA-resistant EGFP-Rac1-wt caused only little change in this phenotype and only leads to occasional formation of membrane ruffles In contrast, expression of EGFP-Rac1-P29S resulted in pronounced membrane ruffling and a marked loss of stress fibers (Fig. 14C, D green arrows).

In addition to wide-field fluorescence imaging of the global cell morphology, we also used confocal microscopy to investigate adhesion formation together with actin organization upon depletion of Rac1-P29S and re-introduction of siRNA-resistant Rac1 variants (Fig. 14D). To do so, we used immunofluorescence to visualize the adhesion protein Paxillin as

a marker for adhesion sites. While in control cells distinct adhesion structures were visible (n.t siRNA), merely sporadic formation of adhesions was observed after Rac1 depletion (Fig. 14D). Similar to the weak recovery of membrane ruffles, transfection of EGFP-Rac1-wt resulted in the formation of small adhesions, while EGFP-Rac1-P29S stimulated strong adhesion formation (Fig. 14D orange arrows, enlargements).

Thus, data shown in this part demonstrate that the fast-cycling mutation Rac1-P29S has an essential role in regulating the cell morphology in UKE-Mel-55b melanoma cells, inducing membrane ruffling, lamellipodia and adhesion formation.

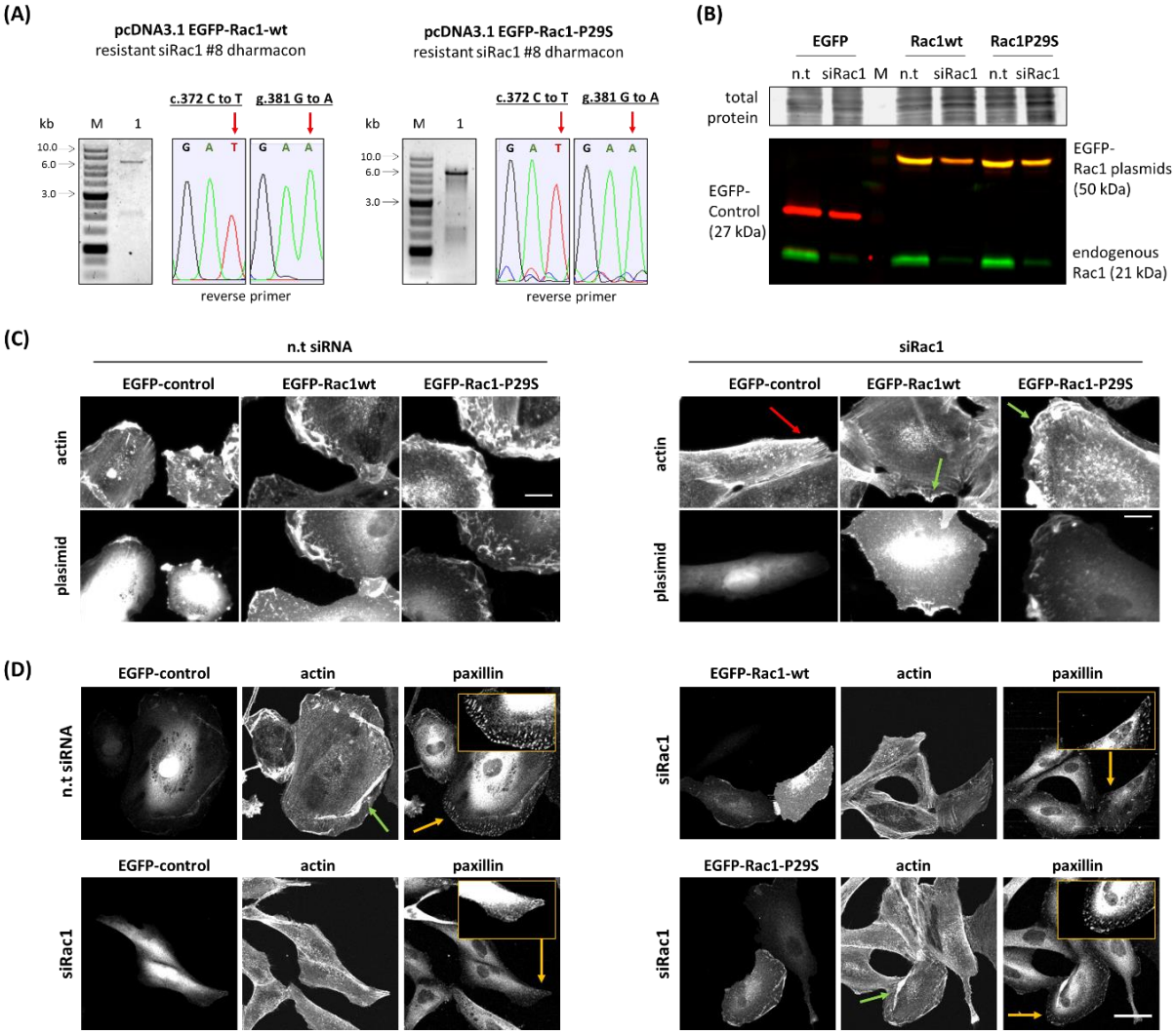

Figure 14: Rac1-P29S is required for the formation of membrane ruffles and focal adhesion formation in melanoma cells. To confirm that Rac1-P29S is important for cell morphology, siRNA resistant Rac1-plasmids were designed by introducing two silent point mutations. One was in the amino acid Asp124 at position c.372 with a C to T transition and the second was in Glu127 at g.381 from G to A. **(A)** HDgreen stained agarose gel and sanger-sequencing results for the pcDNA3.1 EGFP-Rac1-wt construct are shown. **(B)** Similar is in (A) for the pcDNA3.1 EGFP-Rac1-P29S plasmid. **(C)** Representative western blot after 72 h treatment with n.t siRNA or siRac1 (dharmacon #8). Cells were transfected with EGFP-control plasmid (left), pcDNA3.1-EGFP-Rac1wt (middle) and pcDNA3.1-EGFP-Rac1P29S (right) 24 h after siRNA treatment. **(D)** Wide field images for EGFP-control and EGFP-Rac1-plasmids 72 h after Rac1-depletion. F-actin was stained with rhodamin-phalloidin. Scale bar 20 µm. Transfected Rac1-P29S induces membrane ruffling in Rac1 siRNA treated melanoma cells. **(E)** Fluorescent confocal images after Rac1 depletion and transfection with EGFP-control, EGFP-Rac1-wt and EGFP-Rac1-P29S. Z-stacks used for max projection generation. F-actin stained with rhodamin-phalloidin and an antibody for paxillin was used. Membrane ruffles indicated with green arrows and Paxillin localized on focal adhesions with orange arrows. Scale bar 50 µm.

3.2 Rac1-P29S promotes cell adhesion, cell spreading and migration in melanoma cells

The integrin protein family mediates the signal transmission between the various extracellular matrix (ECM) components and the cellular response (Hynes, 2002). Depending on the properties of the cell-surrounding matrix, different integrins are involved and activate signaling pathways that control cellular processes such as cell migration (Rho-GTPases) or proliferation (MAKP) (Huveneers and Danen, 2009; Lopez-Colome et al., 2017; Schaks et al., 2019). Based on results presented in the previous chapter, Rac1-P29S alter cell-matrix adhesion formation. As integrin-dependent adhesion signaling is critical for early cell adhesion to the extracellular matrix and as well for the spreading of the cell body at later time points, we were interested how Rac1-P29S might affect these dynamic cell behaviors in melanoma.

3.2.1 Rac1-P29S enhances early cell adhesion behavior in UKE-Mel-55b cells

To investigate how Rac1-P29S controls cell adhesion in UKE-Mel-55b cells, we performed cell adhesion assays for which we used glass as uncoated control condition, collagen I for integrin-mediated cell adhesion and poly-L-lysine (PLL) as additional control to induce adhesion via electrostatic interactions.

To assess how the Rac1-wt background affects this behavior, we used Ma-Mel-86c cells as control. First, cells were fixed 15, 30, 60 and 90 minutes after cell seeding, followed by rhodamin-phalloidin and Hoechst 33342 staining for F-Actin and nuclei, respectively. Next, we collected epifluorescence images at randomly chosen positions and counted the number of adherent cells for each time point. Individual mean values and SEM see in Tab. 36. Cell adhesion on PLL was strong for both cell lines already from the beginning (15 min) and stayed constant (90 min) (Fig. 15B, D). These results suggest that the maximum number of adherent cells is already reached before the first sampling point (15 min). Thus, adhesion via electrostatic interactions is faster when compared to the other ECMs. In contrast to PLL, on glass and collagen I we observed substantial difference in adhesion dynamics between Rac1-wt expressing Ma-Mel-86c cells and Rac1-P29S expressing UKE-Mel-55b cells. With Rac1-wt cells, we obtained a gradual increase of adhesion starting from very low levels at 15 min until 60 min and a steady-state after 90 min (Fig. 15B). Of note, we did not observe any significant differences between the

uncoated glass and collagen I samples. In contrast to Rac1-wt cells, adhesion of UKE-Mel-55b cells on glass and collagen I was strong already at 15 min after seeding (Fig. 15D). Furthermore, the number of adherent UKE-Mel-55b cells on collagen I converged with cell numbers on PLL already at 60 min, whereas cell numbers on glass only reached saturation after 90 min (Fig. 15D). This behavior is in line with the long-established mechanism that efficient cell adhesion is integrin dependent. Results presented in this part suggest that endogenous expression of Rac1-P29S stimulates this integrin-mediated adhesion signaling above the level observed measured with endogenous Rac1-wt.

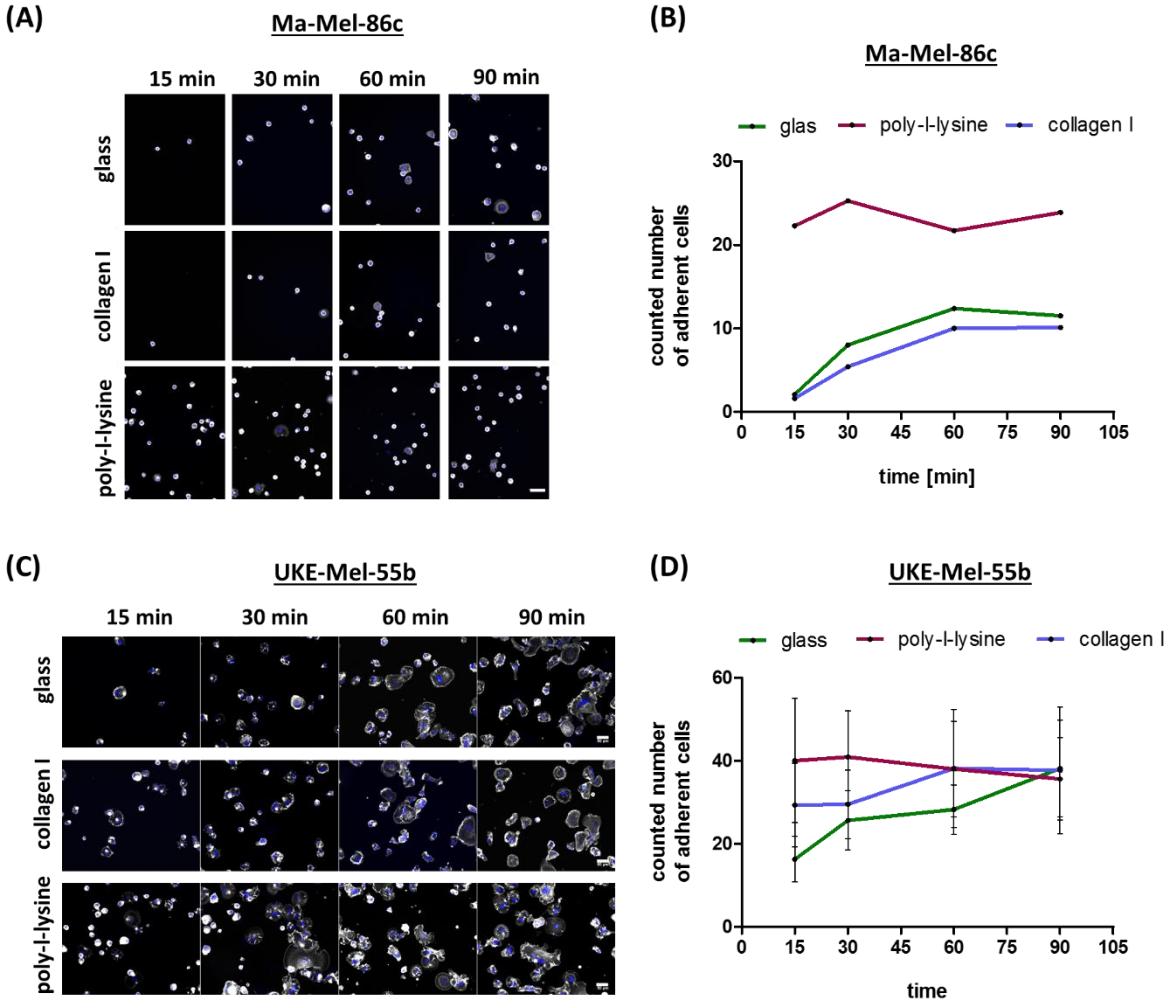

Figure 15: Melanoma cells with endogenous expression of Rac1-P29S showed increased cell adhesion. Both melanoma cell lines were seeded on coated (collagen I/poly-L-lysine) or uncoated glass coverslips. Cells were fixed at different time points after seeding (15, 30, 60, 90 min). Cells were stained with rhodamin-phalloidin (F-actin, grey) and Hoechst 33342 (nuclei, blue). **(A)** Representative microscope images (Nikon-Ti Eclipse) of different time points and ECMs for the Rac1-wt cell line (Ma-Mel-86c). Scale bar 50 µm. **(B)** Shown mean values of number of adherent cells for each ECM and time point from one experiment with 5-10 random imaging positions/condition. **(C)** Representative images (Zeiss Axio observer 7) for different time points and ECMs. Scale bar 50 µm. **(B)** Mean value of adherent cells at each time point from n=2 independent experiments with 5-10 random imaging positions /condition.

Table 36: Mean values of adhered cell numbers on different ECMs at the respectively time points. Ma-Mel-86c cells: one experiment. Mean values were calculated by the random imaging positions for each time point. UKE-Mel-55b cells: Mean values from two individual experiments based on the random imaging. SEM indicate standard-error-of-the-mean of the two experiments.

Time	Ma-Mel-86c			UKE-Mel-55b		
	glass	collagen I	PLL	glass	collagen I	PLL
15 min	2.1 cells	1.6 cells	22.3 cells	16.3 cells ± 5.5 SEM	29.3 cells ± 10.1 SEM	40.1 cells ± 15 SEM
30 min	8 cells	5.4 cells	25.3 cells	25.7 cells ± 7.2 SEM	29.6 cells ± 8.3 SEM	40.9 cells ± 11.1 SEM
60 min	12.4 cells	10 cells	21.7 cells	28.3 cells ± 6 SEM	38.2 cells ± 14.3 SEM	38 cells ± 11.6 SEM
90 min	11.5 cells	10.1 cells	23.9 cells	38.2 cells ± 11.7 SEM	37.7 cells ± 15.3 SEM	35.6 cells ± 9.9 SEM

To further understand the relevance of Rac1-P29S for the enhanced adhesion capacity of UKE-Mel-55b cells as compared to Rac1-wt cells, we performed the above-described adhesion assays with Rac1 depleted cells.

In line with the previous findings (Fig. 15), we observed a gradual increase in number of adherent cells during the experiment for each control group (n.t siRNA) as well as upon Rac1 depletion in both cell lines (siRac1) (Fig. 16B). Furthermore, we confirmed the substantially lower adhesion capacity of Rac1-wt cells (Ma-Mel-86c) as compared to Rac1-P29S expressing UKE-Mel-55b cells throughout.

Depletion of Rac1-wt in Ma-Mel-86c cells did not affect cell adhesion markedly. However, depletion of Rac1-P29S in the UKE-Mel-55b cell line caused dramatic reduction of adherent cells at all measured time-points. Single results for adherent cell numbers under the different conditions were collected in Tab. 37.

Taken together our findings suggest that Rac1-P29S is an important regulator for cell adhesion but observed cell adhesion in Rac1 depleted cells reveal that also other pathways are involved in the formation of early adhesions. Nevertheless, endogenous expression of Rac1-P29S significantly enhances cell adhesion capacity in melanoma cells compared to Rac1-wt cells.

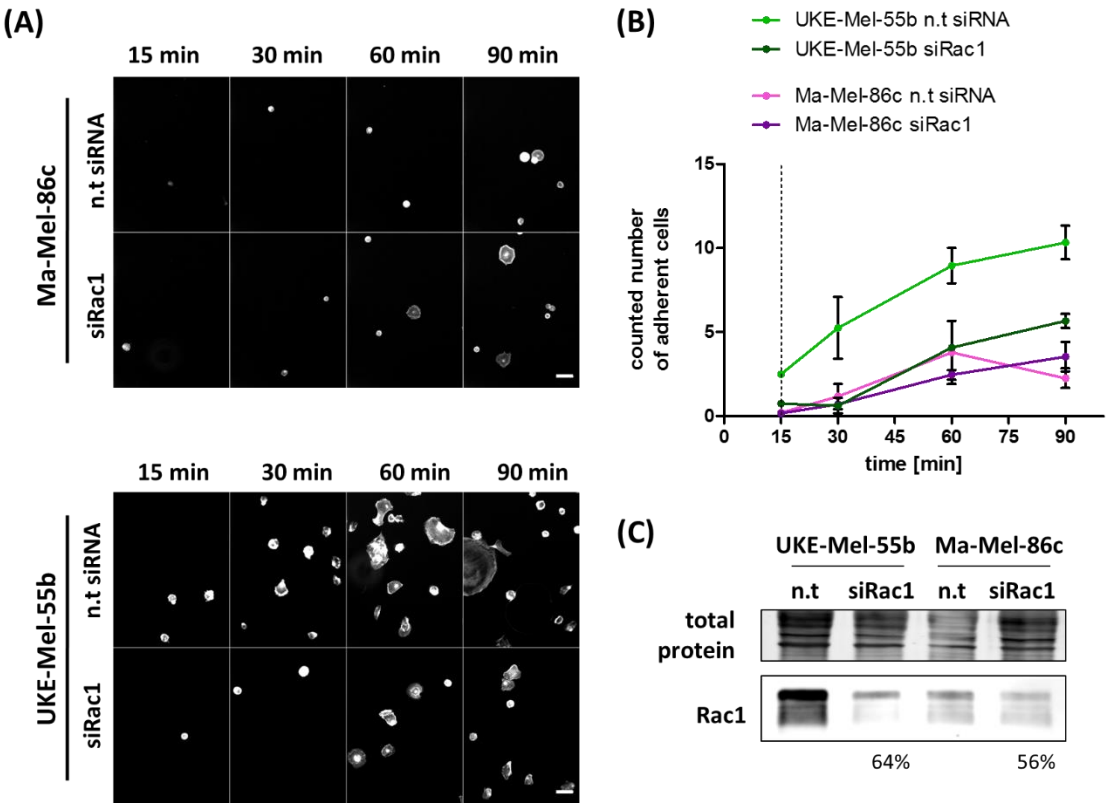

Figure 16: Figure 16: Depletion of Rac1-P29S causes reduced cell adhesion, while depletion of Rac1-wt does not affect basal adhesion behavior. Melanoma cells treated with n.t siRNA and siRac1 for 72 h were re-plated on uncoated glass coverslips, fixed at different time points (15, 30, 60 and 90 min after re-plating) and stained with rhodamine-phalloidin for F-actin. **(A)** Representative wide field microscope images for both melanoma cell lines at the indicated time points. Scale bar 50 µm. **(B)** Graph shows the mean number or adherent cells at each time point from n=2 independent experiments with 12 each random imaging positions per condition. Only Rac1 depletion in UKE-Mel-55b and 15 min after re-plating was calculated by one experiment. See Tab. 37 for calculated values and SEMs. **(C)** Showing representative western blot for Rac1 depletion.

Table 37: Calculated mean values of adherent cell numbers for both melanoma cell lines after Rac1 depletion. Rac1 depletion in UKE-Mel-55b cells and fixation after 15 min n=1 experiment. N=2 experiments for UKE-Mel-55b cells after 30, 60, 90 min and for all time point of the Rac1-wt cell line (Ma-Mel-86c).

time	UKE-Mel-55b		Ma-Mel-86c	
	n.t siRNA	siRac1	n.t siRNA	siRac1
15 min	2.5 cells	0.7 cells	0.2 cells ± 0.1 SEM	0.2 cells ± 0.1 SEM
30 min	5.3 cells ± 1.8 SEM	0.6 cells ± 0.5 SEM	1.2 cells ± 0.8 SEM	0.7 cells ± 0.2 SEM
60 min	8.96 cells ± 1 SEM	4.1 cells ± 0.1 SEM	3.8 cells ± 1.9 SEM	2.5 cells ± 0.3 SEM
90 min	10.3 cells ± 1 SEM	5.7 cells ± 0.4 SEM	2.3 cells ± 0.6 SEM	3.5 cells ± 0.9 SEM

3.2.2 Integrin-signaling and Rac1-P29S activity are relevant for cell spreading in UKE-Mel-55b melanoma cells

In addition to the role of Rac1-P29S mutant in dynamics of melanoma cell adhesion behavior, we were also interested in studying its potential effect on cell spreading. For this purpose, we plated both, Rac1-wt and Rac1-P29S expressing, melanoma cell lines on glass, collagen I and poly-L-lysine and allowed them to adhere and spread for 24 h, followed by wide field fluorescence microscopy to visualize F-actin and nuclei (Fig. 17A, C). Based on our imaging data, UKE-Mel-55b cells formed membrane ruffles on both, collagen I coated and uncoated glass coverslips (Fig. 17C), whereas these dynamic structures were not present in Ma-Mel-86c cells with Rac1-wt (Fig. 17A). In addition, we found that the Rac1-P29S melanoma cells formed mixed populations of larger and smaller cells under both conditions. Detailed analysis of the cell area using the free hand selection tool from Fiji revealed that spreading cell area of cells plated on poly-L-lysine coated coverslips was clearly reduced in both cell lines as compared to glass surface or collagen I. (Ma-Mel-86c: box plot with 95% CI for glass: 1099 μm^2 ± 889.3-1308 CI; collagen I: 1226 μm^2 ± 1039-1413 CI; PLL: 315 μm^2 ± 249.1-380.9 CI, Fig. 17B). (UKE-Mel-55b: box plot with 95% CI for glass: 8123 μm^2 ± 6609-9636 CI; collagen I: 7608 μm^2 ± 6217-8998 CI; PLL: 3362 μm^2 ± 2517-4206 CI, Fig. 17D). Thus, our findings revealed that the UKE-Mel-55b cell population with excessively large size, substantially decreased on PLL further confirming that excessive spreading of Rac1-P29S expressing melanoma cells is linked to integrin signaling.

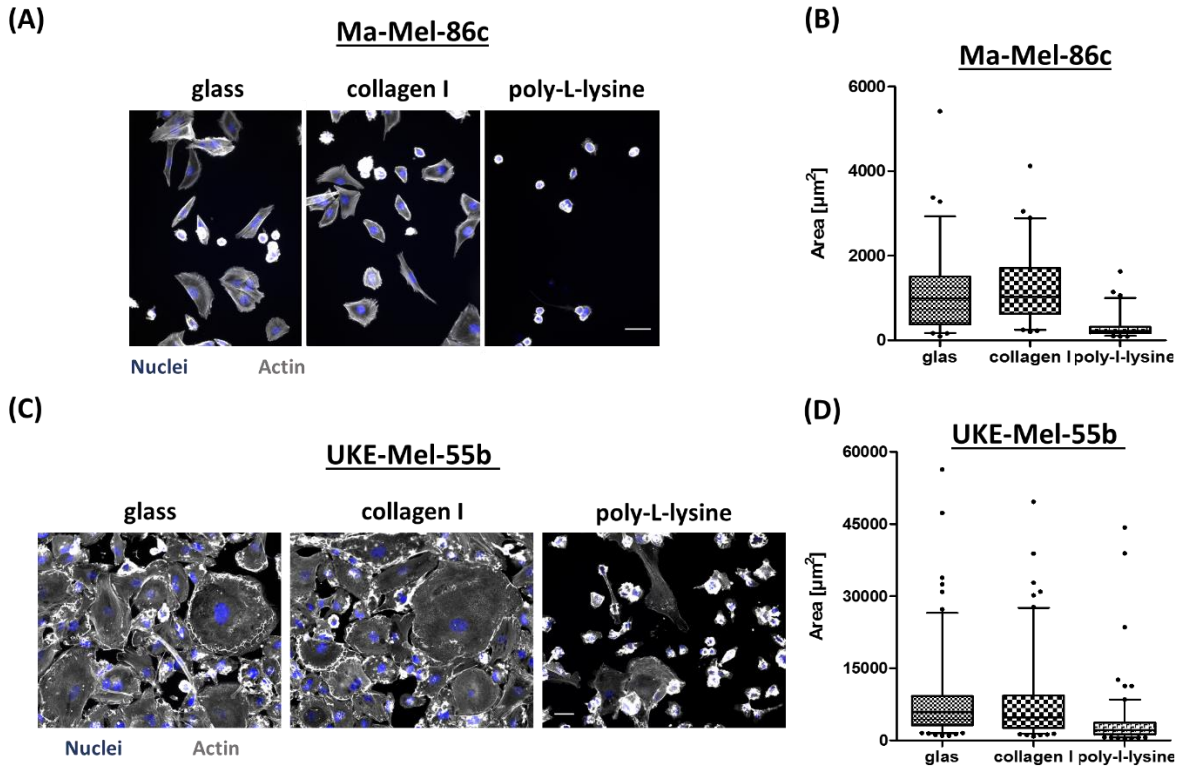

Figure 17: Integrin-mediated signaling is necessary for cell spreading in melanoma cell lines. Cells were seeded on coated (collagen I/poly-L-lysine) or uncoated glass coverslips and fixed after 24 h. **(A)** Representative wide field images (Nikon-Ti) for Rac1-wt cells (Ma-Mel-86c) after 24 h with nuclei (blue, Hoechst 33342) and F-actin (grey, rhodamin-phalloidin) staining. Scale bar 50 µm. **(B)** Graph for measured cell area [µm²] of Ma-Mel-86c cells on different ECMs. N=1 experiment with 70 cells. Error bars indicate 95% confidence interval. **(C)** Representative wide field images (Zeiss) for Rac1-P29S cells (UKE-Mel-55b) after 24 h on different ECMs with nuclei (blue, Hoechst 33342) and F-actin (grey, rhodamin-phalloidin) staining. Scale bar 50 µm. **(D)** Graphs depict cell area [µm²] of UKE-Mel-55b cells on different substrates. N=132-150 cells from two independent experiments. Error bars indicate 95% confidence interval.

Next, we used RNAi to deplete Rac1-P29S in UKE-Mel-55b cells and measured cell spreading 24 h after re-platting on glass, collagen-I and PLL-coated coverslips. In agreement with the findings shown in Fig. 11, 17, Rac1 depletion resulted in F-actin remodeling, i.e. membrane ruffles to stress fiber formation, and in an elongated cell shape on all three substrates (Fig. 18A, B). Furthermore, Rac1 depletion reduced cell spreading on all three substrates as indicated by measured cell area (Fig. 18C, Tab. 38).

In summary, our results reveal that Rach1-P29S strongly stimulates integrin dependent cell adhesion and cell spreading in UKE-Mel-55b melanoma cells.

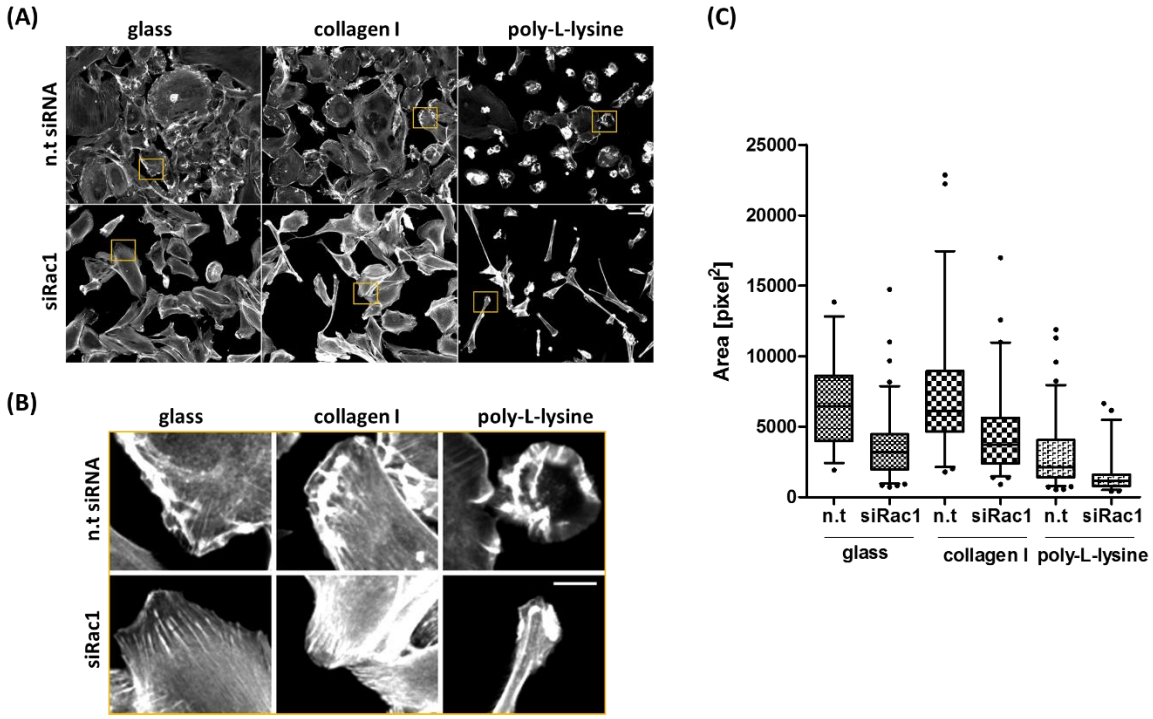

Figure 18: Rac1-P29S stimulates integrin-mediated signaling during cell spreading behavior of UKE- Mel-55b cells. UKE-Mel-55b cells were seeded on coated (collagen I/poly-L-lysine) or uncoated glass coverslips 72 h after Rac1 depletion and incubated for another 24 h. Imaging was performed on a Zeiss Axio observer 7 with 20x air objective. **(A)** Representative F-actin (grey, rhodamin-phalloidin) images . Scale bar 50 µm. **(B)** Enlargements of selected regions in (A), indicated by orange boxes. Scale bar 20 µm. **(C)** Graph with measured cell area 24 h after cell seeding on different ECMs and error bars indicate 95% confidence interval. N=1 experiment with 34-90 cells/condition.

Table 38: Mean values of cell area with 95% confidence interval (CI). Detailed mean values from figure 18B for Rac1 depleted UKE-Mel-55b on different ECMs.

ECM	UKE-Mel-55b	
	n.t siRNA	siRac1
glass	6613 µm² ± 5529-7697 CI	3591 µm² ± 3114-4068 CI
collagen I	7400 µm² ± 6138-8662 CI	4450 µm² ± 3733-5168 CI
poly-L-lysine	3060 µm² ± 2547-3573 CI	1523 µm² ± 1153-1892 CI

3.2.3 Cell migration of Rac1-P29S melanoma cells is Rac1-dependent

As we have already shown that Rac1-P29S is required for cell adhesion, we also want to study the role of Rac1-P29S in cell migration on different ECMs. Depletion of Rac1-P29S clearly reduced the average migration velocity on glass and collagen I surfaces (box plot in µm/min with 95% CI for glass n.t siRNA: 0.38 ± 0.33-0.41 CI; glass siRac1: 0.27 ± 0.23-0.32 CI; collagen I n.t siRNA: 0.38 ± 0.33-0.44 CI; collagen I siRac1: 0.29 ± 0.23-0.36 CI) (Fig. 19C). In contrast, Rac1-P29S knock-down increased the migration velocity on poly-L-lysine substrate (PLL n.t siRNA: 0.35 ± 0.3-0.4CI; PLL siRac1: 0.42 ± 0.35-0.5 CI) and the accumulated distance (box plot in µm with 95% CI for PLL n.t siRNA: 200.9 ± 172-229.7 CI; PLL siRac1: 245 ± 203.2-286.9 CI) (Fig. 19C). Furthermore, glass (box plot in µm with 95% CI for glass n.t siRNA: 216 ± 192.8-239.1 CI; siRac1: 156.9 ± 131.3-182.5 CI) and collagen I showed a reduced migration distance (box plot in µm with 95% CI for collagen I n.t siRNA: 222.5 ± 192.7-252.4 CI; collagen I siRac1: 169.4 ± 131.7-207.2 CI) (Fig. 19C).

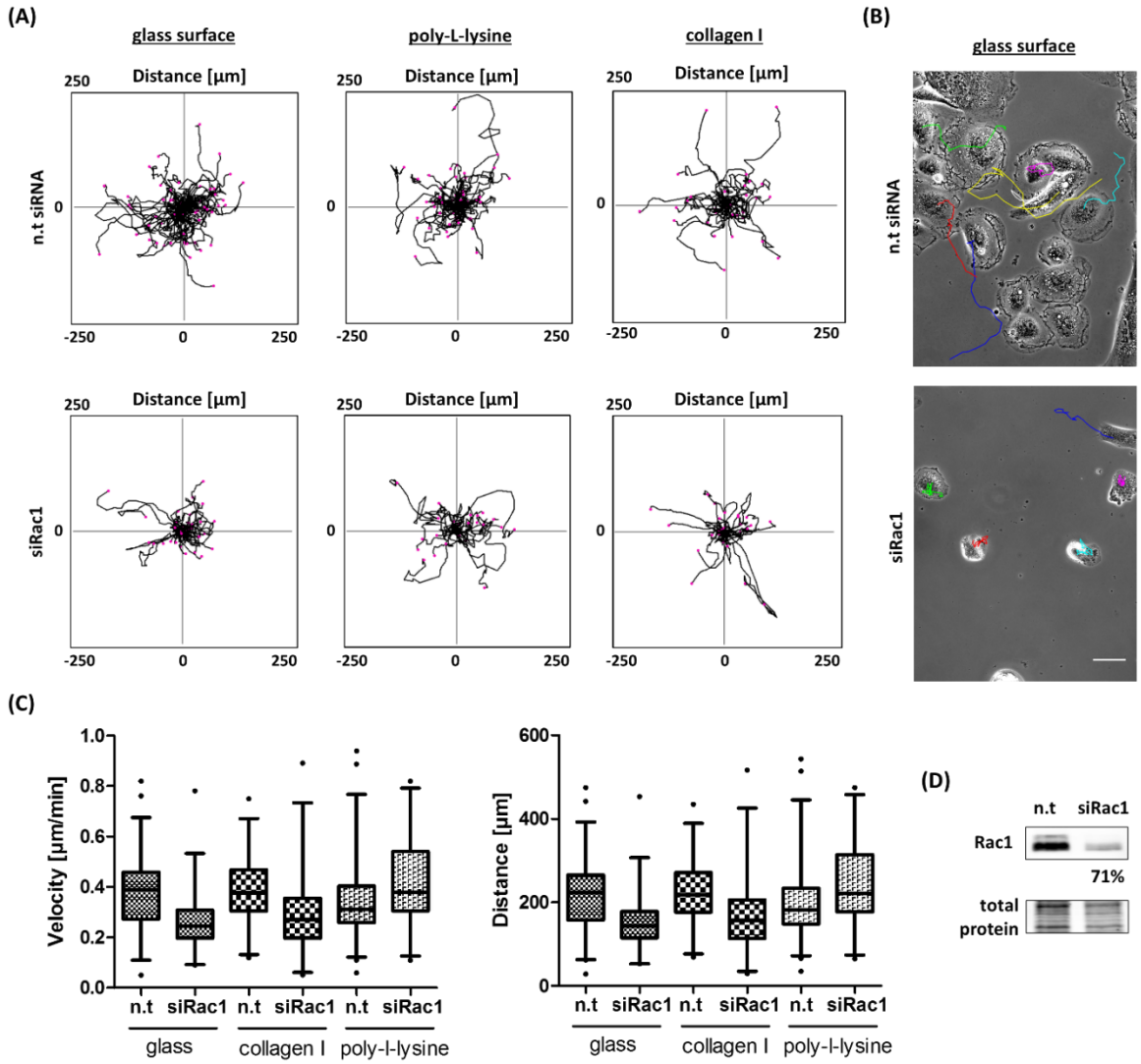

Figure 19: Rac1-P29S is required for cell migration on collagen I and glass surface. UKE-Mel-55b cells were treated with n.t siRNA and siRac1 for 72 h and then re-plated on 4-well IBIDI glass bottom dishes for phase-contrast microscopy. For coating collagen I and poly-L-lysine were used and compared with glass as uncoated condition. After re-plating, cells were incubated for 2 h before imaging was performed with a 20 minutes frame rate for 10 h in total. On collagen I and glass Rac1 depletion resulted in reduced cell migratory behavior. **(A)** Representative migration plots of individual cells for all conditions are shown. **(B)** Showing representative phase-contrast images of cell migration on uncoated dishes. Colored lines indicate cell migration trajectories. Scale bar 50 µm. **(C)** Graphs for migration velocity [µm/min] and accumulated distance [µm] are depicted. Error bars indicate 95% confidence interval. **(D)** Western blot for Rac1 protein level and total protein staining for loading control. Collagen I N=1 experiment with 27-31 cells and N=2 independent experiments for glass and PLL with 23-56 cells.

Overall, this part of the study revealed that endogenous expression of the fast-cycling Rac1-P29S mutant in melanoma resulted in extensive formation of dynamic actin protrusions and enhanced cell adhesion and spreading, all processes that are critically involved in efficient cell migration. Interestingly, melanoma cells expressing Rac1-wt exhibited a lower Rac1-dependency in these processes.

3.3 Role of Rac1-P29S in melanoma cell proliferation

In addition to its regulatory function in actin dynamics, Rac1 has been linked to cell cycle and proliferation-related processes such as G1/S phase transition in cancer cells, enhanced MAPK signaling and Cyclin D1 expression (Liu et al., 2014; Prudnikova et al., 2015; Villalonga and Ridley, 2006).

The Rac1-P29S mutant is suggested to stimulate cell proliferation and survival in melanoma (Lionarons et al., 2019; Watson et al., 2014). In this part of the study, we aimed to dissect potential pathways that mediate this function.

3.3.1 Endogenous Rac1-P29S promotes cell proliferation and survival pathways in melanoma cells

Previous studies have shown in IGR1 melanoma cells that Rac1-P29S expression increase MAPK signaling (Watson et al., 2014). Here, we used the established cell proliferation marker ki-67 (Dowsett et al., 2011; Sun and Kaufman, 2018) to investigate how depletion of Rac1-P29S in our melanoma cell model UKE-Mel-55b affects cell proliferation. We also studied the Rac1-wt expressing Ma-Mel-86c cell line as control to assess potential adaptation processes in UKE-Mel-55b cells due to endogenous expression of Rac1-P29S.

To measure proliferation, cells were fixed and stained with an anti-ki-67 antibody and Hoechst 33342 to detect nuclei. Imaging data were collected by epi-fluorescence microscopy (Fig. 20A). The number of cells with positive ki-67 signal was determined and normalized by the total cell number to calculate the percentage of proliferating cells (Fig. 20B). We measured a significant reduction of proliferating cells after Rac1 depletion in the UKE-Mel-55b cell line as compared to control (n.t siRNA: 74.5 % ± 2.8 SEM; siRac1: 22.7 % ± 3.5 SEM). Interestingly, depletion of Rac1 in Ma-Mel-86c cells, that express Rac1-wt endogenously, did not cause such dramatic reduced cell proliferation (n.t siRNA: 86.3 % ± 4.7 SEM; siRac1 85.9 % ± 7.9 SEM) (Fig. 20B). Thus, this data suggests that proliferation in these cells is Rac1 independent, whereas Rac1 activity is required in melanoma cells with the endogenous Rac1-P29S mutant.

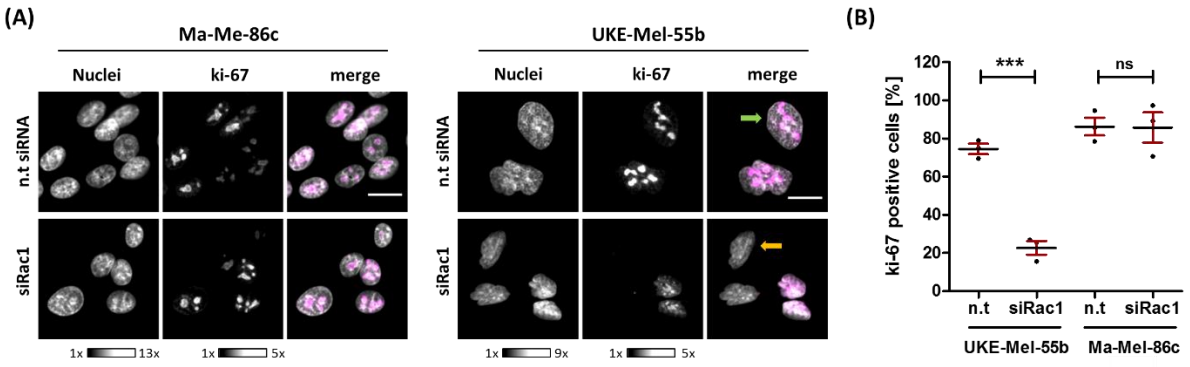

Figure 20: Depletion of endogenous Rac1-P29S in melanoma cells distinctly decreases cell proliferation. (A) Representative wide field images depicting ki-67 nuclear localization. Merge: Nuclei (grey); ki-67 (magenta). Green arrow indicates ki-67 in the nucleus, orange arrow indicates nucleus without ki-67. Scale bar 20 µm **(B)** Percent cells with nuclear ki-67 signal [%]. Statistical analysis was performed with a two-tailed unpaired t-test. p<0.0001:***, ns=non-significant. Error bars indicate SEM. N=3 independent experiments.

To better understand the mechanisms, by which the endogenously expressed fast-cycling mutant Rac1-P29S controls cell proliferation in melanoma, we depleted the protein using RNAi and measured activity of its prominent downstream effector (PAK 1/2) as well as canonical proliferation and survival pathways such as ERK 1/2, AKT and Yap/Taz signaling.

Cells, expressing Rac1-P29S (UKE-Mel-55b) showed significantly reduced phosphorylated ERK 1/2 levels (pERK 1/2 for n.t siRNA 100 %; siRac1 59.8 % ± 5 SEM), resulting in a rise of the levels of the inactive un-phosphorylated form (ERK for n.t siRNA 100 %; siRac1 127.7 % ± 10.3 SEM) (Fig. 21B). This inhibition of signaling activity was also observable by the pERK/ERK ratio (ratio pERK/ERK for n.t siRNA 100 %; siRac1 49.8 % ± 4.7 SEM). Rac1-wt cells did not show such a reduced ERK activity upon Rac1 depletion (ratio pERK/ERK for n.t siRNA: 100 %; siRac1 88.5 % ± 3.9 SEM) (Fig. 21B). Based on the distinct reduction of ERK 1/2 activity upon depletion of Rac1-P29S, MAPK signaling might mediate stimulation of cell proliferation by this fast-cycling Rac1 mutant.

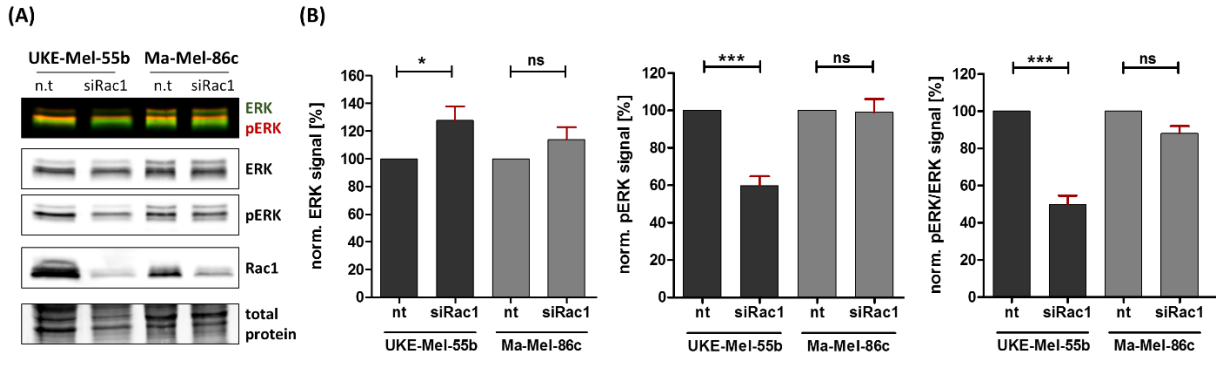

Figure 21: Depletion of endogenous Rac1-P29S significantly reduces ERK activity in melanoma cells. Melanoma cell lines were treated with n.t siRNA or siRac1 for 72 h and analyzed by western blot for protein level quantification. Only melanoma cells expressing Rac1-P29S showed Rac1 dependent ERK signaling. **(A)** Representative western blot showing relative protein levels of Rac1, ERK1/2 and pERK1/2 (pT202/pY204). Total protein was used as loading control and for signal normalization. **(B)** Graphs showing normalized protein levels. Signals were plotted against n.t siRNA, which acted as reference (100 % protein expression). N=13 independent experiments. Statistical analysis was performed with column statistic, one-sample t-test against 100. P<0.05:*, p<0.0001:***, ns=non-significant. Error bars indicate SEM.

Next, we wanted to investigate how the elevated activity of the Rac1-P29S mutant might influence tumor related survival pathways such as activity of the anti-apoptotic kinase AKT (protein kinase B). To measure the AKT activity state after Rac1 depletion, protein levels for AKT and phosphorylated-AKT (active) were quantified via western blot analysis (Fig. 22A). Rac1 depletion significantly reduced AKT activity in both melanoma cell lines, as measured by the ratio pAKT/AKT (UKE-Mel-55b: n.t siRNA 100%; siRac1 61.7 % ± 3.2 SEM; Ma-Mel-86c: n.t siRNA 100 %; siRac1 71.4 % ± 3.5 SEM) (Fig. 22B). In contrast to cell proliferation and MAPK signaling, AKT activity in melanoma is not differentially affected by endogenous Rac1-P29S mutant as compared to Rac1-wt protein.

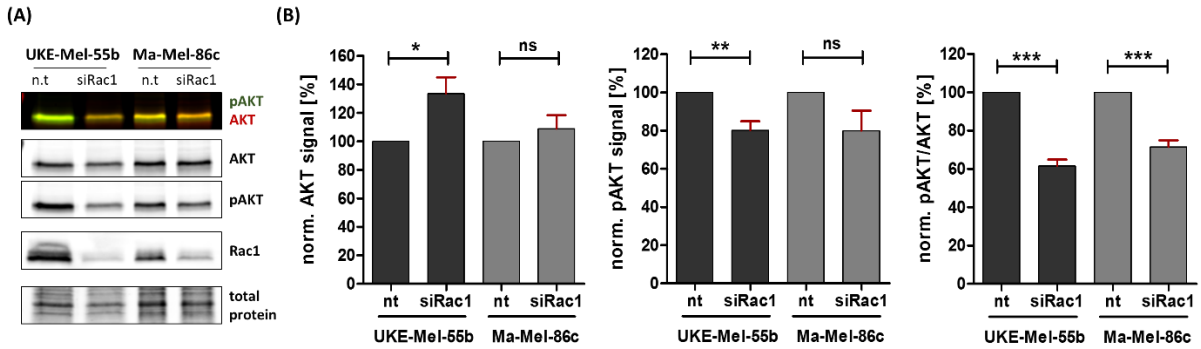

Figure 22: Depletion of Rac1 reduces AKT activity in both melanoma cell lines. Melanoma cell lines were treated with n.t siRNA or siRac1 for 72 h and analyzed by western blot for protein level quantification. **(A)** Representative western blot showing relative protein levels of Rac1, AKT and pAKT. Total protein was used as loading control and for signal normalization. **(B)** Graphs showing normalized protein levels. Signals were plotted against n.t siRNA, which acted as reference (100 % protein expression). UKE-Mel-55b n=9; Ma-Mel-86c n=11. Statistical analysis was performed with column statistic, one-sample t-test against 100. P<0.05:*, p<0.0001:***, ns=non-significant. Error bars indicate SEM. AKT level in UKE-Mel-55b: n.t siRNA 100%; siRac1 133.7 % ± 11.2 SEM. AKT level in Ma-Mel-86c: n.t siRNA 100%; siRac1 109 % ± 9.4 SEM. pAKT level in UKE-Mel-55b: n.t siRNA 100 %; siRac1 80.3 % ± 4.7 SEM; pAKT in Ma-Mel-86c: n. siRNA 100 %; siRac1 80.1 % ± 10.4 SEM).

In addition to the above studied canonical signaling pathways that control cell proliferation (ERK) and survival (AKT), we also measured the effect of Rac1 depletion on the transcriptional coactivators Yap/Taz that are controlled by actin regulatory mechanisms (Dupont et al., 2011). Yap/Taz are only active in the nucleus when they are de-phosphorylated. To investigate whether Yap/Taz activity is also Rac1 dependent, immunofluorescence analysis was performed to visualize Yap/Taz localization with epi-fluorescence imaging (Fig. 23A). Cells with predominant nuclear Yap/Taz signal were counted and normalized to total number of cells. Interestingly, nuclear Yap/Taz localization in melanoma cells expressing the active Rac1-P29S mutant (UKE-Mel-55b) was significantly higher as compared to Rac1-wt cells (UKE-Mel-55b n.t siRNA 70.5 % ± 4.7 SEM ; Ma-Mel-86c n.t siRNA: 17.6 % ± 3.3 SEM) (Fig. 23B). Upon depletion of Rac1, percentage of cells with nuclear Yap/Taz significantly reduced in UKE-Mel-55b cells (n.t siRNA: 70.5 % ± 4.7 SEM; siRac1: 35.8 % ± 3.6 SEM), whereas Yap/Taz signal was not affected in the Rac1-wt (Ma-Mel-86c) cell line (n.t siRNA: 17.6 % ± 3.3 SEM; siRac1: 20.8 % ± 3.6 SEM) (Fig. 23B).

Overall, this finding suggested that the strongly elevated Yap/Taz activity in UKE-Mel-55b melanoma cells is due to increased activity of the fast-cycling Rac1-P29S mutant.

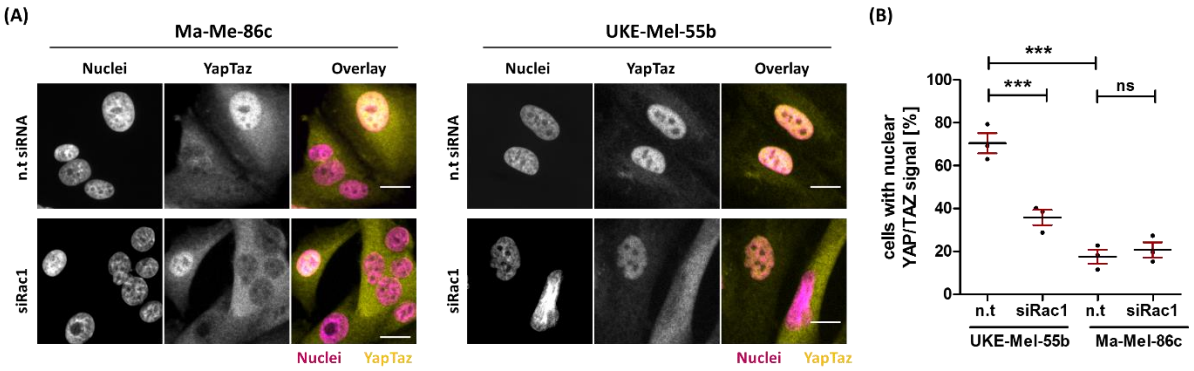

Figure 23: Rac1-P29S is required for increased nuclear Yap/Taz localization in UKE-Mel-55b cells. Melanoma cells treated with n.t siRNA or siRac1 for 72 h. **(A)** Representative wide field images for nuclear Yap/Taz localization. Cells fixed and stained for nuclei with Hoechst 33324 (magenta) and Yap/Taz (yellow). Scale bar 20 µm. **(B)** Graph with cells displaying nuclear localized Yap/Taz in [%]. Overall threshold was set to count cells with positive Yap/Taz signal. N=3 independent experiments. Statistical analysis was performed with a two-tailed t-test unpaired. p<0.0001:***, ns=non-significant. Error bars indicate SEM.

To further test the specificity of Rac1-P29S effects on nuclear Yap/Taz localization, we performed rescue experiments after Rac1-P29S knock-down in UKE-Mel-55b cells. For this, we transfected siRNA-resistant EGFP-control, EGFP-Rac1-wt and EGFP-Rac1-P29S plasmids in these cells 24 h after Rac1-siRNA treatment. Western blot analysis were performed to confirm Rac1 knock-down and transfection efficiency of the siRNA-resistant plasmids (Fig. 24A). In Fig. 24A, the lower red bands at around 21 kDa indicate the endogenous Rac1-P29S protein level for control (n.t siRNA) and Rac1 depleted cells (siRac1), whereas the green bands depict the EGFP antibody signal. The EGFP-control vector is visible at 27 kDa, while EGFP-Rac1-wt and EGFP-Rac1-P29S are detected at around 50 kDa with green or yellow colored patterns due to the superposition of antibody signals for Rac1 and EGFP. The western blot studies revealed a sufficient Rac1 depletion and expression of the siRNA resistant plasmids (Fig. 24A).

Yap activity was determined via western blot to detect Yap and pYap (inactive) protein (Fig. 24B) as well as by Yap/Taz staining and fluorescent microscopy (Fig. 24C). In n.t siRNA-treated cells, overexpression of Rac1-wt did not alter Yap phosphorylation level as compared to EGFP-control plasmid, whereas YAP phosphorylation was somewhat elevated with Rac1-P29S overexpression.

Rac1 depletion substantially increased the level of phosphorylated inactive Yap (pYap) in EGFP-control and EGFP-Rac1-wt expressing cells as compared to the corresponding n.t siRNA-treated cells. In contrast, pYap levels did not change upon Rac1-depletion in

EGFP-Rac1-P29S transfected cells. Furthermore, wide-field fluorescence imaging was performed to analyze Yap/Taz localization in transfected cells (Fig. 24C). In agreement with increased pYap signal in the western blot analysis, microscopy studies revealed substantial reduced percentage of cells with nuclear localized Yap/Taz upon Rac1 depletion in EGFP-transfected control cells (n.t siRNA 90.4 %; siRac1: 61.8 %). Overepression of EGFP-Rac1-wt in Rac1 depleted cells did not rescue Yap/Taz nuclear localization suggesting that activity level of Rac1-wt is not sufficient to stimulate Yap/Taz activity in this cell system (n.t siRac1: 92.1 %, siRac1: 67.2 %). In contrast, expression of EGFP-Rac1-P29S restored Yap/Taz localization to control levels in Rac1 depleted cells, confirming that elevated activity of the fast-cycling mutant Rac1-P29S stimulates activity of the transcriptional coactivators Yap/Taz in UKE-Mel-55b cells (n.t siRac1: 89.9 %; siRac1: 87.5 %).

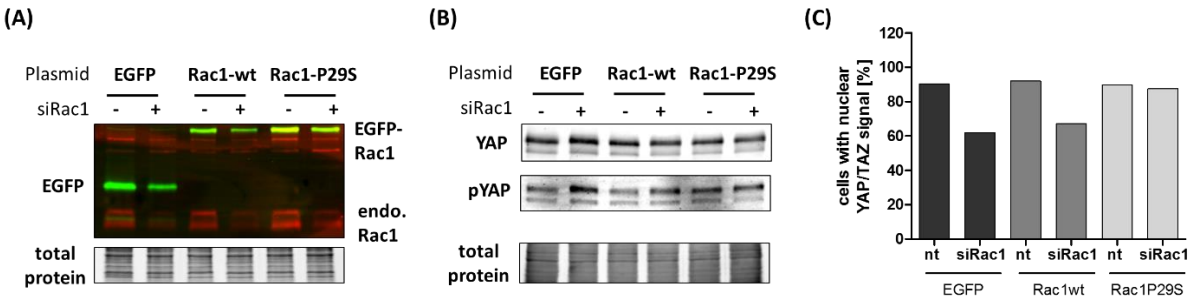

Figure 24: Exogenous Rac1-P29S leads to recovery of reduced nuclear Yap/Taz localization in UKE-Mel-55b cells after Rac1 depletion. UKE-Mel-55b cells that endogenously express Rac1-P29S were treated with n.t siRNA and siRac1 for 72 h. After 24 h siRNA-resistant EGFP-Rac1-plasmids and EGFP-control vector were transfected. Rac1 depletion reduced nuclear Yap/Taz levels. However, we obtained an increase of cells with nuclear Yap/Taz after transfection with EGFP-Rac1-wt and EGFP-Rac1-P29S plasmids. **(A)** Western blot for endogenous Rac1 and transfected plasmids (EGFP-control vector, EGFP-Rac1-wt and EGFP-Rac1-P29S) together with total protein signal. **(B)** Western blot analysis of Yap and phosphorylated Yap (pYap; cytosolic, inactive). **(C)** Graph with percentage of cells with nuclear Yap/Taz after Rac1 depletion and transfection with the indicated plasmids. Only transfected cells were analyzed (microscopy images are not shown). N=1 experiment.

3.3.2 Rac1 downstream effector PAK2 is a potential mediator of Rac1-P29S related proliferation

Several studies have established that proteins of the PAK (p21-activated kinases) protein family are major mediators of Rac1 signaling in multiple pathways and lead to activation of ERK1/2, AKT and Yap/Taz (Knaus et al., 1998; Lu et al., 2017). Therefore, we were interested if PAK activity might also play a role in Rac1-mediated enhanced proliferation signals in melanoma. For this purpose, we first evaluated PAK1/2 activity in melanoma cell systems that distinctly express either Rac1-wt (Ma-Mel-86c) or Rac1-P29S (UKE-Mel-55b) on endogenous level. Western blot analysis revealed similar protein levels for PAK in both cell lines (Fig. 25A), whereas PAK activity, as evident through phosphorylation of PAK1/2, was substantially elevated in Rac1-P29S expressing cells as compared to cells that express Rac1-wt (Fig. 25A). To study if the elevated PAK activity in the UKE-Mel-55b melanoma cells was due to the presence of the Rac1-P29S mutant, we performed western blot analysis after Rac1 depletion in this cell system (Fig. 25B). PAK protein level was significantly reduced in Rac1 depleted cells (PAK: n.t siRNA: 100 %; siRac1: 67 % ± 6.4 SEM) (Fig. 25C). However, a reduced PAK phosphorylation (pPAK) in these cells was even more pronounced (pPAK: n.t siRNA: 100 %; siRac1: 34.3 % ± 10.2 SEM). Our measurements resulted in significantly reduced PAK activity ratio upon Rac1 depletion (pPAK/PAK: n.t siRNA: 100%; siRac1: 53.3 % ± 21.8 SEM) (Fig. 25C).

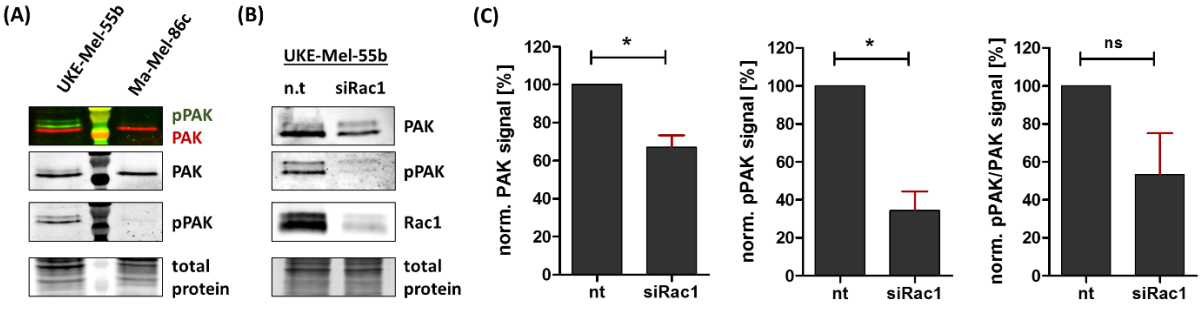

Figure 25: Rac1-P29S is required for elevated PAK activity in UKE-Mel-55b cells. Both melanoma cell lines were analyzed for PAK-signaling activity. **(A)** PAK activity is strongly elevated in UKE-Mel-55b cells as compared to Rac1-wt expressing Ma-Mel-86c cells. Western blot analysis of protein levels of PAK1/2/3 and phosphorylation of PAK1/2 (PAK1 at S199/204 and PAK2 at S192/197). N=1 experiment. **(B)** Representative western blot to analyze PAK activity in UKE-Mel-55b cells after Rac1 knock-down. Increased PAK1/2 activity in UKE-Mel-55b cells is Rac1-P29S dependent. **(C)** Graphs depict normalized PAK1/2/3 and phosphorylated PAK1/2 (pPAK) levels as well as activity ratio of PAK calculated as pPAK/PAK. Protein levels were normalized with total protein staining and values for n.t siRNA were set to 100%. N=3 independent experiments. Statistical analysis was performed with a two-tailed unpaired t-test. $p<0.05$:*, ns=non-significant. Error bars indicate SEM.

As shown above, Rac1 depletion resulted in significantly reduced ERK1/2, AKT and PAK activity in UKE-Mel-55b cells. Thus, we next investigated how depletion of the Rac1 effector PAK affects ERK and AKT protein levels and activity in this cell system.

We utilized two different smart pool siRNA mixes to deplete PAK1 or PAK2 protein (Fig. 26). The PAK protein signal was almost entirely lost with the PAK2 siRNA, whereas no change was evident with siRNA against PAK1 (Fig. 26A). AKT protein levels were not affected after either PAK1 or PAK2 depletion (Fig. 26B). In comparison, depletion with siPAK2 showed a slight decrease in pERK level (Fig. 26C). These first findings suggest that PAK2 might be more involved in signaling pathways in UKE-Mel-55b cells compared to PAK1. However, since the PAK antibody that was used in this study detects all three PAK isoforms, it cannot be exclude that depletion with the siPAK2 smart pool mix also reduce the other protein levels of PAK1 or PAK3. Here further detailed studies would be necessary to characterize the role of the different PAK forms in UKE-Mel-55b cells.

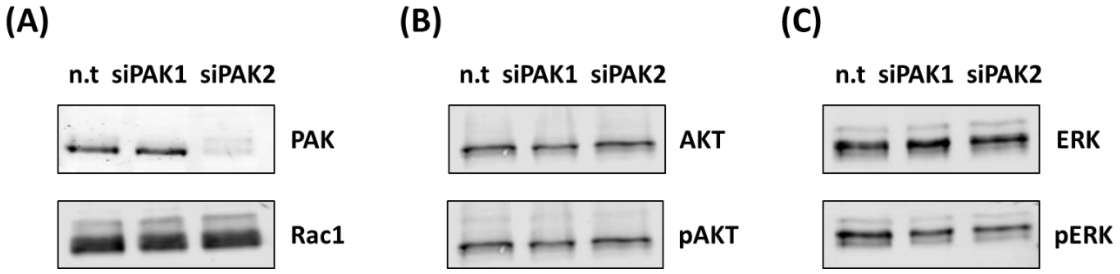

Figure 26: PAK2 depletion in Rac1-P29S expressing melanoma cells decrease ERK activity. UKE-Mel-55b cells were transfected with smart pool siRNA mixes for PAK1 and PAK2 for 72 h, individually. **(A)** Western blot images for PAK and Rac1 levels after PAK depletion are shown. Antibody for PAK detects PAK1/2/3, while antibody for pPAK detects pPAK1/2. **(B)** Western blot images for AKT and pAKT after PAK depletion. **(C)** Western blot images for ERK1/2 and pERK1/2 after PAK knock-down. Only siPAK2 reduced PAK levels whereas Rac1 expression and AKT activity was not affected. PAK2 depletion caused a slight decrease in pERK level. N=1 experiment.

3.3.3 Depletion of Rac1-P29S in UKE-Mel-55b cells causes mitotic defects

Based on our observation that proliferation is significantly reduced upon depletion of endogenous Rac1-P29S in UKE-Mel-55b cells, we wondered if mitosis in these cells is perturbed too. To analyze the effects of Rac1-P29S depletion during cell division in UKE-Mel-55b cells, phase-contrast imaging was performed after treatment with siRNA for 72 h (Fig. 27). The number of mitotic cells was counted during the course of imaging (10 h) and divided by the total cell number to determine the percentage of mitotic events.

Cell division after Rac1 depletion was significantly reduced as compared to control siRNA-treated cells (n.t siRNA 24.9 % ± 3.6 SEM; siRac1: 10 % ± 2.6 SEM) (Fig. 27B). To further understand the underlying reasons for this substantial reduction of mitosis, we assessed morphodynamic behavior of individual cells. We found that the majority of control cells (n.t siRNA) formed elongated membrane extensions during mitotic entry that appeared to support cell adhesion to the substrate (n.t siRNA: 72.1 % ± 2.1 SEM) (Fig. 27C, E; green arrow). In contrast, Rac1 depletion, significantly diminished the percentage of cells with these cell-substrate adhesions (siRac1: 25 % ± 8.3 SEM) (Fig. 27C). Moreover, we found that cells lacking Rac1 require a longer time period for mitosis as compared to control cells (n.t siRNA: 93.8 min ± 0.2 SEM; siRac1: 125.8 min ± 9.2 SEM) (Fig. 27D, E). Based on these findings, Rac1-P29S might therefore promote cell division in UKE-Mel-55b via generation of cell extensions that support substrate adhesion during mitosis and that by that facilitate efficient cell division.

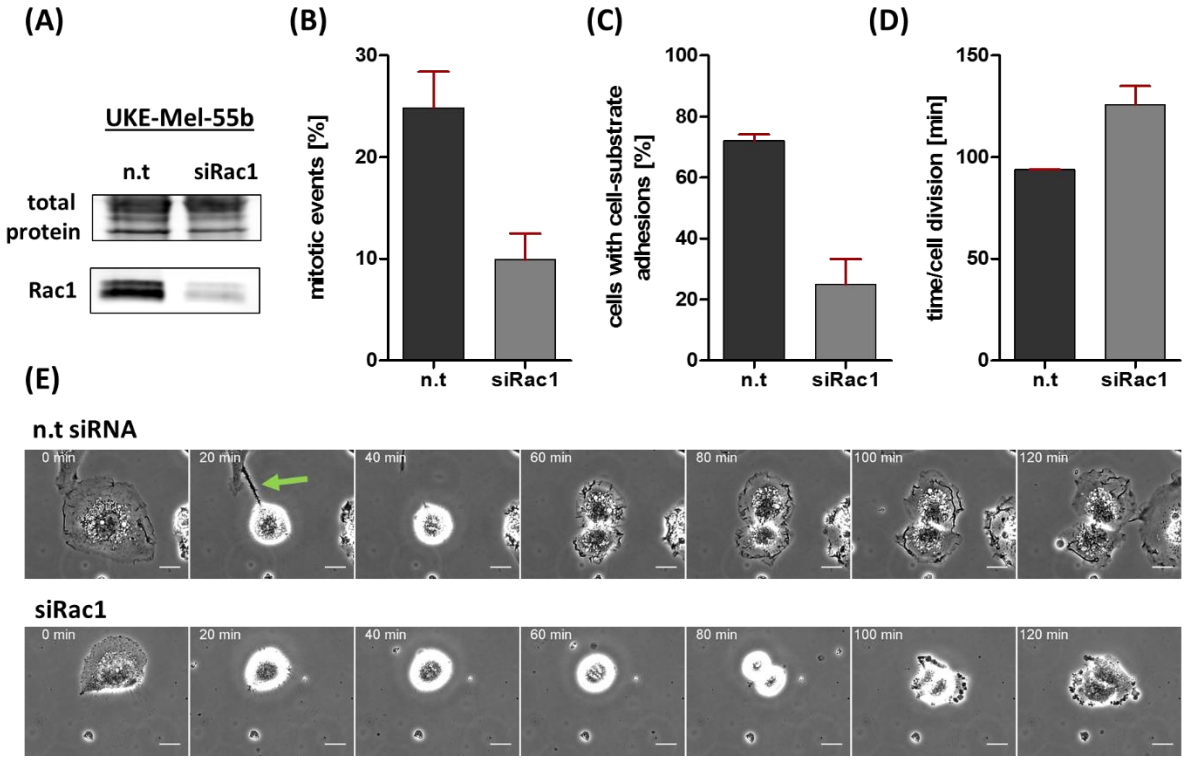

Figure 27: Depletion of Rac1-P29S cause mitotic defects in UKE-Mel-55b cells. Cells were re-plated 72 h after n.t siRNA and siRac1 treatment on IBIDI glass phase-contrast dishes. Imaging was started 2 h after seeding. Cells were imaged every 20 minutes for 10 h. **(A)** Representative western blot for Rac1 protein level and total protein as loading control. **(B)** Graph depicting mitotic events [%]. **(C)** Percentage of dividing cells, which shown cell-substrate adhesions upon entering mitosis. **(D)** Duration of mitosis [min]. All graphs shown mean of n=2 independent experiments (total number of cells for n.t siRNA: 142; siRac1: 129; total number of mitotic cells: n.t siRNA 17 and 8 for siRac1-treated cells. Error bars indicate SEM. **(E)** Representative mitotic events for n.t siRNA and Rac1 siRNA treated cells. Scale bar 20 µm.

In summary, data presented in this part of the study revealed that endogenous expression of Rac1-P29S stimulates cell proliferation and survival pathways in UKE-Mel-55b melanoma cells.

3.4 Rac1-P29S expression is associated with adaptation of resistance to BRAF inhibitor (Vemurafenib; PLX-4032) in melanoma cells

Previous studies showed that 50 % of all melanoma patients carry an activating BRAF mutation. This causes an increased activity in MAPK signaling and results in an enhanced cell proliferation (Ascierto et al., 2012). As a consequence, patients were often treated with specific BRAF inhibitors. One of those is vemurafenib (PLX-4032), which specifically inhibits the activity of BRAF bearing V600K/E mutations and thus blocks the MAPK pathway (Yang et al., 2010). However, patients can develop a resistance against the BRAF inhibitor, which typically occurs within 6 months after treatment begin (Villanueva et al., 2011). Interestingly, these patients frequently express the Rac1-P29S mutation in addition to the BRAF mutation (Watson et al., 2014). As an effective inhibition of BRAF results in the down regulation of MAPK signaling, it has been hypothesized, that tumor cells utilize the highly active Rac1-P29S mutation to sustain continuous proliferation via an alternative pathway (Watson et al., 2014). However, the role of Rac1-P29S in the adaptation of melanoma cells to BRAF inhibition and potential mechanisms that could mediate this role remain unknown. Based on our findings in the previous chapter, Rac1-P29S stimulates signaling pathways in melanoma cells that are linked to cell survival and proliferation.

Here, our goal was to investigate how endogenous expression of the Rac1-P29S mutant in melanoma cells (UKE-Mel-55b) affects these pathways and how this might be linked to adaptation to BRAF inhibitor resistance.

3.4.1 Melanoma cells endogenously expressing Rac1-P29S partially recover proliferation defects during the course of BRAF inhibition

To understand potential mechanistic differences we used PLX-4032 treatment of cells that express either Rac1-wt (Ma-Mel-86c) or the fast-cycling mutant Rac1-P29S (UKE-Mel-55b). First, we treated both melanoma cell lines for three, six and nine days with PLX-4032 and DMSO as control. The number of cells was determined for each time point using the Neubauer counting chamber, together with trypan blue staining to assess cell vitality (Fig. 28A) (performed by a master student under my supervision (Ramminger, 2018)).

As expected, we observed a significantly reduced cell number for the Rac1-wt expressing melanoma cell line (Ma-Mel-86c) under PLX-4032 treatment as compared to DMSO. Moreover, the differences to DMSO increases over time (Fig. 28A, Tab. 39).

Interestingly, PLX-4032 also resulted in reduced cell numbers in cells that endogenously express Rac1-P29S (Fig. 28A, Tab. 39). However, this decrease was statistically not significant and remained stable throughout the entire experiment, suggesting a survival advantage of these cells during PLX-4032 treatment. Surprisingly, DMSO treatment cause reduced cell numbers during the course of experiment indicating that other factors such as cell density might also involved in cell proliferation in these cells.

Next, we investigated how altered cell numbers correlated to cell proliferation rate during drug treatment experiments. For this purpose, we fixed treated cells on the indicated time points and use immunofluorescence to detect the proliferation marker ki-67 (Fig. 28B).

PLX-4032 treatment caused a significant reduction of proliferation as compared to DMSO in both cell lines (Fig. 28C, Tab. 39, 40). The substantial difference between DMSO control and PLX-4032 treatment remained in Rac1-wt cells (Ma-Mel-86c) over the entire time course of the experiment (Fig. 28C, Tab. 39). Interestingly, the initially low proliferation rate in Rac1-P29S expressing UKE-Mel-55b cells caused by PLX-4032, constantly increased over time reducing the gap to DMSO control cells (Fig. 28C, Tab. 40).

Thus, our experiments show that cells endogenously expressing Rac1-P29S are able to partially recover proliferation after several days of BRAF inhibition using PLX-4032.

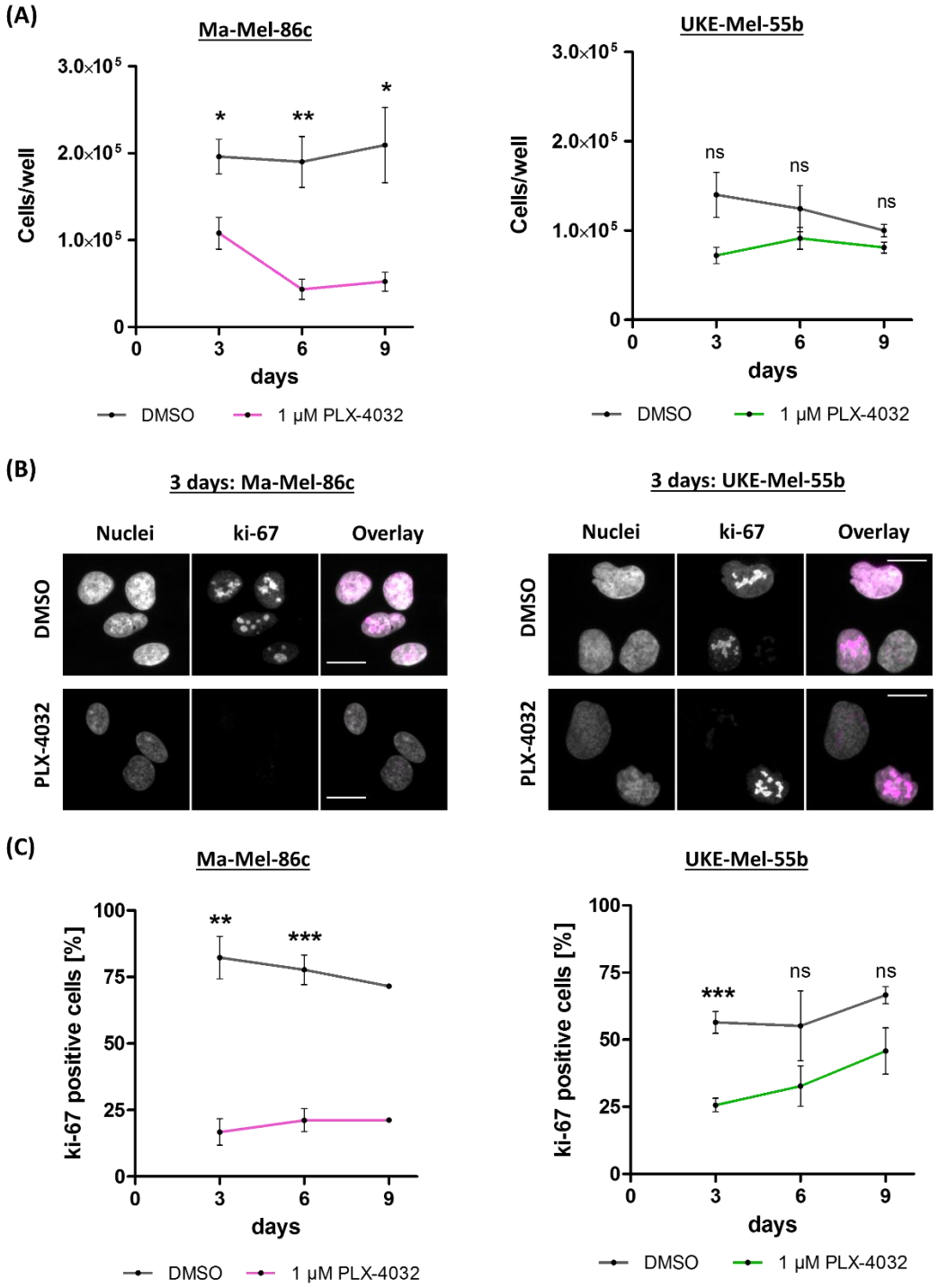

Figure 28: Proliferation rate in Rac1-P29S expressing melanoma cells recovers after six days of PLX 4032 induced BRAF inhibition. Melanoma cell lines expressing Rac1-wt (Ma-Mel-86c) or Rac1-P29S (UKE-Mel-55b), were treated with PLX-4032 (c=1 µM) for three, six and nine days. At each time point, the total cell numbers were counted and cells were stained with an antibody for ki-67 to determine cell proliferation rate. **(A)** Cell numbers at three, six and nine days of drug treatment. Mean values from three independent experiments (Ramminger, 2018). **(B)** Representative wide field images after three days of treatment for both cell lines. Nuclei were stained with Hoechst 33324. Antibody for ki-67 staining was used for immunofluorescence. Single images in grey scale. Overlays: Nuclei grey; ki-67 magenta. Scale bar 20 µm. **(C)** Percentage of ki-67 positive cells at indicated time points of treatment. Mean values are shown. Ma-Mel-86c: n=3 independent experiments for three and six days, n=1 for nine days. UKE-Mel-55b: n=3 for all time points. Statistical analysis performed with two-tailed t-test, unpaired. P<0.05:*, p<0.001:**, p<0.0001:***, ns=non-significant. Error bars indicate SEM.

Table 39: Mean values of calculated cell number and percentage of ki-67 positive Ma-Mel-86c cells under BRAF inhibition with PLX-4032 for three, six and nine days.

time	Cellnumber		ki-67	
	DMSO	1 µM PLX	DMSO	1 µM PLX
3 days	$1.9 \cdot 10^5$ cells ± $0.2 \cdot 10^5$ SEM	$1 \cdot 10^5$ cells ± $0.2 \cdot 10^5$ SEM	82.3 % ± 8 SEM	16.72 % ± 4.97 SEM
6 days	$1.9 \cdot 10^5$ cells ± $0.3 \cdot 10^5$ SEM	$0.4 \cdot 10^5$ cells ± $0.1 \cdot 10^5$ SEM	77.7 % ± 5.6 SEM	21.2 % ± 4.3 SEM
9 days	$2 \cdot 10^5$ cells ± $0.4 \cdot 10^5$ SEM	$0.5 \cdot 10^5$ cells ± $0.1 \cdot 10^5$ SEM	71.5 % ± 2.6 SEM	21.2% ± 4 SEM

Table 40: Mean values of calculated cell number and percentage of ki-67 positive UKE-Mel-55b cells under BRAF inhibition with PLX-4032 for three, six and nine days.

time	Cellnumber		ki-67	
	DMSO	1 µM PLX	DMSO	1 µM PLX
3 days	$1.4 \cdot 10^5$ cells ± $0.25 \cdot 10^5$ SEM	$0.7 \cdot 10^5$ cells ± $0.1 \cdot 10^5$ SEM	56.4 % ± 4 SEM	25.7 % ± 2.6 SEM
6 days	$0.25 \cdot 10^5$ cells ± $0.3 \cdot 10^5$ SEM	$0.9 \cdot 10^5$ cells ± $0.1 \cdot 10^5$ SEM	55.2 % ± 13 SEM	32.7 % ± 7.5 SEM
9 days	$1 \cdot 10^5$ cells ± $0.1 \cdot 10^5$ SEM	$0.8 \cdot 10^5$ cells ± $0.1 \cdot 10^5$ SEM	66.6 % ± 3.2 SEM	45.8 % ± 8.6 SEM

We next wanted to understand, if Rac-P29S is required for the partial recovery of cell proliferation in UKE-Mel-55b cells during PLX-4032 treatment. For this, we first depleted Rac1-P29S using RNAi for 72 h prior to drug treatment. Rac1-P29S depleted cells were then re-plated for 24 h before treatment with either DMSO control or PLX-4032 started. After three and six days of drug treatment, cell numbers and proliferation rates (ki-67 as marker) were determined (Fig. 29; Tab. 41).

As also shown in untreated cells in the previously chapter (Fig. 20), Rac1 depletion clearly reduce cell proliferation (Fig. 29A, before drug treatment). After three days of DMSO treatment, we observed a lower cell proliferation in Rac1 depleted cells, albeit with a milder effect (Fig. 29B). However, the difference in cell proliferation between n.t siRNA and siRac1 treated cells in the DMSO group diminished after six days of treatment. This was mainly due to decreased proliferation in n.t siRNA cells (Fig. 29C).

PLX-4032 treatment of n.t siRNA cells caused a dramatic decrease of cell proliferation after three days as compared to DMSO (Fig. 29B). Rac1 depletion did not further add to this significant effect at this time point. Interestingly, after six days, proliferation in n.t siRNA control cells recovered substantially as compared to three days of PLX-4032 treatment (Fig. 29C). In contrast, proliferation rate in Rac1-depleted cells remained at a

similar low level, as it was after three days of PLX-4032 treatment (Fig. 29B, C). These results supporting that Rac1-P29S is required for partial adaptation of cell proliferation in melanoma cells to PLX-4032 treatment.

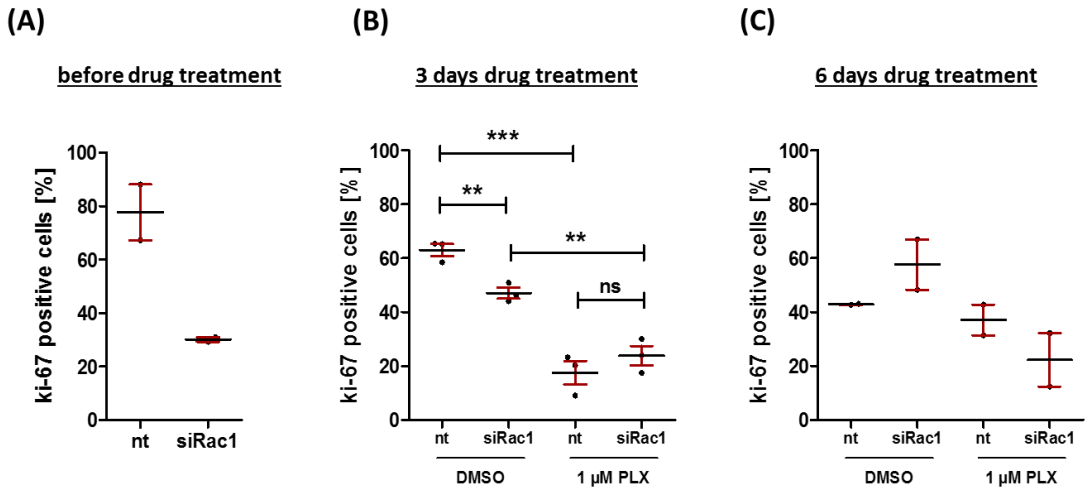

Figure 29: Rac1-P29S depletion leads to further reduction of cell proliferation after six days of BRAF inhibition. UKE-Mel-55b cells were treated with n.t siRNA and siRac1 for 72h (before drug treatment) and exposed to DMSO or PLX-4032 for another 3 or 6 days respectively (3 days and 6 days of drug treatment). **(A)** Graphs with percentage of ki-67 positive cells after 72 h Rac1 depletion. **(B)** Graph with ki-67 positive cells [%] after three days drug treatment and **(C)** shown graph after six days DMSO/PLX-4032 treatment in Rac1 depleted cells. See Tab. 41 for mean values and SEM. 3 days drug treatment: n=3; 6 days drug treatment: n=2 independent experiments. Statistical analysis was performed with two-tailed t-test, unpaired. p<0.001:**, p<0.0001:***, ns=non-significant. Error bars indicate SEM.

Table 41: Mean values of the percentage of ki-67 positive cells after Rac1 depletion and DMSO/PLX 4032 treatment in UKE-Mel-55b cells.

time	DMSO		PLX-4032	
	n.t siRNA	siRac1	n.t siRNA	siRac1
before drug treatment	77.6 % ± 10.4 SEM	30 % ± 0.9 SEM	--	--
3 days of drug treatment	63.3 % ± 2.3 SEM	47.3 % ± 2 SEM	17.5 % ± 4.3 SEM	23.8 % ± 3.6 SEM
6 days of drug treatment	42.9 % ± 0.2 SEM	57.6 % ± 9.4 SEM	37.1 % ± 5.7 SEM	22.3 % ± 9.9 SEM

3.4.2 PLX-4032 treatment stimulates PAK signaling in Rac1-P29S melanoma cells

Next, we want to understand how activity of the Rac1 effector PAK might be involved in cell proliferation in the context of BRAF inhibition. Western blot analyses revealed that PLX-4032 treatment caused increased pPAK1/2 signals in UKE-Mel-55b cells (pPAK 3 days: PLX-4032: 181.5 % ± 0.5 SEM; 6 days: 212.5 % ± 47.5 SEM; 9 days: 241 %) (Fig. 30A, B). Interestingly, PLX-4032 treatment was not sufficient to increase pPAK1/2 levels in Rac1-wt cells (Ma-Mel-86c) (Fig. 30A). To determine the activation status of PAK1/2 in UKE-Mel-55b cells, the ratio between pPAK and PAK levels was calculated. Here, PLX-4032 treatment strongly upregulate active PAK1/2 (ratio pPAK/PAK) levels as compared to DMSO treatment with maximum activity at six days of PLX-4032 treatment (pPAK/PAK 3 days: PLX-4032: 182 % ± 1.5 SEM; 6 days: 250.5 % ± 5.5 SEM; 9 days: 152 %) (Fig. 30C).

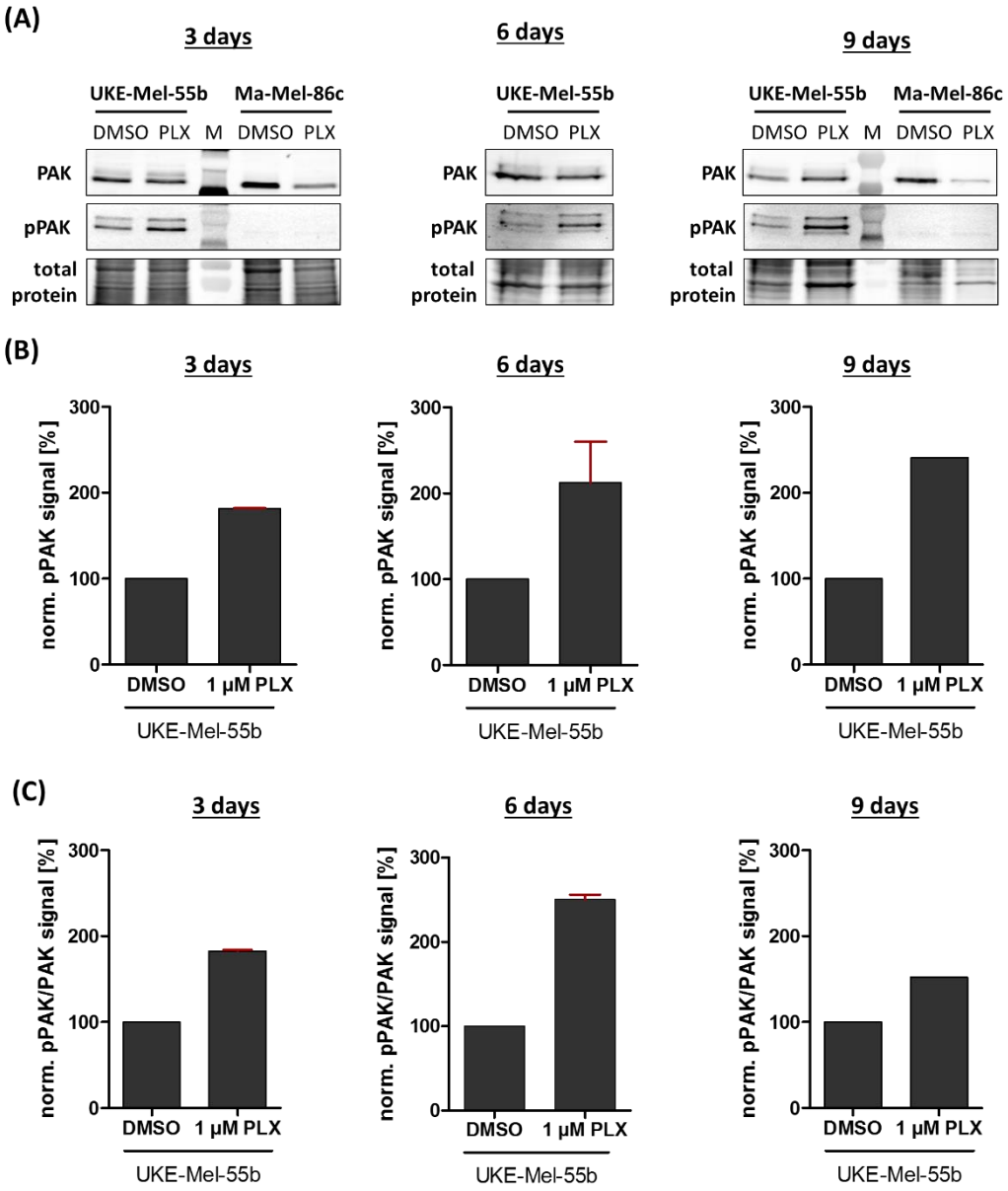

Figure 30: BRAF inhibition with PLX-4032 increases pPAK1/2 level in Rac1-P29S expressing melanoma cells. Melanoma cell lines were treated with DMSO or 1 µM PLX-4032 for three, six and nine days. **(A)** Representative western blot analysis of protein levels of PAK1/2/3 and phosphorylation of PAK1/2 (PAK1 at S199/204 and PAK2 at S192/197) after 3, 6 and 9 days of PLX-4032 treatment. (C) Graphs shown measured pPAK1/2 signals for all three time points in UKE-Mel-55b cells. **(C)**. Graphs depict normalized activity ratio of PAK1/2 calculated as pPAK/PAK. Protein levels were normalized with total protein staining and values for DMSO were set to 100%. N=2 independent experiments for 3 and 6 days and n=1 experiment for 9 days drug treatment.

To examine whether the increase of PAK1/2 phosphorylation upon PLX-4032 treatment is Rac1 dependent, we depleted Rac1-P29S in UKE-Mel-55b cells, and measured protein levels of PAK1/2/3 as well as their active forms pPAK1/2 using western blot analysis. Without drug treatment, Rac1 depletion resulted in strongly reduced PAK activity,

indicated by the substantial reduction of pPAK1/2 signal, while protein levels were decreased only moderately (Fig. 31). Due to the low pPAK1/2 signal intensities in Rac1-depleted cells, protein levels for PAK and pPAK were not quantified.

After three and six days of PLX-4032 treatment pPAK1/2 was substantially increased in n.t siRNA cells compared to DMSO treated n.t siRNA cells (Fig. 31B, C; n.t siRNA).

In contrast to n.t siRNA, PLX-4032 treatment in Rac1-depleted cells did not cause this upregulated pPAK level (Fig. 31B, C; siRac1). These findings support that Rac1-P29S activity is required for PLX-4032 mediated increase of pPAK in UKE-Mel-55b cells.

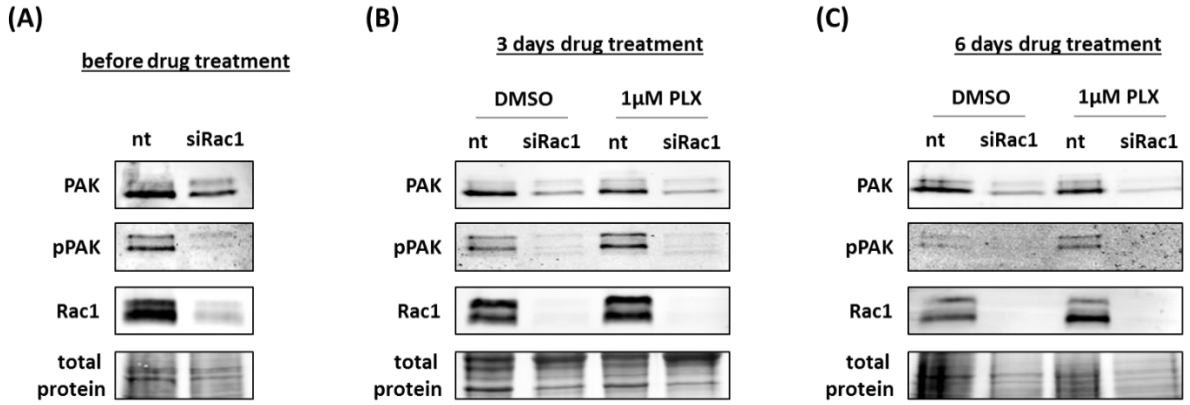

Figure 31: Rac1-P29S depletion in UKE-Mel-55b cells prevents enhanced phosphorylation of PAK1/2 induced by PLX-4032 treatment. Rac1-P29S expressing cell line UKE-Mel-55b was first treated with n.t siRNA and siRac1 for 72 h, re-plated for additional 24 h before treatment with DMSO or 1 µM PLX-4032 started. After 3 and 6 days of drug treatment, cells were lysed and western blot analysis for was performed to measure Rac1 depletion, PAK protein and pPAK level. Representative western blot images are shown in **(A)** for before drug treatment: n=3; **(B)** 3 days of drug treatment: n=3; **and (C)** 6 days of drug treatment: n=2 independent experiments.

3.4.3 Rac1-P29S expression partially prevents reduction of ERK activity upon BRAF inhibition

To determine whether the Rac1-P29S mutant affects MAPK signaling under PLX-4032 treatment, activity of the MAPK protein ERK1/2 was analyzed in both melanoma cells lines. Western blot studies were performed to measure ERK1/2 protein and pERK1/2 levels after three, six and nine days of inhibitor treatment and the pERK/ERK ratio was calculated to quantify relative activity (Fig. 32). After three days, both cell lines exhibited a significant reduced ERK1/2 activity after BRAF inhibition as compared to DMSO control (Fig. 32B). However, while the decrease upon PLX-4032 was almost complete in the Rac1-wt cell line (Ma-Mel-86c pERK/ERK 3 days: 2.9 % ± 0.1 SEM; 6 days:

10.5% ± 0.5 SEM; 9 days: 9 %), ERK1/2 activity in cells with Rac1-P29S remained at higher level at three days drug treatment and seemed even to recover throughout the experiment (UKE-Mel-55b pERK/ERK 3 days: 22 % ± 2.3 SEM; 6 days: 38 % ± 6 SEM; 9 days: 37 %). Interestingly, Rac1-P29S protein levels in UKE-Mel-55b cells also increased upon six and nine days of PLX-4032 treatment, which correlated with increase of ERK1/2 suggesting a molecular link between these signaling pathways (Fig. 32A).

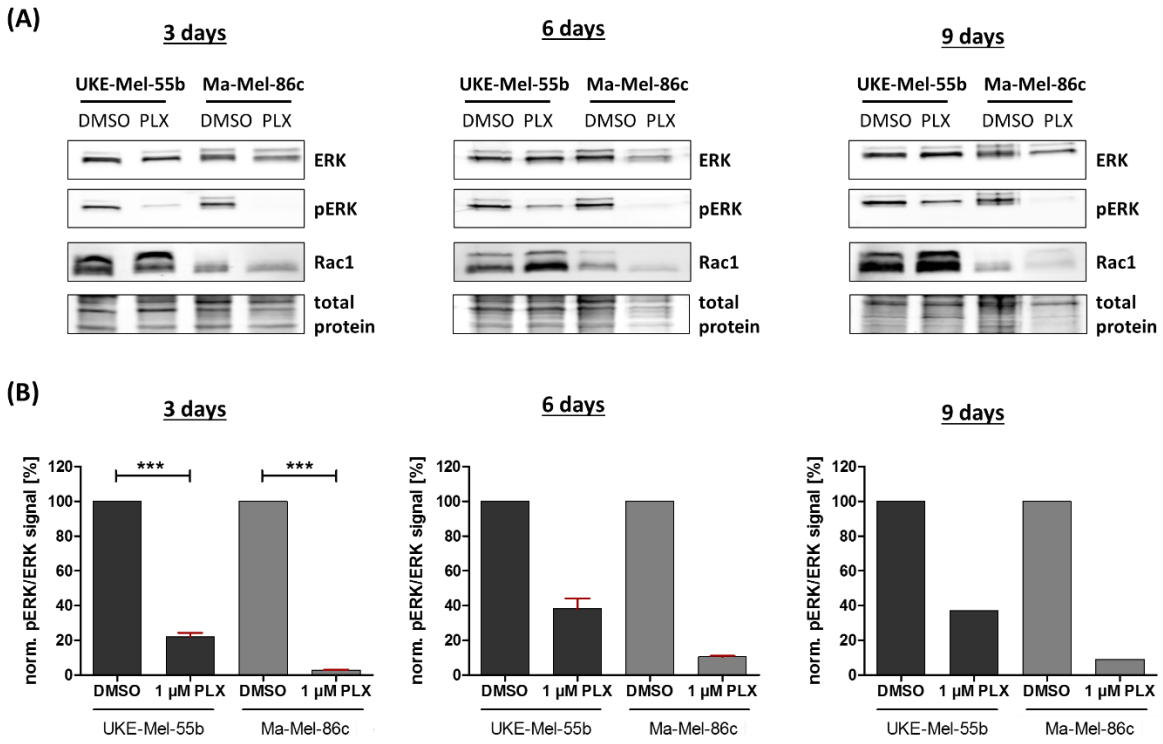

Figure 32: ERK1/2 activity in Rac1-P29S expressing melanoma cells is not fully inhibited upon BRAF inhibitor treatment. Protein levels of ERK1/2, pERK1/2 (pT202/pY204) and Rac1 were analyzed after 3, 6 and 9 days PLX-4032 treatment in both melanoma cell lines. **(A)** Representative western blots for the indicated time-points. **(B)**. Protein signals were first normalized with total protein amount and values for DMSO treated cells were set to 100%. The ratio pERK/ERK describes relative ERK1/2 activity. N=3 experiments for 3 days. N=2 experiments for 6 days and n=1 experiment for 9 days of drug treatment. Statistical analysis was performed with column statistic, one-sample t-test against 100. p<0.0001:***. Error bars indicate SEM.

Overall, we found that relative pERK1/2 levels were considerably reduced under BRAF inhibition and Rac1 activity in UKE-Mel-55b cells might compensate for the loss of BRAF signaling and thus prevent complete decrease of ERK1/2 activity upon PLX-4032 treatment. To test this idea, we next analyzed ERK1/2 activation level after depletion of Rac1-P29S in this cell line. The n.t siRNA cells under DMSO treatment were defined as a control group in order to analyze the effects of Rac1 depletion and PLX-4032 treatment individually and in combination.

Rac1-P29S protein levels dropped by more than 80 % after 72 hours in Rac1 siRNA-treated cells as compared to control treatment (n.t siRNA: 100 %; siRac1: 16.5 % ± 5.1 SEM) (Fig. 33; left). At three and six days of drug treatment, Rac1 knock-down was almost complete with barely detectable signal levels in western blot images (Fig. 33; middle, right). In contrast, we measured increased Rac1 expression levels when cells were treated with PLX-4032 in n.t siRNA conditions as has been already observed before (3 days DMSO: n.t siRNA: 100 %; siRac1: 7.3 % ± 1.8 SEM) (PLX-4032: n.t siRNA: 127.1 % ± 20.2 SEM; siRac1: 3.5 % ± 1.7 SEM) (Fig. 33; middle).

Rac1 knock-down in untreated cells (DMSO) lead to a substantial reduction of ERK1/2 activity after 72 hours siRNA treatment (n.t siRNA: 100 %; siRac1: 55 % ± 3.5 SEM) (Fig. 33; left). This effect on ERK1/2 activity was constant after three days and slightly reduced after six days of drug treatment (DMSO pERK/ERK n.t siRNA: 100 %; 3 days: siRac1: 56.4 % ± 2.4 SEM; 6 days: siRac1: 37.2 % ± 35.2 SEM) (Fig. 33; middle, right). As also found in the previous section without siRNA (Fig. 32), PLX-4032 treatment of n.t siRNA-treated cells resulted in significantly reduced ERK1/2 activity levels after three days, and similar reduction was observed at six days of treatment (pERK/ERK 3 days PLX-4032: n.t siRNA: 28.8 % ± 1.5 SEM; 6 days: n.t siRNA: 40.1 % ± 10. SEM) (Fig. 33; middle, right). In cells that were both, depleted of Rac1-P29S and treated with PLX-4032, we found that the effect of decreased ERK1/2 activity at three days drug treatment was additive compared to the individual treatments (pERK/ERK 3 days PLX-4032: 3 days: 12.2 % ± 5 SEM; 6 days siRac1: 15.9 % ± 15.9 SEM) (Fig. 33; middle, right). Again, similar effects were observed at six days of drug treatment, however, values at this time point fluctuated rather strongly between the individual experiments as represented by the high standard error (DMSO: n.t siRNA: 100 %; siRac1: 37.2 % ± 35.2 SEM) (Fig. 33; right).

Thus, our results provide evidence that the Rac1-P29S mutant prevents complete MAPK inactivation downstream of BRAF inhibition in UKE-Mel-55b cells.

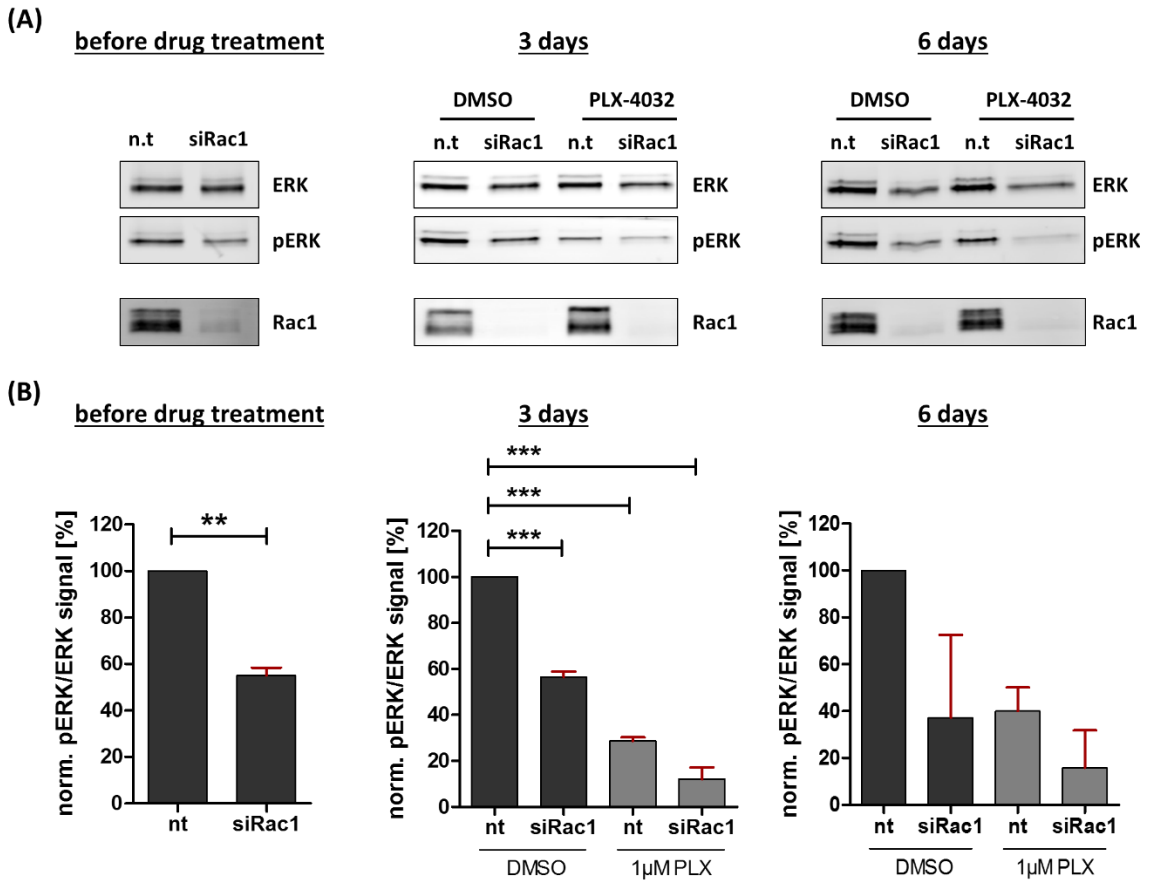

Figure 33: Rac1-P29S depletion UKE-Mel-55b cells augments decrease of ERK1/2 activity upon BRAF inhibition. The Rac1-P29S expressing UKE-Mel-55b melanoma cells were first treated with n.t siRNA and siRac1 for 72h. After three days, cells were re-plated and after additional 24 h, treatment with DMSO or 1 µM PLX-4032 was started (3 days vs. 6 days drug treatment). **(A)** Representative western blot images for all time points with protein signals for Rac1, pERK1/2 and ERK1/2. **(B)**. Graphs for calculated pERK/ERKT signaling activity. Protein signals were first normalized with total protein amount and values for DMSO treated cells were set to 100%. The ratio pERK/ERK describes relative ERK1/2 activity. Before drug treatment: n=3; 3 days drug treatment: n=3; 6 days drug treatment: n=2 individual experiments. Statistical analysis was performed with two-tailed t-test, unpaired for condition – before drug treatment. Statistical analysis was performed with a One-Way-Anova test, post-test: Dunnett`s Multiple Comparison Test for three and six days drug treatment; $P<0.05$:*, $p<0.001$:**, $p<0.0001$:***, ns=non-significant. Error bars indicate SEM.

3.4.4 Endogenous Rac1-P29S is required for elevated YAP/TAZ activity in melanoma cells upon BRAF inhibition

Studies in primary melanoma suggested that high Yap/Taz activity promotes BRAF inhibitor resistance (Zanconato et al., 2016). In chapter 3.3.1 (Fig. 23), it was shown that Rac1-P29S mediates nuclear localization of the transcription coactivator Yap/Taz in

UKE-Mel-55b cells. As shown above, results also suggested that Rac1-P29S stimulates ERK1/2 activity in BRAF-inhibited cells. We next tested how this Rac1 mutant might control Yap/Taz activity in this context. For this purpose, we first used antibody staining to analyze Yap/Taz cellular localization via wide-field fluorescence microscopy at different time points of BRAF-inhibitor treatment in both melanoma cell lines (Fig. 34A) (experiments partially performed by a master student under my supervision (Ramminger, 2018)). As in the previous experiment (chapter 3.3.1; Fig. 23), we observed strongly elevated nuclear Yap/Taz localization in UKE-Mel-55b cells treated with DMSO and this was further augmented upon PLX-4032-treatment for three days (DMSO: 84.8 % ± 0.7 SEM, PLX-4032: 92.3 % ± 1.9 SEM). Unlike the UKE-Mel-55b cell line that express Rac1-P29S endogenously, Rac1-wt expressing Ma-Mel-86c cells showed significantly less nuclear Yap/Taz localization (Fig. 34B). However, treatment with PLX-4032 caused in this cell line a strong and significant increase in percentage of cells with nuclear Yap/Taz (Ma-Mel-86c DMSO: 31.8 % ± 5.6 SEM, PLX-4032: 68.6 % ± 6.7 SEM). Similar observations were made after nine days of drug treatment. Here, Rac1-P29S expressing cells still exhibited a high degree of nuclear localized Yap/Taz for both, DMSO control and PLX-4032 treatment, albeit no significant difference could be measured (DMSO: 90.5 % ± 3.1 SEM, PLX-4032: 92 % ± 2.9 SEM). In contrast, PLX-4032 treatment of Rac1-wt expressing Ma-Mel-86c cells resulted in enhanced nuclear Yap/Taz localization as compared to the DMSO control (9 days DMSO: 30.1 % ± 1.6 SEM, PLX-4032: 67.9 % ± 21.6 SEM).

As shown in chapter 3.4.1 (Fig. 28), Rac1-wt expressing Ma-Mel-55b cells are sensitive to PLX-4032-treatment. The significant increase of nuclear Yap/Taz in these cells after short-term inhibitor treatment could indicate an early response mechanism involving the hippo pathway. In contrast to the Ma-Mel-86c cell line (Rac1-wt), UKE-Mel-55b cells are capable of recovering proliferation during BRAF inhibitor treatment (Fig. 28) and the highly elevated basal Yap/Taz nuclear localization in these cells might underlie this recovery.

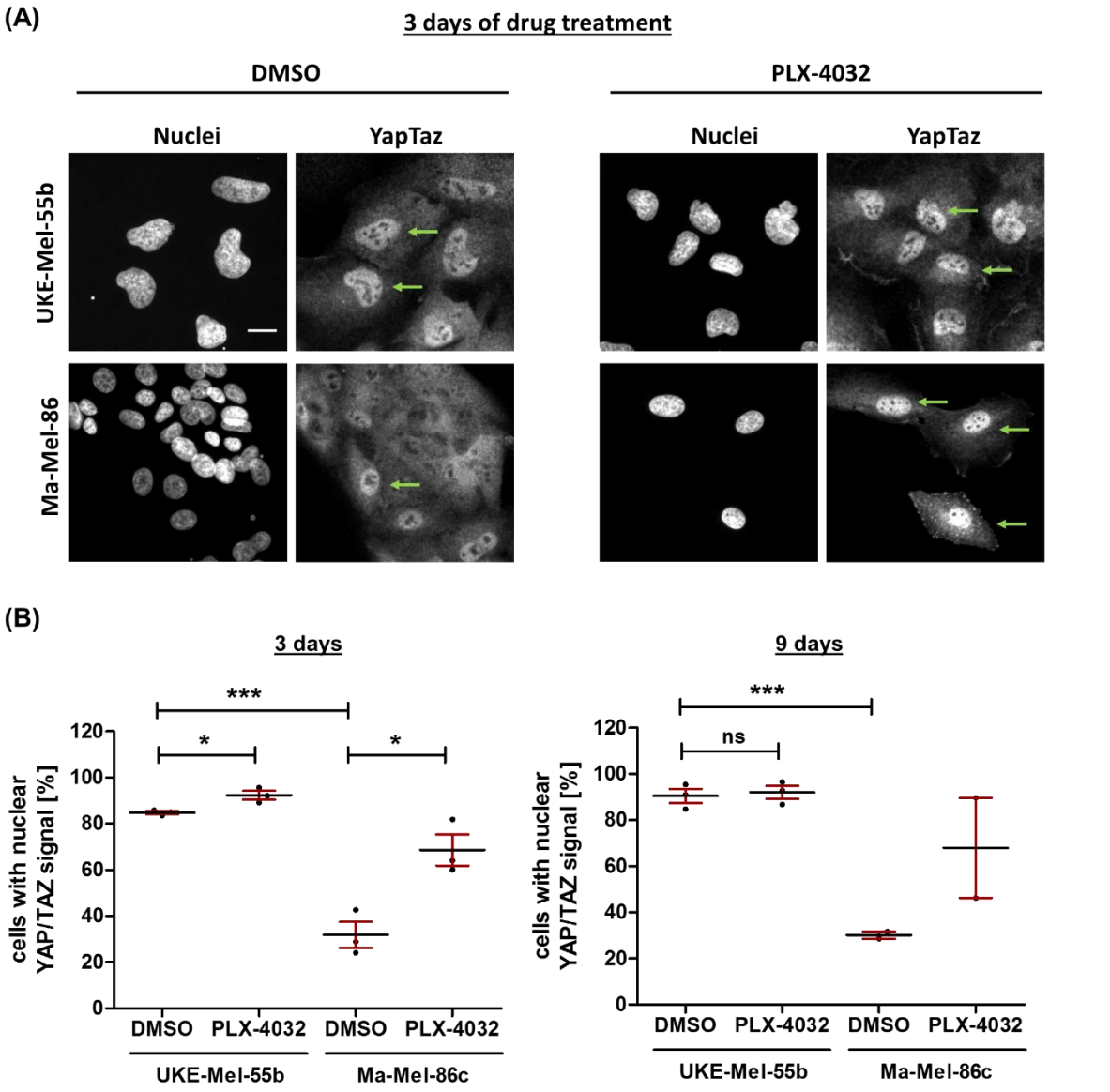

Figure 34: Distinct Yap/Taz response to PLX-4032 treatment in Rac1-P29S and Rac1-wt expressing melanoma cells. Melanoma cells were treated with DMSO as vehicle or Vemurafenib (PLX-4032) for three and nine days. **(A)** Representative wide-field microscopy images for nuclei (Hoechst 33342) and Yap/Taz staining after three days of treatment. Scale bar 30 µm. Examples for cells with nuclear Yap/Taz localization are highlighted with green arrows. **(B)** Graphs represent percentage of cells with nuclear Yap/Taz localization [%] (three days: n=3 experiments; nine days: n=2 experiments). Statistical analysis performed with two-tailed t-test, unpaired. P<0.05:*, p<0.001:**, p<0.0001:***, ns=non-significant. Error bars indicate SEM.

To further understand, how Rac1-P29S could control Yap/Taz activity, we combined PLX-4032 treatment with Rac1-P29S depletion. To do so, UKE-Mel-55b cells were treated with siRNA for 72 h and re-plated for 24 h before drug treatment was started. Cells were then fixed at the same time points as described above and stained with the Yap/Taz antibody (Fig. 35A).

In agreement with previously shown results (chapter 3.3.1, Fig. 23), we observed a relative high level of nuclear Yap/Taz in control cells (n.t siRNA), which was significantly reduced after Rac1 depletion, i.e. prior to drug treatment (n.t siRNA: 76.7 % ± 8.4 SEM; siRac1: 47.6 % ± 5.8 SEM) (Fig. 35B). After three days of drug treatment, nuclear Yap/Taz localization in DMSO control cells decreased significantly upon Rac1-depletion (DMSO: n.t siRNA: 62 % ± 12.8 SEM; siRac1: 21.1 % ± 1.9 SEM). In addition, lack of Rac1-P29S reduced nuclear Yap/Taz similarly to a dramatic low level in PLX-4032-treated cells, revealing that endogenous expression of Rac1-P29S in UKE-Mel-55b cells is required for maintaining activity of hippo transcription coactivators upon BRAF-inhibition (PLX-4032: n.t siRNA: 85.3 % ± 5 SEM; siRac1: 31 % ± 1 SEM).

After six days of DMSO treatment, we observed comparable levels of cells with nuclear Yap/Taz in the control (n.t siRNA) and Rac1 depleted group (DMSO: n.t siRNA: 51.3 % ± 8.2 SEM; siRac1: 47.9 % ± 9.5 SEM) (Fig. 35B). In contrast, after PLX-4032 treatment n.t siRNA cells exhibited more cells with nuclear Yap/Taz at the same time point, while Rac1 depletion resulted in a clearly reduce nuclear Yap/Taz localization (PLX-4032: n.t siRNA: 5.6 % ± 3.4 SEM; siRac1: 45.4 % ± 1.2 SEM) (Fig. 35B).

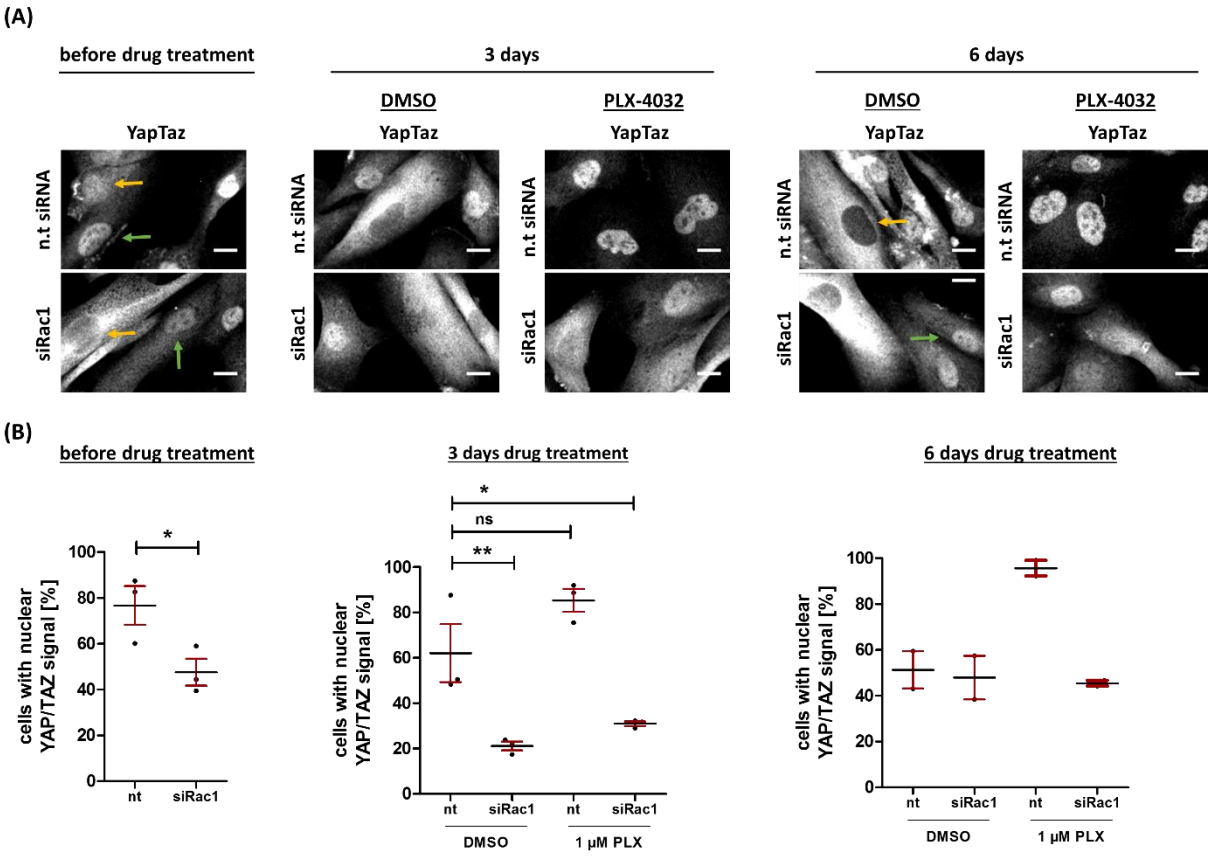

Figure 35: Depletion of endogenous Rac1-P29S reduces nuclear Yap/Taz localization in PLX-4032 treated UKE-Mel-55b cells. Rac1-P29S expressing UKE-Mel-55b cells were treated with n.t siRNA and siRac1 for 72h and re-plated for another 24 h before treatment with DMSO or 1 µM PLX-4032 was started. Cells were fixed after three days and Yap/Taz immunostaining with antibody was performed. **(A)** Representative wide-field fluorescence images of Yap/Taz immunostaining. Scale bar 20 µm. Cells with Yap/Taz located in the nuclei are marked with a green arrow. Negative result are highlighted with an orange arrow. **(B)** Graph shows percentage of cells with nuclear Yap/Taz [%].n=3 independent experiments. Statistical analysis was performed with a One-Way-Anova test, post-test: Dunnett`s Multiple Comparison Test with n.t siRNA (DMSO) as control; P<0.05:*, p<0.001:**, ns=non-significant. Error bars indicate SEM.

In summary, data in this section revealed that the highly active Rac1-P29S mutant is a key regulator for cellular morphogenesis and proliferation signaling in melanoma cells and provide evidence that the fast-cycling Rac1 mutant promotes proliferation and survival signaling via activation of the MAPK and Yap/Taz signaling under BRAF inhibitor treatment.

3.5. Potential role of other Rho-GTPases in proliferation and survival pathways in melanoma cells endogenously expressing Rac1-P29S

Cell proliferation in UKE-Mel-55b melanoma cells is majorly dependent on the endogenous expression of the highly active Rac1-P29S mutant variant (chapter 3.3). Moreover, partial recovery of MAPK signaling and Yap/Taz upon BRAF inhibition requires Rac1 signaling. Interestingly, we found that despite Rac1 depletion in this context, around 20% of UKE-Mel-55b cells were still able to proliferate upon PLX-4032 treatment (chapter 3.4; Fig. 29) and also Yap/Taz activity was not entirely diminished (chapter 3.4.4; Fig. 35). These findings suggested that additional signaling pathways that are independent of Rac1-P29S might be involved in the regulation of cell proliferation in these cells.

Importantly, localization and activity of the transcription coactivators Yap/Taz is regulated by F-actin dynamics and both Rac1 and RhoA have been reported to mediate this mechanism (Dupont et al., 2011; Seo and Kim, 2018). First studies from Kim *et al.* indicate that PLX-4032 treatment promotes actin remodeling and increase nuclear Yap/Taz level (Kim et al., 2016). Thus, we next investigated whether actin reorganization by Rho-GTPase proteins might underlie the elevated nuclear localization of Yap/Taz upon PLX-.4032 treatment. We first treated UKE-Mel-55b and Ma-Mel-86c cells with PLX-4032 and visualized the F-actin network using rhodamin-phalloidin staining followed by wide-field fluorescent microscopy imaging (Fig. 36). For both cell lines we observed, already after the first three days of PLX-4032 treatment, increased actin bundling (orange arrows) while DMSO treated control cells still generated the typical cellular morphology.

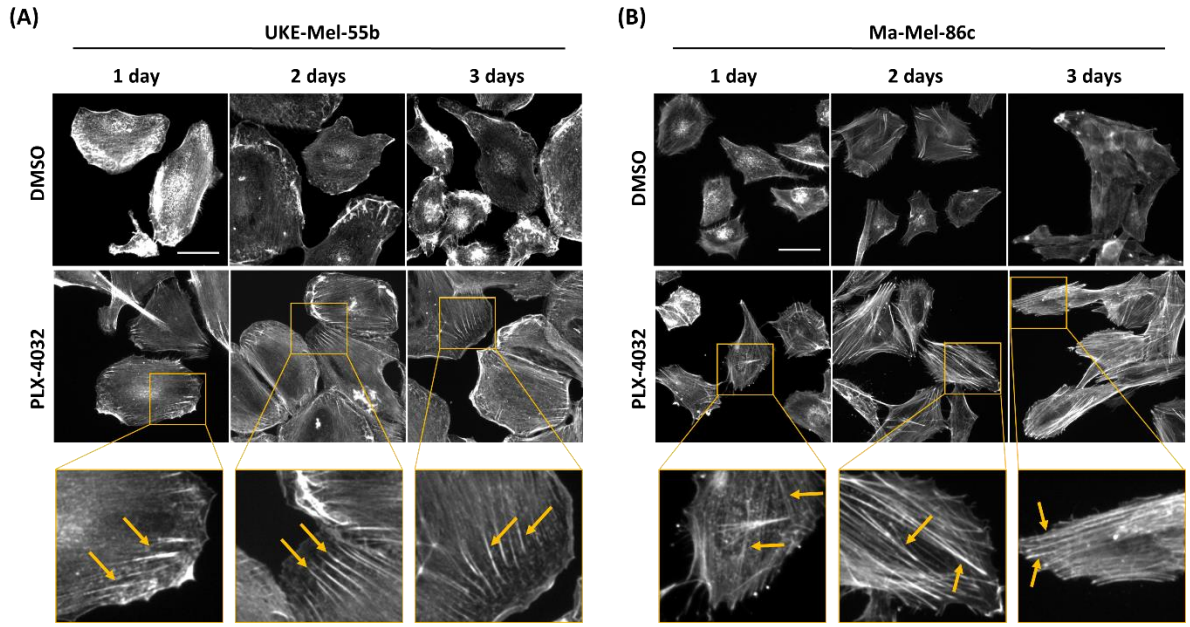

Figure 36: PLX-4032 treatment cause actin bundle formation in melanoma cell lines. Both melanoma cell lines were seeded on glass coverslips and cultured for 72 h with PLX-4032 and DMSO as control. **(A)** Representative wide-field images for F-actin (rhodamin-phalloidin) for Rac1-P29S expressing cells (UKE-Mel-55b). **(B)** Images for the Rac1-wt cell line (Ma-Mel-86c). Enlargements were shown for actin bundles under PLX-4032 treatment. Actin bundles are highlighted with orange arrows. Scale bar 50 µm.

As the effect was markedly pronounced after three days of treatment, we used this time point to determine whether the actin bundles are indeed contractile stress fibers and performed immunostaining with a Myosin-IIa antibody as a marker (Fig. 37A, B). While the Myosin-II signal in DMSO treated control cells was only localized in a few disordered regions similar to membrane ruffles, the signal was highly ordered in PLX-4032 treated cells and localized to distinct fibrous structures indicating stress fibers (Fig. 37A, B). In order to further confirm the formation of stress fibers in PLX-4032 treated melanoma cells, we also visualized cell-adhesions using antibody staining for the focal adhesion kinase (FAK) as marker (Fig. 37C, D). Wide-field imaging revealed that treatment with PLX-4032 resulted in strongly enhanced formation of focused dot-like structures that were localized to peripheral cell regions, whereas FAK positive dots in the control group were formed to a lesser extent and were of substantially smaller size (Fig. 37C, D; orange arrows). Together, data presented in this section confirmed that actin bundles, which are formed upon PLX-4032 treatment in both melanoma cells, are indeed contractile stress fibers.

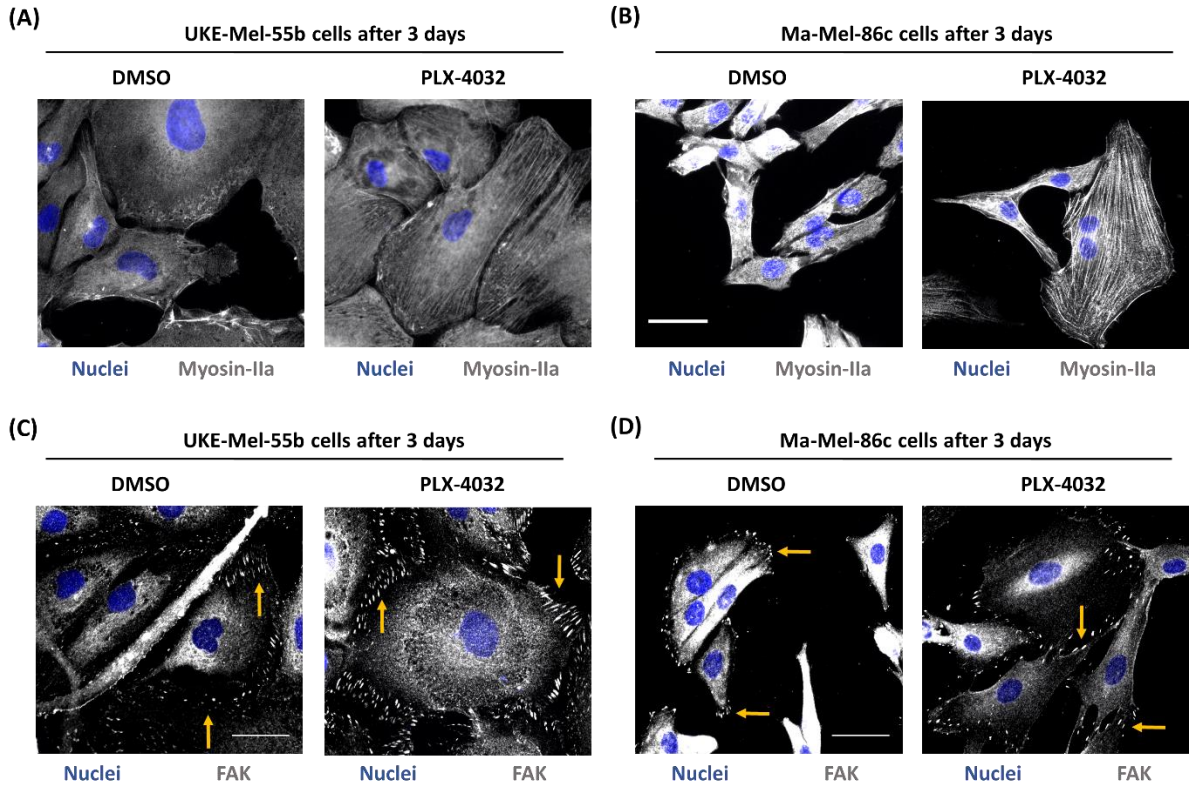

Figure 37: BRAF inhibition with PLX-4032 induced contractile stress fiber and focal adhesion formation after three days in melanoma cell lines. Both melanoma cell lines were seeded on glass coverslips and cultured for 72 h with PLX-4032 and DMSO as control. **(A+B)** Epi-fluorescent images with Hoechst 33342 for nuclei detection and for Myosin-IIa (anit-Myo2a AB) to determined, if the motor protein is localized to the actin bundles, which allows generating of contraction forces. Scale bar 50 µm. **(C+D)** Representative images for FAK localization (AB anti-focal adhesion kinase, FAK). Scale bar 50 µm. Peripheral localized FAK is highlighted with orange arrows.

Based on the finding that PLX-4032 treatment caused enhanced formation of stress fibers, we next studied the role of RhoA, the major regulator of cell contractility, in UKE-Mel-55b cells.

3.5.2 RhoA does not control basal ERK, AKT and Hippo signaling in Rac1-P29S expressing melanoma cells

Several studies have shown that RhoA controls multiple poliferation and survival pathways such as MAPK, AKT and Yap/Taz (Feng et al., 2014; Liu et al., 2004; Mahajan-Thakur et al., 2017).

To study the role of RhoA in these pathways in UKE-Mel-55b cells, we depleted RhoA by RNA interference and analyze protein activities of ERK1/2, AKT and Yap/Taz localization. Depletion of RhoA was highly efficient as measured by western blot analysis (Fig. 38A). Despite the strong decrease in RhoA protein level, activities of both ERK1/2 and AKT were not altered (pERK1/2/ERK1/2: n.t siRNA 100 %; siRhoA: 105.5 % ± 3.5 SEM pAKT/AKT: n.t siRNA 100 %; siRhoA: 100 % ± 9 SEM) (Fig. 38B).

As RhoA mediated actin stress fiber formation, it was previously associated to control activtiy of the transcriptional coactivators Yap/Taz (Seo and Kim, 2018). We also measured nuclear localization of these proteins after RhoA depletion in UKE-Mel-55b cells. Strikingly, depletion of RhoA did not alter nuclear Yap/Taz localization (n.t siRNA 79.6 %; siRhoA: 75 %; Fig. 38C) and caused only a minimal decrease in the proliferation rate, as estimated by ki-67 labeling (n.t siRNA 86.2 %; siRhoA: 70.4 %) (Fig. 38D).

Thus, RhoA does not seem to play a major role in proliferation and survival signaling in UKE-Mel-55b cells.

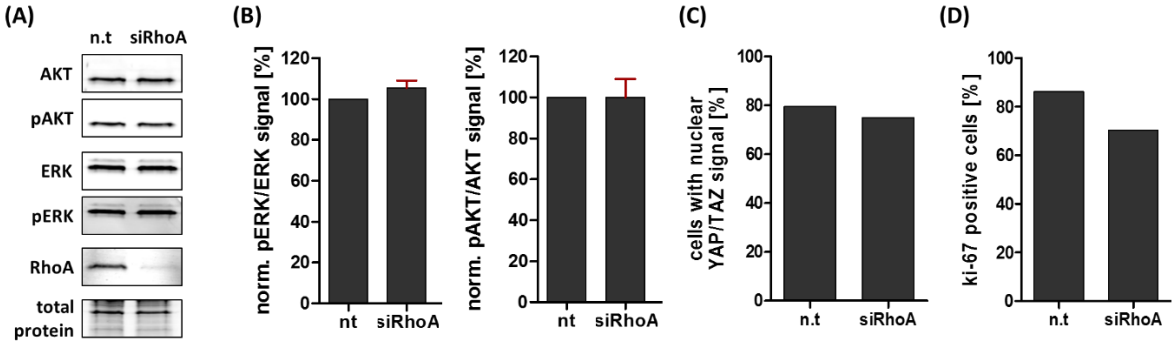

Figure 38: RhoA depletion did not affect proliferation and survival signaling in Rac1-P29S expressing melanoma cells. UKE-Mel-55b cells treated with n.t siRNA or siRhoA for 72 h. **(A)** Western Blots images for AKT, ERK1/2 and RhoA knock-down efficiency. **(B)** Graphs shown normalized protein signals compared to n.t siRNA as control (set to 100 % protein expression). N=2 experiments for RhoA depletion, ERK and AKT signaling. Error bars indicate SEM. **(C)** Graph with percentage of cells with nuclear Yap/Taz. **(D)** Graph with ki-67 positive [%] cells. Mean values from one experiment with five random images/condition.

3.5.3 RhoB and RhoC partially regulate nuclear Yap/Taz localization in melanoma cells with endogenous Rac1-P29S

The results shown above indicated that RhoA might not be an essential regulator of Yap/Taz activation in UKE-Mel-55b cells. This was surprising as RhoA was previously suggested to activate these transcriptional cofactors via control of contractile actin stress fibers.

Thus, we next tested if two closely related Rho proteins, RhoB and RhoC, which also promote stress fibers, might mediate the elevated Yap/Taz activity instead. In a first step, we confirmed the expression of RhoB and RhoC in both melanoma cells using western blot analysis (Fig. 39A). Next, we used the well-established C3 transferase based Rho inhibitor to inhibit all three, RhoA, B and C, simultaneously. After five hours of Rho-inhibitor treatment, UKE-Mel-55b cells were fixed and the actin cytoskeleton as well as Yap/Taz localization was assessed. As expected, treatment with the Rho-inhibitor caused dramatic morphological changes, including loss of membrane ruffles and formation of thin elongations instead (Fig. 39B). The percentage of cells with nuclear Yap/Taz localization was determined as described in previous experiments (chapter 3.3.1 Fig. 23). Similar as in the previous chapters, nuclear Yap/Taz localization in control UKE-Mel-55b cells was prominent (H_2O control: 87.2 % ± 2.5 SEM) (Fig. 39C). This value was clearly reduced when cells were treated with the Rho inhibitor (Rho inhibitor: 39 % ± 3.9 SEM, Fig. 39C), implicating that Rho protein activity is involved in the elevated nuclear localization of Yap/Taz.

However, as depletion of RhoA did not cause any effects on Yap/Taz localization in UKE-Mel-55b cells, these findings suggest that RhoB and RhoC may have a more prominent role in this context as compared to RhoA.

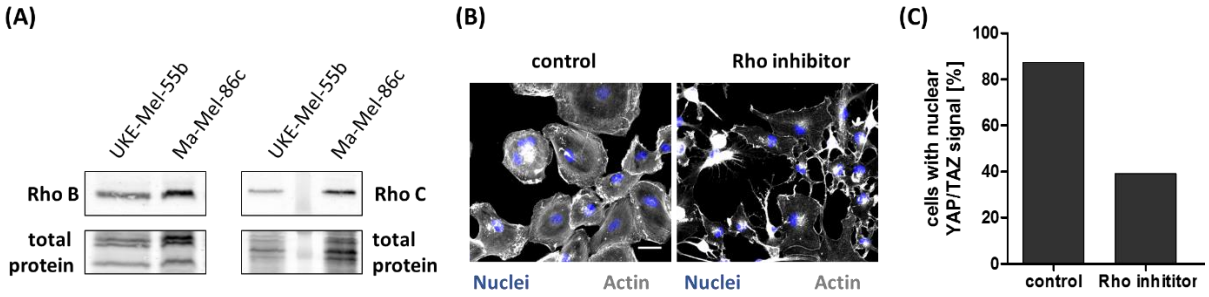

Figure 39: Inhibition of Rho-GTPases reduce nuclear Yap/Taz localization in UKE-Mel-55b melanoma cells. (A) Western blot images depicting RhoB and RhoC expression in both melanoma cells **(B)** Representative wide-field microscope images of the actin (rhodamin-phalloidin) cytoskeleton and nuclei (Hoechst 33324) after H_2O (control) or Rho inhibition. Scale bar 50 µm. UKE-Mel-55b showed disturbed actin organization. **(C)** Percentage of cells with nuclear Yap/Taz. N=1 experiment.

We found that Rac1-P29S substantially contributes to acquisition of BRAF inhibitor resistance of UKE-Mel-55b melanoma cells. Our Data also suggests that additional mechanisms, potentially involving other Rho proteins, are involved in the complex adaptation process to develop drug resistance. Thus, including these additional Rho signal network proteins could facilitate developing improved novel pharmacological treatment strategies of melanoma patients.

4. Discussion

The small Rho-GTPase Rac1 is an important key regulator in actin dynamics, which control cellular processes such as adhesion, morphodynamics and migration (Haga and Ridley, 2016). Moreover, Rac1 is involved in cell cycle progression, proliferation and cell survival (Hein et al., 2016; Watson et al., 2014). In particular, the highly active fast-cycling Rac1-P29S mutation was identified as new driver mutation in melanoma cells and was linked to tumor progression (Davis et al., 2013; Hodis et al., 2012). In addition, recent studies have implicated that this mutation might also contribute to adaptation of resistance to common BRAF inhibitor treatment in melanoma patients (Watson et al., 2014).

To understand how endogenous expression of the Rac1-P29S driver mutant contributes to tumor-related processes in melanoma, we studied two patient-derived melanoma cell lines. The Ma-Mel-86c cell line expresses the Rac1-wt and was served as a control, whereas the UKE-Mel-55b cell line expresses the fast-cycling Rac1-P29S mutant.

4.1 Endogenous Rac1-P29S induces enlarged circular cell shape and enhanced cell migration in melanoma cells

In contrast to melanoma cells that endogenously express Rac1-wt, cell morphology of cells expressing Rac1-P29S (UKE-Mel-55b) was predominantly circular and enlarged. In this study, we found that Rac1-P29S is required for this morphological phenotype. It is well-established that exogenous expression of active Rac1-variants, including the fast-cycling Rac1-P29S and the constitutively active Rac1-Q61L mutant, induces a highly dynamic cell phenotype with increased lamellipodia and membrane ruffle formation (Davis et al., 2013).

In agreement with this, we observed a higher degree of lamellipodia and membrane ruffle formation in the Rac1-P29S expressing melanoma cell line as compared to the Rac1-wt cell line. Membrane ruffles are generated when weakly adherent sheet-like membrane protrusions are formed, which loose contact with the substrate over time and fold subsequently back. In some cases, these structures can even propagate towards the dorsal cell side (Chhabra and Higgs, 2007). The pronounced phenotype in the UKE-Mel-55b cell line expressing the Rac1-P29S driver mutant was expected, as strong activation of Rac1

has long been known to promote lamellipodia dynamics and ruffling behavior. Using RNA interference and overexpression of siRNA-resistant mutants, we were able to confirm that endogenous expression of Rac1-P29S is indeed responsible for the dramatic ruffling phenotype, which was observed in the UKE-Mel-55b cell line. The formation of lamellipodia requires active Rac1 at the cell front (Ridley et al., 1992), where it promotes actin polymerization through activation of multiple downstream effectors. One of the best-characterized pathways is the activation of the actin nucleation factor Arp2/3 via WAVE (ASP-family verprolin-homologous protein) proteins, downstream of Rac1 (Chen et al., 2017; Steffen et al., 2004). Actin nucleation by this complex facilitates the formation of the dendritic branched actin network, characteristic for lamellipodia and membrane ruffles (Chhabra and Higgs, 2007; Goley and Welch, 2006). In addition to this direct effect on actin polymerization, Rac1 also activates PAK (p21-activated kinase) proteins, which phosphorylate and activate the LIM-kinase (LIMK), thereby causing inhibition of the F-actin disassembling protein cofilin (Manetti, 2012). As a result, activation of these distinct pathways by Rac1 promotes F-actin polymerization and formation of the dendritic actin network. Our data suggest that high Rac1 activity due to the P29S mutation reinforces these effects. In agreement with this, we found elevated PAK activity in Rac1-P29S expressing UKE-Mel-55b cells compared to Rac1-wt melanoma cells (Ma-Mel-86c). In addition, depletion of Rac1-P29S in UKE-Mel-55b cells resulted in strongly reduced PAK activity. Furthermore, inhibition of cofilin by the LIM-kinase, can induce a positive feedback loop to activate Rac1 via PL-D1 (phospholipase D1) and the Rac1-specific GEF DOCK2 (Dedicator of cytokinesis 2) (Bamburg and Bernstein, 2010). Interestingly, PL-D1 was found to correlate with cell polarity and motility in cancer cells by recruiting Rac1 to the leading edge (Zhang and Frohman, 2014). Riebeling *et al.* showed that melanoma cells have a higher expression level of PL-D1 compared to melanocytes (Riebeling et al., 2003). Moreover, high protein levels for PL-D1 were observed in metastatic and superficial spreading melanoma cells and were correlated with high invasive potential (Oka et al., 2003). Albeit the highly elevated activity of the driver mutant Rac1-P29S in UKE-Mel-55b cells, it is also possible that further stimulation of Rac1 signaling is facilitated by an enhanced positive feedback loop involving the PL-D1/DOCK2 pathway.

Depletion of Rac1-P29S in UKE-Mel-55b cells cause actin remodeling ranging from upregulated lamellipodia and membrane ruffle formation to stress fiber formation. While lamellipodia and membrane ruffles are linked to Rac1 activity, stress fiber formations is

typically associated with RhoA signaling (Hall, 1998). Several studies have described a mutual antagonistic relationship between the GTPases Rac1 and RhoA. The RhoA/ROCK pathway causes inhibition of Rac1 by activating Rac1 GAPs such as FilGAP or ArhGAP22 (Ohta et al., 2006; Parsons et al., 2010). In contrast, Rac1 can inhibit RhoA in different ways. First, it can either directly activate specific RhoA GAPs such as p190RhoGAP to facilitate the GTP hydrolysis or inhibit RhoA GEFs (e.g. GEF-H1) via activation of PAK signaling (Nimnual et al., 2003; Parsons et al., 2010; Zenke et al., 2004). Both have a reducing effect on RhoA signaling due to Rac1 activation. This can explain why we observed increased membrane ruffling and less stress fiber formation in Rac1-P29S melanoma cells as compared to Rac1-wt cells. Thus, we suggest that the increased Rac1 activity caused by the Rac1-P29S mutation inhibits RhoA more efficiently than the Rac1-wt form. Moreover, Rac1 depletion causes enhanced RhoA activity and thus promotes stress fiber formation in Rac1-depleted UKE-Mel-55b cells.

The coordinated formation of dynamic actin-based protrusions together with integrin-based cell substrate adhesions is essential for efficient cell spreading in cellular processes such as cell migration (Huveneers and Danen, 2009; Lawson and Burridge, 2014). Multiple independent studies in various cell lines showed that elevated Rac1 activity correlates with extended cell area (Chang et al., 2011; Vidali et al., 2006). Data presented in this work, showed that endogenously expressed Rac1-P29S in UKE-Mel-55b cells was essential for both, the significantly enlarged cell area and formation of large peripheral cell-matrix adhesions. To investigate effects of the Rac1-P29S mutant on the formation of cell-matrix adhesions, we studied the localization of key adhesion-associated proteins such as Paxillin and the focal adhesion kinase (FAK). Similar to Rac1-wt and Rac1-P29S overexpression studies in A375 cells (Mohan et al., 2019), our data in U2-OS cells showed, that overexpression of EGFP-Rac1-wt, EGFP-Rac1-P29S and EGFP- Rac1-Q61L induced Paxillin re-localization from the cytosol to focal complexes in the cell front and that this process is correlated with Rac1 activity (supplementary data). Endogenous expression of Rac1-P29S in UKE-Mel-55b cells leads to Paxillin recruitment to focal complexes in the cell front. This Paxillin localization to focal complexes was not detectable after Rac1 depletion in UKE-Mel-55b cells, but could be restored by overexpression of siRNA-resistant EGFP-Rac1-wt and EGFP-Rac1-P29S constructs. Such cell-substrate adhesions mediate transduction of extra cellular signals to intracellular response (Hynes, 2002). Integrins are activated by ECM substrate binding and act as receptors during signal

transmission (Hynes, 2002). Integrin-mediated cell-surface signaling recruited the scaffold protein Paxillin to nascent adhesions and focal complexes in an early state of adhesion formation (Lopez-Colome et al., 2017). Paxillin can then form different multi-protein complex, which activate different signaling pathways. We speculate that the complex formation with the Rac1 specific GEF β-PIX and the Rac1 effector PAK1/2 could be involved in the observed upregulated adhesion and lamellipodia formation that was observed in UKE-Mel-55b cells (Fig. 40) (Nayal et al., 2006; Tang et al., 2018). There, Paxillin is recruited by integrin heterodimers and can be activated via phosphorylation by pPAK1 (Clayton and Ridley, 2020). Paxillin phosphorylation enables the binding to the adaptor protein GIT1 (G-protein-coupled-receptor-kinase–interacting-protein-1) and facilitates the localization of β-PIX and PAK to focal complexes (Nayal et al., 2006). β-PIX can then directly activate Rac1 to stimulate actin polymerization and induces a positive feedback loop over PAK (Tang et al., 2018). We performed western blot studies to analyze β-PIX expression and PAK activity in both melanoma cells. Our results confirmed that both cell lines express similar levels of β-PIX (supplementary data). PAK1/2 are important downstream effectors of Rac1 (Clayton and Ridley, 2020). Interestingly, active PAK1/2 has been observed only in UKE-Mel-55b cells, whereas we could not detect any PAK phosphorylation in the Ma-Mel-86c cell line. An increased PAK1/2 activity together with Rac1-P29S expression was recently observed in mouse melanocytes (Lionarons et al., 2019). In line with previous observations in mast cells (Kosoff, 2015), we detected high activity of PAK2 and lower activity for PAK1 in UKE-Mel-55b melanoma cells. Both, PAK1 and PAK2 activity was significantly reduced after Rac1 depletion in UKE-Mel-55b cells. Thus, we suggest that higher Rac1 activity (Rac1-P29S) is responsible for the upregulated PAK signaling in UKE-Mel-55b cells.

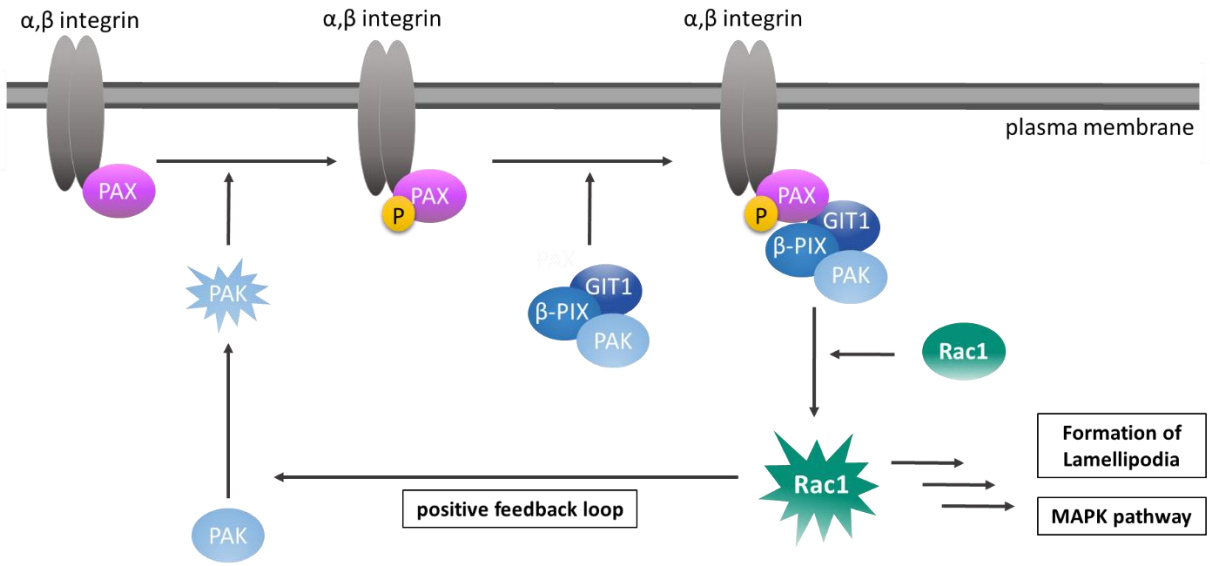

Figure 40: Model for Paxillin-induced Rac1 recruitment to focal complexes. Active integrin dimers bind Paxillin in an early state of adhesion formation. Active Rac1 binds and activates PAK, which facilitates phosphorylation of Paxillin on Ser273. This enables Paxillin binding to the GIT1/β-PIX/PAK complex. Rac1 in turn can interact with the multi-protein complex, becomes activated via the GEF β-PIX, and binding to PAK enables direct downstream signaling. This results in actin polymerization, proliferation and in a positive feedback loop. Modified from (Huveneers and Danen, 2009; Nayal et al., 2006; Tang et al., 2018).

Rac1-wt expression and limited PAK signaling in Ma-Mel-86c cells indicated less Rac1 signaling activity. Accordingly, lower Rac1 activity resulted in less pronounced RhoA inhibition, which enabled increased stress fiber formation in Rac1-wt expressing melanoma cells. We hypothesize, that active Rac1-P29S enhanced PAK1/2 activity, which then promoted focal complex formation over the Paxillin/GIT1/PAK/β-PIX complex. Both, the enhanced Rac1-P29S recruitment to focal complexes and the increase actin polymerization due to the higher Rac1 activity can explain the striking cell morphology in UKE-Mel-55b cells.

In addition to the described positive feedback mediated by Paxillin/GIT1/β-PIX/PAK complex, Paxillin can further recruit the focal adhesion kinase (FAK), resulting in the activation of various signaling pathways (Huveneers and Danen, 2009; Lopez-Colome et al., 2017). FAK binding can phosphorylate Paxillin at Tyr118, which then promotes binding of DOCK180 (Rac1 GEF) and induces Rac1 activation (Huveneers and Danen, 2009; Kiyokawa et al., 1998; Lopez-Colome et al., 2017). Therefore, we performed western blot studies to analyze the activation status of FAK in both melanoma cell lines. Interestingly, Rac1 depletion caused different effects in the two melanoma cell lines. Rac1-wt cells showed a reduced FAK activity after Rac1 knock-down, whereas we

observed an upregulated FAK activity in Rac1-P29S expressing cells. These findings suggest that the fast-cycling Rac1-P29S mutant has a negative regulatory effect on FAK activity compared to Rac1-wt. Moreover, we investigated the localization of FAK in UKE-Mel-55b cells after Rac1 knock-down with fluorescent microscopy. Cells, expressing Rac1-P29S, exhibited varying FAK localization patterns. While we observed cells with clear FAK localization to focal complexes in the cell periphery, other showed only weak adhesion formation. In agreement with our western blot results, we detected a more homozygous population with clear FAK localization to cell-matrix adhesions after Rac1-P29S depletion in UKE-Mel-55b cells. While Rac1 is required for the early formation of nascent adhesions and focal complexes, RhoA is involved in adhesion maturation to generate focal adhesions (Parsons et al., 2010). Together with our findings that Rac1-P29S depletion enhances stress fiber formation in UKE-Mel-55b cells, we speculate that increased RhoA activity facilitates focal adhesion maturation after Rac1 depletion. Therefore, localized RhoA activation at the lamellum and cell rear facilitates Myosin II phosphorylation via ROCK (Rho-associated protein kinase) signaling, which sustains adhesion maturation (Parsons et al., 2010). In contrast, Rac1 promotes ERK1/2 activation, which is associated with the phosphorylation of Paxillin and the re-localization from focal complexes to the cytosol and therefore control adhesion turnover (Woodrow, 2003). Here, we could confirm that the fast-cycling Rac1-P29S is indeed responsible for lamellipodia and membrane ruffle formation in UKE-Mel-55b cells. We showed that this mutant induces formation of nascent adhesions and focal complexes via Paxillin localization and reduces activity of the focal adhesion kinase. We hypothesize that the higher Rac1 activity in the mutant can suppress RhoA more efficient than Rac1-wt, which enables the formation of this striking phenotype in UKE-Mel-55b cells.

Since our data indicate a strong influence of Rac1-P29S in adhesion behavior, we further analyzed the cell behavior on different extra-cellular matrix (ECM) components. Collagen I was used to promote integrin-mediated signaling, poly-L-lysine (PLL) for electrostatic interactions as well as an uncoated glass surface. Poly-L-lysine is a synthetic cationic polymer, which absorbs onto glass surfaces. There, its cationic sites are exposed so that it can interact with the anionic sites of cell surfaces to facilitate cell adhesion (Mazia et al., 1975). This kind of cell adhesions does not require protein activity or specific protein interactions and therefore promotes cell adhesion exclusively by electrostatic interactions. We observed fast cell adhesion on PLL for both melanoma cell lines in our

adhesion assays during the first 15-90 min. Rac1-wt expressing melanoma cells showed less cell adhesion on glass and collagen I compared to PLL. Interestingly, we observed similar cell adhesion on PLL, collagen I and glass for the UKE-Mel-55b cell lines, while depletion of Rac1 resulted in reduced cell adhesion on glass. Together with our results that Rac1-P29S promotes the formation of early adhesions by Paxillin recruitment, we suggest that cells expressing the fast-cycling Rac1-P29S mutant have an upregulated adhesion formation, which enables fast cell adhesion on different ECM substrates. In contrast, lower Rac1 activity in Ma-Mel-86 cells caused a slowdown of cell adhesion.

In addition to cell adhesion behavior, we studied the cell spreading behavior of both melanoma cell line on glass, collagen I and PLL. Both cell lines showed a clearly enhanced cell spreading on glass and collagen I as compared to PLL. This could be facilitated by the high Rac1 activity and integrin-mediated pathways, which activate Rac1 in an early cell spreading state. After 24 h, Rac1-wt cells exhibit only a small round cell shape in PLL, while we observed small populations with spreaded cells for the Rac1-P29S expressing cell line (UKE-Mel-55b). Our results suggested a correlation between cell spreading, cell survival and proliferation and that the expression of Rac1-P29S promoted these cell processes in an ECM-independent way. We speculate that PLL has only a cell adhesion advantage in early adhesion states in Rac1-wt cells, but is not sufficient to facilitate cell survival or proliferation, indicated by the small round cell shape on PLL after 24 h.

Rac1-P29S depletion in UKE-Mel-55b cells caused the previously described phenotype switch to higher stress fiber formation and reduced cell area on all three substrates. Albeit, the effect was even stronger on PLL, indicating that other integrin-mediated pathways could be involved in cell spreading behavior in UKE-Mel-55b cells. We speculate that the induced RhoA activity after Rac1 depletion may be involved in later stages of cell spreading. RhoA facilitates stress fiber formation, which includes phosphorylation of Myosin II. Several studies have shown that cell spreading could be regulated over force-induced activation of protein kinases on focal adhesions (Nisenholz et al., 2014). Although the detailed mechanism is still under debate, several Rho GEFs such as p115GEF, LARG and p190RhoGEF haven been suggested to be involved in these pathway (Huveneers and Danen, 2009).

While formation of cell-matrix adhesions in UKE-Mel-55b cells was clearly detectable on glass and collagen I coated surfaces, only a few cells exhibited these prominent adhesion

structures on PLL. Thus, upon initial adhesion, cell spreading on PLL appeared delayed, likely due to the lack of integrin-mediated activation of Rac1 by via β-PIX or DOCK180 (Kiyokawa et al., 1998; Nayal et al., 2006). Nevertheless, we observed elevated early cell adhesion and cell spreading on all three substrates, when cells endogenously expressed Rac1-P29S (UKE-Mel-55b) as compared to Rac1-wt expressing cells (Ma-Mel-86c), suggesting that presence of Rac1-P29S enables other signaling pathways during adhesion and spreading that also contribute. Marcoux and Vuori reported Rac1 activation as a result of EGFR (epidermal growth-factor receptor) signaling, which could be activated by growth factors stimulation or by integrin-mediated signaling (Marcoux and Vuori, 2003). Our collaborator detected upregulated protein levels of the EGF-receptor in UKE-Mel-55b cells as compared to the Rac1-wt cell line (Paschen, unpublished data). Taken together these findings can explain how Rac1-P29S expressing cells adhere and spread in the absence of integrin-mediated adhesion formation.

Interestingly, 2D migration of Rac1-P29S expressing cells (UKE-Mel-55b) was not affected by different substrates, but was substantially reduced after Rac1-P29S depletion on both, glass and collagen I. Unexpectedly, the migration velocity slightly increased on PLL after Rac1 knock-down. Thus, similar migration behavior of UKE-Mel-55b cells on different substrates as well as the integrin-independent adhesion behavior suggests that the endogenous expression of the Rac1-P29S mutant in melanoma cells enables adaptation of cell migration to changing extracellular matrix environment during tumor progression and acquisition of invasive behavior.

4.2 Role of Rac1-P29S in cell proliferation and survival signaling

Most melanoma patients harbor an activating mutation in the oncogene BRAF, which promotes upregulation of the MAPK signaling pathway and enhances cell proliferation (Ascierto et al., 2012; Holderfield et al., 2014). Previous studies also reported that the fast-cycling Rac1-P29S mutation can also increase MAPK signaling through PAK and ERK activation (Krauthammer et al., 2012; Lionarons et al., 2019).

As reported recently for other human melanoma cell lines (Lionarons et al., 2019), we also found that endogenously expressed Rac1-P29S was required for efficient cell proliferation as measured by the proliferation marker ki-67, while Rac1-wt expressing

cells were not markedly sensitive to Rac1 depletion. Thus, we propose that the higher activity in the Rac1-P29S mutant is more involved in proliferation signaling than the Rac1-wt form.

Several studies have shown that Rac1 activates proliferation-related signaling pathways such as MAPK signaling in melanoma cells (Wang et al., 2010; Watson et al., 2014). For example, RNAi studies showed that Rac1-P29S was required for elevated activity of MEK and ERK proteins in the melanoma cell line IGR1 (Watson et al., 2014). In agreement with these reports, we observed that depletion of Rac1-P29S significantly reduced ERK1/2 activity in UKE-Mel-55b cells, while ERK1/2 activity was not altered in Ma-Mel-86c cells with endogenous Rac1-wt. Thus, MAPK signaling is activated by the fast-cycling Rac1 mutant in UKE-Mel-55b cells and further promotes cell proliferation in addition to the already enhanced proliferation by the constitutively active BRAF mutation in melanoma. Moreover, the contrasting effects of Rac1 depletion in the different cell lines suggest that its role in MAPK signaling strongly depends on the Rac1 activity level.

In addition to the MAPK pathway, Rac1 was also shown to be involved in the control of the cell cycle and survival signaling via activation of the multifaceted kinase AKT. Studies in human prostate cancer cells have shown that Rac1 controls cyclin D1 expression and thus regulates S-phase transition (Ewen, 2000; Fournier et al., 2008; Yoshida et al., 2010). This process could be mediated via activation of PAK1, which phosphorylates AKT leading to cyclin D1 expression (Zins et al., 2013). Consistent with this mechanism, our study revealed markedly reduced AKT activity upon Rac1 depletion in both Rac1-P29S and Rac1-wt expressing melanoma cells. Interestingly, proliferation in melanoma cells that express Rac1-wt (Ma-Mel-86c) was not reduced upon Rac1 depletion despite having reduced AKT activity. This persistent proliferation level suggests that Rac1-independent proliferation signaling exists in these cells. This observation is also in agreement with our finding that ERK1/2 activity in the Rac1-wt cell line is not reduced upon Rac1 depletion. Taken together, the results in both melanoma cell lines suggest that cells with higher Rac1 activity are more dependent on Rac1 signaling pathways to control cell proliferation than Rac1-wt expressing cell lines.

Interestingly, multiple independent studies also suggest a reciprocal relationship between Rac1 and AKT (Murga et al., 2002; Zhu et al., 2015). Besides AKT activation via Rac1 signaling (Murga et al., 2002), AKT activity induced by EGF-receptor (EGFR) signaling was shown to stimulate Rac1 activity via activation of the Rac1-specific GEF

Tiam1 by PI3K (phosphatidylinositol 3-kinase) in several cancer cell lines (Zhu et al., 2015). Based on the reduced AKT activity after Rac1 depletion, we propose that UKE-Mel-55b cells primarily activate AKT via Rac1. Due to increased EGFR expression in these cells (Paschen, unpublished data), it is also conceivable that there is a combination of both pathways. This could then generate a positive feedback loop from AKT to Rac1 via Tiam1 and reinforce the signal pathway (Zhu et al., 2015). However, such positive feedback mechanism are rather unlikely in the UKE-Mel-55b cells due to the already highly elevated level of Rac1 activity as consequence of the fast-cycling Rac1 mutant.

To investigate, if PAK proteins could mediate the effects of Rac1-P29S on cell proliferation and survival, we first used the chemical drug FRAX597 to inhibit PAK1/2/3 (supplementary data). Remarkably, ERK activity was significantly reduced upon PAK inhibition, while the proliferation rate (ki-67) and AKT activity were not altered. Several studies reveal that PAK could promote ERK1/2 activity by activation of RAF or MEK (Eblen et al., 2002; Lu et al., 2017). Here, we used RNAi to knock-down PAK1 and PAK2 and confirm the inhibitor findings as well as determine which PAK protein might have a dominant role in this process. We found that only PAK2 depletion cause reduced ERK activity, revealing that PAK2 is more critical in mediating Rac1 downstream signaling in UKE-Mel-55b cells as compared to PAK1. We also observed a slightly reduced proliferation rate upon PAK2 depletion, which we did not detect when we used pharmacological inhibition. This substantial difference in our findings might be due to the shorter time-course that was used for inhibitor treatment (1 h) as compared to siRNA treatment (72 h), potentially preventing long-term effects. Thus, our findings suggest that ERK1/2 activity in UKE-Mel-55b cells is regulated by PAK family kinases, while AKT signaling is independent of this pathway.

In accordance with the significant decrease of cell proliferation signaling, we also observed a reduced number of mitotic events in Rac1-P29S expressing UKE-Mel-55b cells after Rac1 depletion. Recent studies have implicated the Rac1/WAVE/Arp2/-induced branched actin network in the determination of entry into the S-phase (Molinie et al., 2019). The F-actin-rich lamellipodia structure promotes integration of proliferation signals from soluble growth factors such as EGF and mechanotransduced adhesion cues (Molinie et al., 2019). Thus, the disrupted dendritic actin network upon Rac1 depletion in UKE-Mel-55b cells could reduce cell proliferation as a result of perturbed cell cycle

progression. Moreover, we observed that Rac1-P29S expressing cells do not entirely retract their cell extensions during the early entry into mitosis and that these residual extensions appear to stabilize cell adhesion during the entire process of cell division. Upon Rac1 depletion, these extensions were lost and we observed a significantly elongated duration time for cell division. In particular, we observed that Rac1-depleted cells required significantly longer (40 min) from the time-point of the first cell rounding until the re-attachment of the two daughter cells. These findings suggest that Rac1 is not only involved in cell cycle control but also in the adhesion dynamics during cell division. Michaelson *et al.* reported Rac1 accumulation in the nucleus in late G2-phase, which canbe explained by the C-terminal nuclear-localization-sequence (NLS) of Rac1 (Michaelson
et al., 2008). In agreement with this, we observed fluorescently-tagged Rac1-P29S localizing to the nucleus in U2-OS cells (supplementary data). The re-localization of Rac1 during cell division could offer several advantages. Nuclear Rac1 might directly control gene transcription e.g. via STAT3 or NF-κβ to promote cyclin D1 expression. Studies in human breast cancer cell lines showed that cyclin D1 expression is regulated over the Rac1/NF-κβ pathway (Yoshida et al., 2010) and initial western blot studies showed that UKE-Mel-55b cells express NF-κβ (supplementary data). Thus, we propose that the high Rac1 activity in UKE-Mel-55b cells could control cell cycle progression also by this pathway. The lower Rac1-protein level upon Rac1 knock-down could reduce gene transcription and causes a time delay to reach necessary concentrations of mitotic regulators, which are necessary for cell cycle progression. Moreover, the enriched Rac1 in the nucleus promotes a fast release of Rac1 during cytokinesis and might enhance re-adheration of the daughter cells (Michaelson et al., 2008). The protein complex β-PIX/GIT1/PAK was shown to not only mediate adhesion formation, but also be involved in the regulation of spindle orientation during mitosis (Cernohorska et al., 2016; Zhao et al., 2005). We observed strongly reduced PAK1/2 activity upon Rac1 depletion in UKE-Mel-55b cells, which might cause defects on spindle orientation and delayed cell division.

In recent years, the transcriptional coactivators Yap/Taz have been implicated in multiple cellular processes such as proliferation, organ growth and survival (Fisher et al., 2017; Kanai et al., 2000; Sudol et al., 1995). Yap/Taz activity is mostly known to be regulated by the hippo-pathway, but is also affected by ECM stiffness and the actin cytoskeleton (Dupont et al., 2011; Moroishi et al., 2015; Seo and Kim, 2018). Once in the nucleus, it can

interact with DNA-binding proteins and inducesgene expression to control multiple cellular processes such as proliferation and survival (Cao et al., 2008; Fisher et al., 2017; Kim et al., 2013). Here, we observed differences in Yap/Taz activity between the two melanoma cell lines that carry different Rac1 variants. Rac1-P29S expressing cells showed high levels of nuclear located Yap/Taz, which indicate high Yap/Taz activity, while we found low nuclear levels in Rac1-wt melanoma cells. Furthermore, Rac1 knock-down significantly reduced the fraction of nuclear Yap/Taz in UKE-Mel-55b cells. In contrast, we did not observe changes in Yap/Taz localization in Rac1-wt expressing cells. Using RNAi and siRNA-resistant plasmids, we were able to restore the activity level of Yap/Taz in UKE-Mel-55b cells. These results confirm that the fast-cycling Rac1-mutant is indeed required for stimulation of the transcriptional coactivators in this cell system. Higher ECM rigidity and increased F-actin formation has been shown to upregulate Yap/Taz activity and facilitate nuclear localization (Dupont et al., 2011; Moroishi et al., 2015; Seo and Kim, 2018). Only in the non-phosphorylated form, Yap/Taz are translocated into the nucleus where they induce gene transcription (Cao et al., 2008; Fisher et al., 2017; Kim et al., 2013). Dynamic control of F-actin structures by Rac1 and RhoA has been suggested to induce de-phosphorylation of Yap/Taz (Dupont, 2016; Seo and Kim, 2018). This could explain the high level of active Yap/Taz in the Rac1-P29S expressing cell line. In this case, the enhanced Rac1 activity induces actin polymerization and causes cell spreading to promote Yap/Taz activation. It was previously reported that the two Rac1-specific GEFs STEF and Tiam2 promote the formation of the perinuclear actin cap by activating Rac1 and this in turn induces nuclear stretching (Woroniuk et al., 2018). Importantly, this process enables the transport of Yap/Taz into the nucleus and promotes their activity. However, mechanistic details of the molecular processes downstream of Rac1-P29S have yet to be identified. Here, we showed that melanoma cells that constitutively express the fast-cycling Rac1-P29S mutant adopt a prominent morphology characterized by an enlarged cell area and highly dynamic membrane extensions due to enhanced actin polymerization. It is therefore conceivable that the highly dynamic cell morphology and changes in the nuclear shape could underlie elevated Yap/Taz activation. Prior studies also suggested that proteins of the PAK family might mediate this effect. For example, it was shown that Rac1 activates PAK1, which results in Yap de-phosphorylation and enables Yap shuttling into the nucleus (Sabra et al., 2017).

In summary, data presented in this work confirm that the fast cycling Rac1-P29S mutant stimulates cellular morphogenesis in UKE-Mel-55b melanoma cells. In addition, our findings show that endogenous expression of this driver mutant in melanoma cells results in enhanced activation of cell proliferation pathways, involving the MAPK protein ERK1/2, AKT and the hippo-pathway transcriptional coactivators Yap/Taz (Fig. 41). Given that all of these Rac1-dependent signaling pathways are associated with melanomagenesis and metastatic behavior, Rac1 inhibition is an interesting model for cancer therapy.

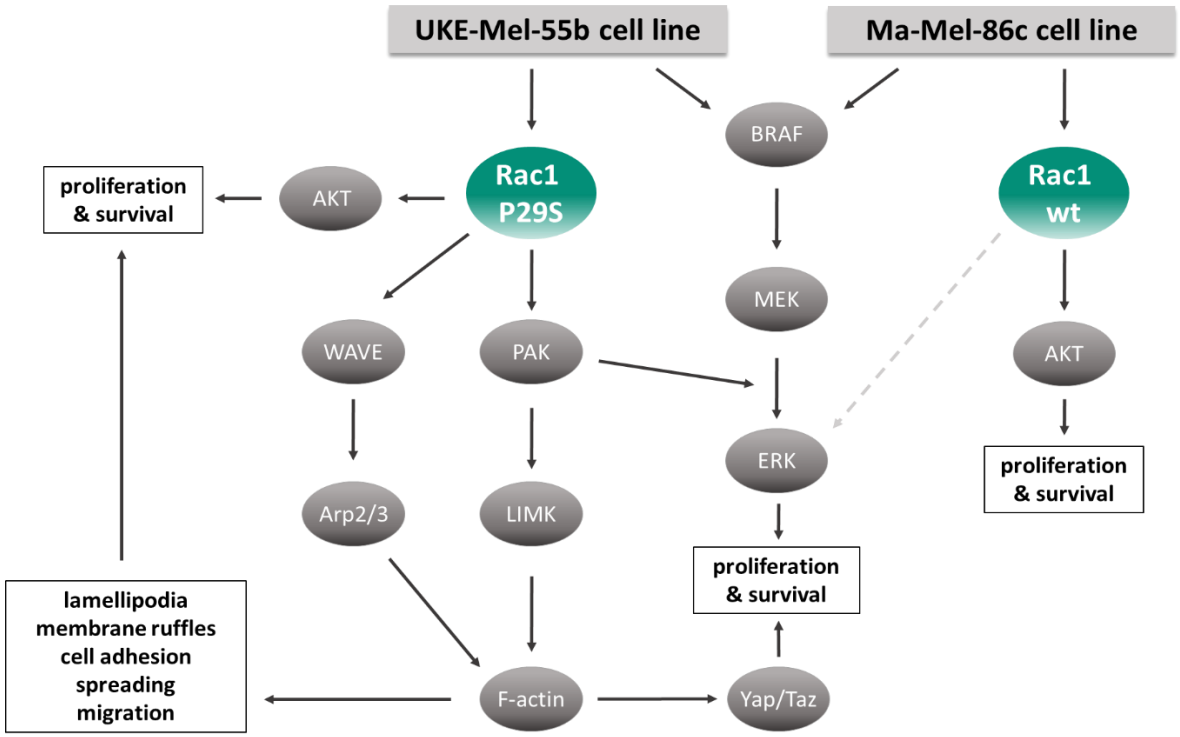

Figure 41: Model for Rac1 function in melanoma cell lines. In distinct patient-derived melanoma cell types that carry an activating BRAF (V600E/K) mutation, two different Rac1 variants have been identified, namely the Rac1-wt and the driver mutant Rac1-P29S. In this thesis, two different melanoma cell lines were studied to understand the role of endogenous Rac1-P29S. **(left)** Melanoma cells that endogenously express the fast-cycling mutation Rac1-P29S (UKE-Mel-55b) exhibit enhanced lamellipodia, membrane ruffles, cell adhesion and spreading. Furthermore, Rac1-P29S is involved in multiple signaling pathways that control cell proliferation and survival. In particular, Rac1-P29S substantially contributes to activity of the MAPK pathway in addition to BRAF signaling. In addition, Rac1-P29S controls Yap/Taz activity, potentially via actin re-modelling and cell shape changes. **(right)** Rac1-wt expressing Ma-Mel-86c cells show Rac1-dependent AKT signaling, whereas ERK was not significantly reduced and activity of the transcriptional coactivators Yap/Taz were not affected after Rac1-depletion. Moreover, Ma-Mel-86c cells did not show active PAK1/2.

4.3 Role of Rac1-P29S in acquisition of resistance to BRAF inhibition

Most of these patients also harbor an activating BRAF mutation and hence were treated with BRAF inhibitors such as vemurafenib (PLX-4032) to suppress cell proliferation and tumor growth. In some patients, however, the tumor develops a resistance against the BRAF inhibitor within the first six month. Interestingly, exome sequencing of these patients identified that some of those tumors harbor the Rac1-P29S mutant (Watson et al., 2014). This new driver mutation Rac1-P29S was identified in 5-9 % of melanoma patients. Thus, it has been suggested that Rac1-P29S might contribute to acquisition of BRAF resistance in melanoma.

As expected, cell proliferation in both melanoma cell lines was significantly reduced upon BRAF inhibition via PLX-4032 (vemurafenib). However, over the course of six and nine days of drug treatment, we observed that proliferation significantly recovered in Rac1-P29S expressing UKE-Mel-55b cells, whereas a similar recovery could not be observed in Rac1-wt melanoma cells. As sustained cell proliferation is critical for acquisition of drug resistance, we further investigated signaling pathways downstream of Rac1-P29S that might mediate such a recovery. Several pathways have been linked to cell resistant behavior to BRAF inhibition.

For example, loss of the tumor suppressor PTEN, which is known to inhibit the PI3K-AKT pathway, was observed in 35% of melanoma that acquire resistance to BRAF inhibitors (Griffin et al., 2017). Indeed, this loss of PTEN was reported to correlate with increased AKT activity that is in agreement with sustained cell survival under BRAF inhibitor treatment (Griffin et al., 2017; Manzano et al., 2016). Our western blot studies showed that PTEN is lost in both melanoma cell lines (supplementary data). And after 72 h treatment with PLX-4032, AKT activity level was restored to control levels in both cell lines (supplementary data). Based on our RNAi studies, AKT activity upon BRAF inhibition does not require Rac1 signaling in both cell lines suggesting that this signaling pathway is not affected by the endogenously expressed Rac1-P29S mutant. Furthermore, AKT activity could be also upregulated by enhanced receptor signaling via EGFR or PDGFR-β (Griffin et al., 2017; Ivanov and Hei, 2005; Zhu et al., 2015). The observed upregulation of EGFR expression in UKE-Mel-55b (Paschen, unpublished data) suggests the EGFR/AKT/Rac1 pathway as an interesting candidate for further studies (Zhu et al., 2015).

As a prominent proliferation regulating pathway, we next investigated activity of the MAPK protein ERK1/2 in the context of BRAF inhibition. As expected due to strong BRAF inhibition, the administration of PLX-4032 significantly reduced ERK1/2 activity in both melanoma cells. However, pERK1/2 levels in in cells that endogenously express Rac1-P29S were significantly higher despite PLX-4032 treatment as compared to Rac1-wt cells. Furthermore, ERK1/2 levels in the Rac1-P29S cell line slightly increased after six days of BRAF inhibition and this increase persisted after nine days of drug treatment. Moreover, we found that Rac1-P29S depletion lead to further reduction of ERK1/2 activity in addition to the effect observed for PLX-4032 treatment alone. This drastically overall reduced ERK1/2 activity to around 10% of control values suggests that BRAF and Rac1-P29S coordinately regulate ERK1/2 activity in UKE-Mel-55b melanoma cells. Interestingly, after additional three days of BRAF inhibition, we observed a slight recovery of ERK1/2 activity in n.t siRNA-treated cells, while we could not detect such an increase in cells lacking Rac1-P29S. Thus, Rac1-P29S appears to be not only important for maintaining basal ERK1/2 activity upon BRAF inhibition, but also to restore activation of this pathway.

In addition to the upregulated proliferation signaling, Lionarons *et al.* observed that Rac1-P29S expression in mouse melanocytes promotes a melanocytic to mesenchymal transition via activation of the Rac1 effector PAK (Lionarons et al., 2019). The findings of this study led to the conclusion that Rac1-P29S induced de-differentiation resulting in progenitor-like cells, which show lower apoptosis and a higher survival rate. Other studies revealed that amplification of the CCND1 gene, which results in increased cyclin D1 expression, correlates with resistance to BRAF inhibitors (Griffin et al., 2017; Smalley et al., 2008). The amplification of CCND1 should result in a BRAF-independent proliferation activity and our observed reduced proliferation rate after Rac1 depletion and BRAF inhibition exclude overexpression of cyclin D1 in our cell system. However, we cannot exclude other effects such as amplification of the BRAF allele (Shi et al., 2012), which can cause BRAF overexpression and decreases sensitivity to the administered inhibitor concentrations. Thus, increased BRAF concentration by overexpression would require correspondingly high PLX-4032 concentrations for treatment in order to obtain sufficient BRAF inhibition. In addition, elevated expression of BRAF has been shown to promote dimerization, which blocks its interaction with PLX-4032 (Griffin et al., 2017; Shi et al., 2012). Thus, the use of inhibitors such as PLX-4032, in cells that overexpress BRAF,

generally complicates patient therapy. Consequently, patients with BRAF mutation derived melanoma often receive combinatorial treatments that include both BRAF and MEK inhibitors. However, in melanoma patients with the additional Rac1-P29S mutation this dual treatment could be problematic as enhanced Rac1 signaling via PAK effectors could overcome inhibitor blockage and still activate ERK1/2 (Halaban, 2015; Watson et al., 2014). Interestingly, PLX-4032 treatment resulted in upregulated pPAK1/2 levels in UKE-Mel-55b cells but not in Ma-Mel-86c cells, suggesting that the fast-cycling Rac1 mutant activates PAK1/2 more efficiently under BRAF inhibition. Rac1 depletion in UKE-Mel-55b cells causes reduced PAK1/2 activation upon PLX-4032 treatment, confirming that PAK1/2 is an important mediator of ERK1/2 signaling activation downstream of Rac1-P29S during BRAF inhibition.

In addition to MAPK signaling, we also provide evidence that Rac1-P29S is involved in activity maintenance of the transcriptional coactivators Yap/Taz upon BRAF inhibition. As discussed earlier, nuclear Yap/Taz level was highly elevated in Rac1-P29S expressing UKE-Mel-55b melanoma cells and consequently treatment with the BRAF inhibitor only caused a small additional increase. Rac1-P29S depletion reduced nuclear Yap/Taz localization in both, control and BRAF inhibitor-treated cells, to similar high degree, suggesting that Rac1-P29S controls basal Yap/Taz activity level to the same extend in untreated cells and when treated with BRAF inhibitors.

4.4 Role of Rho signaling in in the regulation of Yap/Taz activity under BRAF inhibition in Rac1-P29S expressing melanoma cells

In agreement with previous studies (Kim et al., 2016), we observed increased F-actin bundling and elevated Yap/Taz activity in both melanoma cell lines following PLX-4032 treatment. We further confirmed that these actin bundles are decorated with Myosin-II and therefore can generate contractile forces, resulting in enhanced formation of focal adhesions. Similar to our results, Mohan *et al.* also showed that overexpression of Rac1-P29S in A375 melanoma cells together with BRAF inhibition increased focal adhesion formation (Mohan et al., 2019). Both, upregulated stress fiber and focal adhesion formation, indicate that BRAF inhibition caused upregulated activity of the related GTPase RhoA. Indeed, Klein *et al.* described similar effects for the PLX-4032 analogue PLX-4720 (Klein and Higgins, 2011). In their experiments, PLX-4720 treatment reduced the protein

level of RND3, which is considered to be a cellular antagonist of RhoA. In agreement with this, the authors reported that RhoA is required for PLX-4720-induced stress fiber formation (Klein and Higgins, 2011). Enhanced stress fiber formation was also observed for PLX-4032 (Kim et al., 2016). RhoA-mediated acto-myosin reorganization could also contribute to activation of Yap/Taz upon BRAF inhibitor treatment in our cell system. Moreover, BRAF inhibition leads to upregulated collagen I production in the surrounding fibroblast and therefore increases ECM stiffness (Hirata et al., 2015). Higher ECM stiffness is correlated with increased Yap/Taz activity (Zanconato et al., 2016). The ECM rigidity directly influences integrin-mediated signaling such as actin remodeling and is thus an interesting link between Rho-GTPase activity and Yap/Taz signaling to promote tumorigenesis.

RhoA is mostly known to regulate stress fiber formation in eukaryotic cells. We therefore analyzed its role in the regulation of cell proliferation and survival signaling in UKE-Mel-55b cells. Interestingly, RhoA depletion did not cause any effects on ERK, AKT and PAK activity and the proliferation rate was only slightly reduced by 16 %. In contrast, simultaneous inhibition of RhoA along with the two closely related Rho proteins, RhoB and RhoC with the inhibitor C3 transferase, clearly reduced the percentage of cells with nuclear Yap/Taz in the Rac1-P29S expressing cell line. Thus, it would be of further interest to study a combination of Rho protein inhibition via C3 transferase and BRAF inhibition using PLX-4032 in Rac1-P29S expressing melanoma cells. After three days of PLX-4032 treatment and five hours Rho inhibition, actin organization was not perturbed in all cells, indicating that inhibition of the three Rho GTPases for five hours might be too short to antagonize the induction of stress fibers by PLX-4032. However, upon long-term treatment with PLX-4032 for six days and Rho inhibitor for three days, we could not observe any stress fibers as when treated only wiht PLX-4032 treatment, confirming that stress fibers formation during PLX-4032 treatment requires activity of Rho-GTPases.

It was reportat that PLX-4032 treatment increases the protein level of RhoB protein in melanoma cells, which remained high even after PLX-4032 treatment was stopped (Delmas et al., 2015). Therefore, it is conceivable that in our melanoma model system (UKE-Mel-55b) RhoB is more involved in Yap/Taz and actin regulation as compared to RhoA. Thus, it would be of interest to further investigate the molecular mechanism of Yap/Taz activation by individual Rho proteins in melanoma cells and to understand the potential role of this process in the context of BRAF inhibitor resistance in more detail.

5. Conclusion

In this study, we demonstrate that the endogenously expressed fast-cycling mutant Rac1-P29S controls the activity of major proliferation signals including ERK1/2, AKT and Yap/Taz pathways in UKE-Mel-55b melanoma cells. Our findings suggest that the PAK effector family mediates many of these mechanisms downstream of Rac1. As expected, the elevated activity of the Rac1-P29S mutant is also the underlying cause for the highly dynamic cell morphology of UKE-Mel-55b cells. The morphology is characterized by increased lamellipodia formation and membrane ruffling as well as enhanced cell adhesion and spreading. We also show that migration of these cells is independent of the ECM substrate, suggesting profound reprogramming of key adhesion and mechanosensation signaling networks by Rac1-P29S. In addition, enhanced F-actin dynamics by Rac1-P29S activity might also underlie the strong activation of the actin dependent transcriptional coactivators Yap/Taz, thus stimulating cell proliferation programs.

Our study provides evidence that Rac1-P29S also promotes acquisition of BRAF inhibitor resistance in melanoma cells via gradual recovery of cell proliferation, potentially due to activation of the MAPK protein ERK1/2. Furthermore, related Rho-GTPase proteins such as RhoB and RhoC might also contribute to this process by stimulation of acto-myosin contractility and Yap/Taz signaling. Collectively, these findings advance our understanding of the role of the Rac1-P29S driver mutation in tumor-related processes such as proliferation, migration and survival. Thus, this study provides the basis for subsequent work to overcome Rac1-induced resistance against BRAF inhibitors.

6. Supplementary data

6.1 Establishing Rac1-depletion in melanoma cell lines

To established Rac1 knock-down by RNA interference, we used two siRNAs for Rac1. One form the company Qiagen (siRac1 #6Q) and the other from dharmacon (siRac1 #8D). Both were used with a final concentration of 10 nM for 72 h to perfume Rac1 depletion in UKE-Mel-55b cells. Depletion efficiency of Rac1 was studied by western blot analysis and morphological effects were analyzed by F-actin staining (rhodamin-phalloidin) and epi-fluorescent microscopy. Both siRNAs for Rac1 depletion resulted in significantly reduced Rac1 protein level of approx. 80 % and caused reduced ERK and AKT activity (Fig. 42).

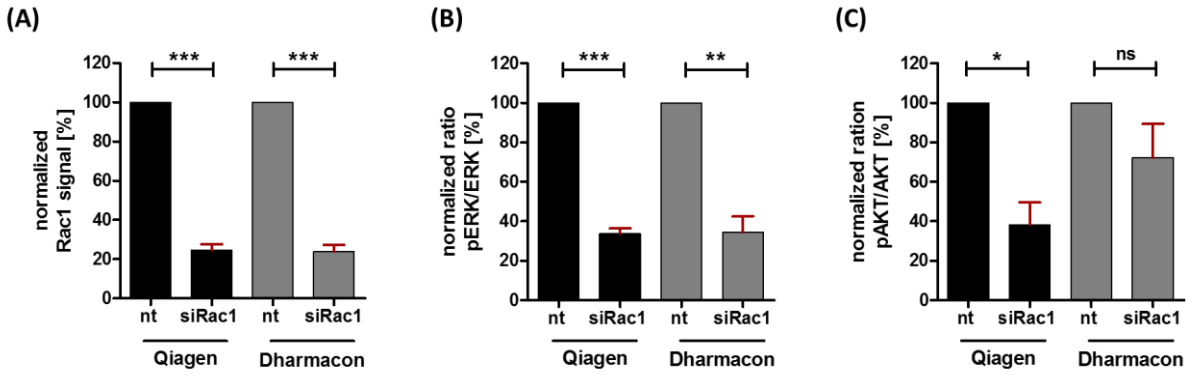

Figure 42: Western blot studies to analyze siRNA efficiency in UKE-Mel-55b cells. Rac1 depletion was performed for 72 h with Qiagen (siRac1#6Q) and Dharmacon (siRac1#8D) siRNA. Protein signals were normalized to total protein signal. Corresponding control group (n.t siRNA) was set to 100 % protein expression. **(A)** Measured Rac1 protein levels in UKE-Mel-55b cells after Rac1 depletion with Qiagen and Dharmacon siRNA. (Rac1: n.t siRNA 100 %; siRac1 #6Q: 24.7 % ± 3 SEM; siRac1 #8D: 24 % ± 3.4 SEM). **(B)** Ratio of pERK/ERK protein signals was calculated to measure ERK activity. (pERK/ERK: n.t siRNA 100 %; siRac1 #6Q: 33.7 % ± 2.8 SEM; siRac1 #8D: 34.3 % ± 8.1 SEM). **(C)** AKT activity was calculated over AKT and pAKT protein levels. (pAKT/AKT: n.t siRNA 100 %; siRac1 #6Q: 38.3 % ± 11.2 SEM; siRac1 #8D: 72.4 % ± 16.9 SEM).N=3 independent experiments. . Statistical analysis was performed with a one-tailed t-test against 100. P<0.05:*, p<0.001:**, p<0.0001:***, ns=non-significant. Error bars indicate SEM.

Similar morphological changes after Rac1 depletion with both siRNAs were observed for area, circularity and roundness. All parameters were significantly reduced after Rac1 depletion by both siRNAs (Fig. 43C-E). Moreover, Rac1 knock-down with both siRNAs leads to actin remodeling from membrane ruffling phenotype to more stress fiber formation (Fig. 43B).

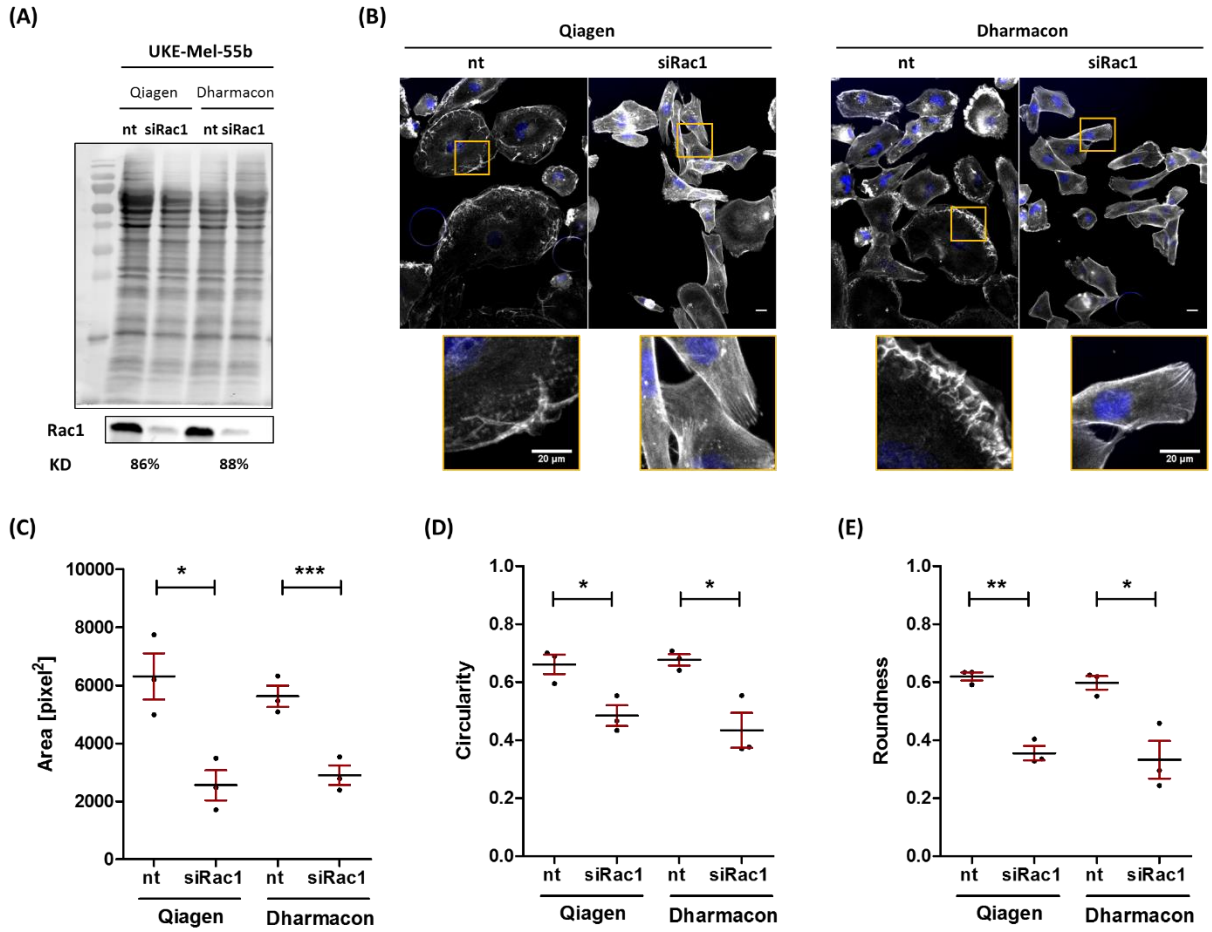

Figure 43: Comparison of different Rac1 siRNA to exclude off-target effects in UKE-Mel-55b cells on a Nikon-Ti Eclipse microscope. Cells were transfected with nt and siRac1 from Qiagen and dharmacon for 72 h. **(A)** Representative western blot with total protein staining and Rac1 signal. **(B)** Cells were fixed with 4 % formaldehyde and stained for nuclei with Hoechst (blue) and for actin rhodamin-phalloidin (grey). Imaging was performed on a Nikon-Ti Eclipse microscope with an 20x air objective. **(C)** Area/cell in square pixel measured with Image J for both Rac1 siRNAs. Shape descriptors circularity **(D)** and roundness **(E)** were measured also with Image J. N=3 experiments. Statistical analysis was performed with a two-tailed t-test, unpaired. P<0.05:*, p<0.001:**, p<0.0001:***, ns=non-significant. Error bars indicate SEM. Scale bar 20µm.

(Area: Qiagen n.t siRNA :6310 µm² ± 796.8 SEM; siRac1#6: 2555 µm² ± 514.7. Dharmacon n.t siRNA: 5622 µm² ± 366; siRac1#8: 2900 µm² ± 335.5 SEM). (Circularity: Qiagen n.t siRNA: 0.66 ± 0.03 SEM; siRac1#6: 0.49 ± 0.04 SEM. Dharmacon n.t siRNA: 0.68 ± 0.02 SEM; siRac1#8: 0.4 ± 0.06 SEM). (Roundness: Qiagen n.t siRNA: 0.6 ± 0.01 SEM; siRac1#6: 0.36 ± 0.02 SEM. Dharmacon n.t siRNA: 0.6 ± 0.02 SEM; 0.3 ± 0.07 SEM).

Rac1 depletion was also established for the Rac1-wt expressing melanoma cell line (Ma-Mel-86c). Protein levels for Rac1 and activity of ERK and AKT was analyzed by western blot studies after depletion of Rac1 with siRNA from Qiagen and Dharmacon (Fig. 44). As it was observed in UKE-Mel-55b cells, Rac1 knock-down in Ma-Mel-86c cells by Qiagen and Dharmacon siRNA reduced Rac1 level to 20 % compared to n.t siRNA-treated cells.

ERK activity showed only minimal decrease, whereas AKT activity was significantly reduced for both siRNAs.

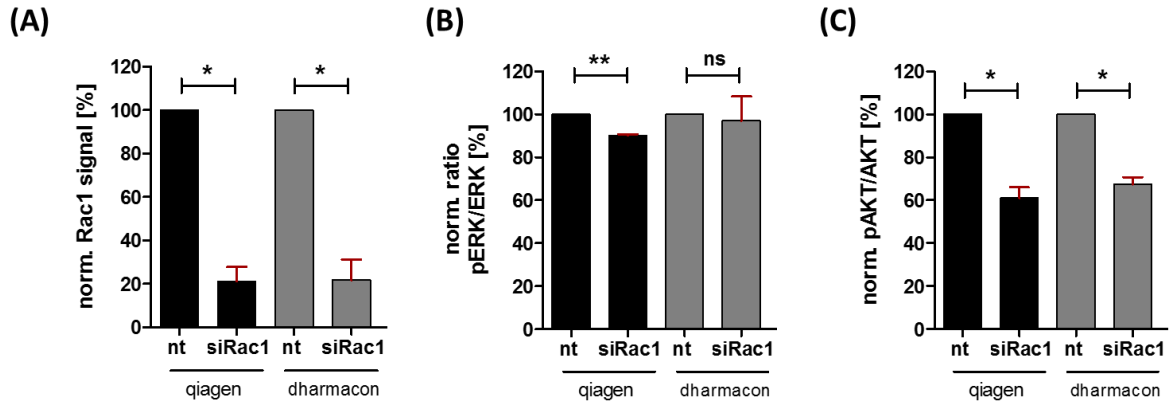

Figure 44: Western blot studies to analyze siRNA efficiency in Ma-Mel-86c cells. Rac1 depletion was performed for 72 h with Qiagen (siRac1#6Q) and Dharmacon (siRac1#8D) siRNA. Protein signals were normalized to total protein signal. Corresponding control group (n.t siRNA) was set to 100 % protein expression. **(A)** Measured Rac1 protein levels in Ma-Mel-86c cells after Rac1 depletion with Qiagen and Dharmacon siRNA. (Rac1: n.t siRNA 100 %; siRac1 #6Q: 21.3 % ± 6.6 SEM; siRac1 #8D: 21.8 % ± 9.4 SEM). **(B)** Ratio of pERK/ERK protein signals was calculated to measure ERK activity. (pERK/ERK: n.t siRNA 100 %; siRac1 #6Q: 90.25 % ± 0.6 SEM; siRac1 #8D: 97 % ± 11.39 SEM). **(C)** AKT activity was calculated over AKT and pAKT protein levels. (pAKT/AKT: n.t siRNA 100 %; siRac1 #6Q: 61 % ± 5 SEM; siRac1 #8D: 67.33 % ± 3.4 SEM). N=3 independent experiments. . Statistical analysis was performed with a one-tailed t-test against 100. P<0.05:*, p<0.001:**, p<0.0001:***, ns=non-significant. Error bars indicate SEM.

6.2 Overexpression of Rac1-P29S leads to lamellipodia and adhesion formation in U2-OS cells

To investigate the influence of Rac1 activity on early cell adhesion formation and actin organization, overexpression studies with different Rac1 mutations were performed.

First, the EGFP-Rac1-P29S plasmid was generated by inserting a point mutation in the EGFP-Rac1-wt plasmid (Fig. 45A-C). To achieve this, the base triplet CCT (coding for proline) was replaced by the TCT triplet (serine) using site-directed PCR mutagenesis. The osteosarcoma cell line U2-OS, which expresses endogenous Rac1-wt, is a commonly used model system to study the actin cytoskeleton. U2-OS cells were analyzed with fluorescent confocal imaging to examine the effect of different Rac1-mutations on F-actin and focal adhesions. Therefore, cells were transfected with an EGFP-control vector, EGFP-Rac1-wt, the fast-cycling EGFP-Rac1-P29S and a dominant active version – EGFP-Rac1-Q61L. After fixation, rhodamin-phalloidin and an anti-Paxillin antibody were used to visualize F-actin and focal adhesions. Rac1 is involved in Paxillin recruitment at an early stage of adhesion formation, which renders it as an interesting candidate to observe Rac1

effects (Deakin and Turner, 2008). Similar as we have observed previously, higher Rac1 activity correlates with an enhanced membrane ruffling and lamellipodia formation (Fig. 45D, green arrows). Moreover, a higher Rac1 activity resulted in increased focal adhesion formation (Fig. 45D, orange arrows). Cells expressing the fast-cycling EGFP-Rac1-P29S or the active EGFP-Rac1-Q61L mutant showed increased adhesion formation as compared to the EGFP-control cells. Moreover, some cells showed nuclear localization of Rac1, indicating Rac1 accumulation during cell proliferation.

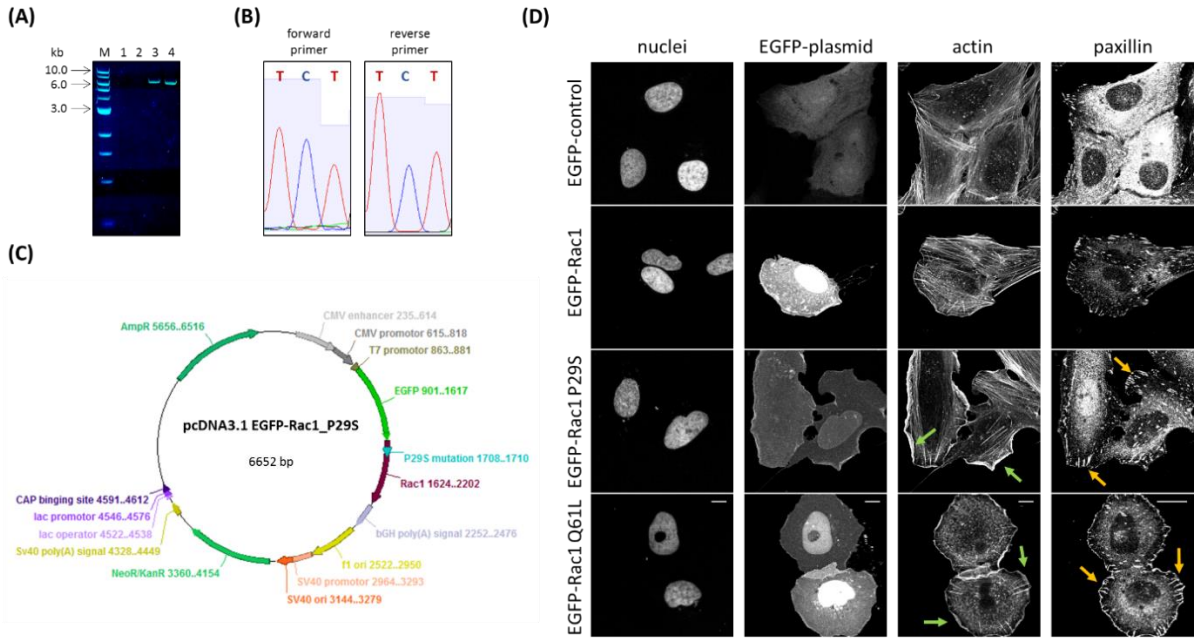

Figure 45: Rac1 activity correlates with lamellipodia and focal adhesion formation in U2-OS cells. The plasmid pcDNA3.1-EGFP-Rac1P29S were designed by introduction of a single point mutation. The introduced C to T transition resulted in the amino acid exchange from proline to serine and caused the gain-of-function mutant Rac1-P29S. **(A)** HDgreen stained agarose gel after mutagenesis. For optimization, different DNA and buffer concentrations were evaluated. M: marker Quick Load 1kb from NEB. Lane 1: 20 ng DNA with 10 µl buffer. Lane 2: 50 ng with 10 µl buffer. Lane 3: 20 ng with 5 µl buffer and Lane 4 with 50 ng and 5 µl buffer. Conditions from Lane 3 were used for further experiments. **(B)** Sequencing results for both primers, showing the expected TCT triplet (coding for the amino acid serine). **(C)** Plasmid map of the generated pcDNA3.1 EGFP-Rac1-P29S construct with important features annotated. **(D)** U2-OS cells, expressing endogenous Rac1wt, were transfected with different Rac1-mutant-plasmids and an EGFP-control plasmid. Cells were fixed and stained with rhodamine-phalloidin for F-actin, Hoechst 33342 for nuclei and an antibody for Paxillin was used to label focal adhesions. Images shown are max projections of confocal z-stacks. Scale bar 20 µm. Higher Rac1 activity resulted in increased formation of lamellipodia (green arrows) and focal adhesions (orange arrows).

6.3 Inhibition of PAK1/2/3 reduce pERK levels in UKE-Mel-55b cells

To analyze the role of the well-characterized Rac1 effector PAK, inhibition of PAK1/2/3 was performed by incubation with FRAX597 for 1 h in UKE-Mel-55b cells. Next, protein activity of PAK, AKT and ERK were analyzed by western blot and microscope experiments were performed for ki-67 and Yap/Taz signaling. PAK inhibition clearly reduced ERK but not AKT activity, while Rac1 protein level was also not perturbed (Fig. 46 A, B). Moreover, proliferation rate (ki-67) and Yap/Taz localization were not alter by PAK inhibition (Fig. 46C). However, PAK inhibition lower membrane ruffle formation in UKE-Mel-55b cells (Fig. 46D).

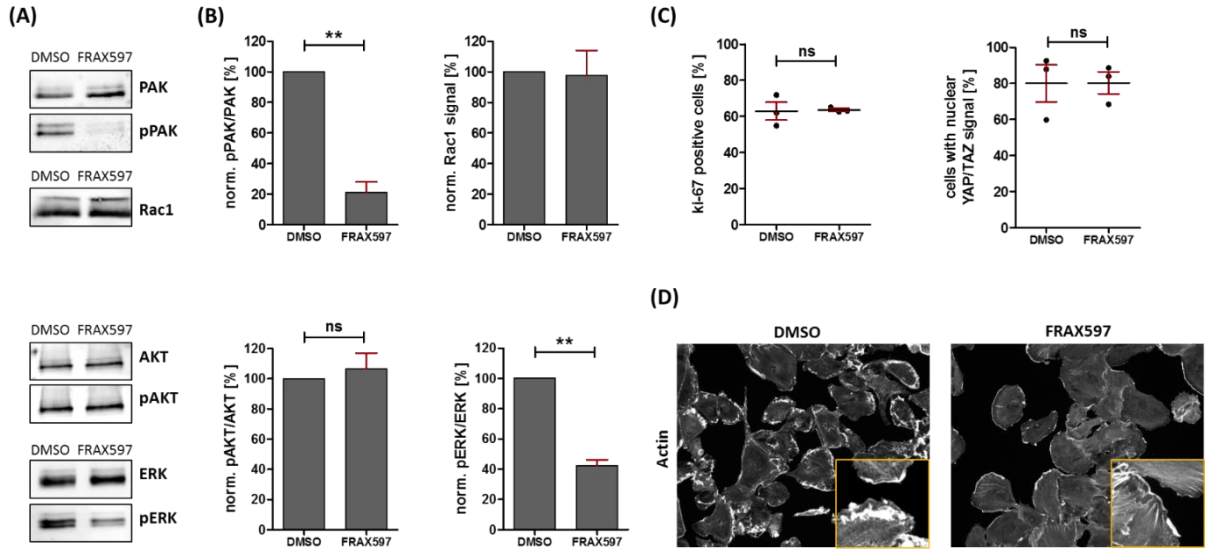

Figure 46: PAK inhibition with FRAX597 cause reduced ERK activity in UKE-Mel-55b cells. UKE-Mel-55b cells were plated 24 h prior drug treatment. 1 µM FRAX597 was added for 1 h, followed by western blot studies and fixation of samples for microscopy analysis. **(A)** Representative western blot images for PAK, pPAK, Rac1 and signaling proteins such as AKT, pAKT, ERK and pERK. Inhibition clearly reduce active PAK (pPAK) level. **(B)** Graphs shown signaling activity for PAK, AKT and ERK by calculated ratio between active protein (phosphorylated) and inactive un-phosphorylated protein levels. Rac1 protein level was not affected through PAK inhibition. N=3 independent experiments. Statistical analysis was performed with a one-tailed t-test against 100. P<0.05:*, p<0.001:**, p<0.0001:***, ns=non-significant. Error bars indicate SEM. **(C)** Ki-67 and Yap/Taz staining was performed and determined to analyze cell proliferation of UKE-Mel-55b after PAK inhibition. PAK inhibition for 1 h did not show downstream effects on ki-67 level and Yap/Taz localization. N=3 independent experiments. Statistical analysis was performed with a two-tailed t-test, unpaired. ns=non-significant. Error bars indicate SEM **(D)** Representative microscope images for F-Actin (rhodamin-phalloidin) after PAK inhibition. Inhibition of PAK proteins reduce membrane ruffles in UKE-Mel-55b cells.

6.4 Migration of the Rac1-P29S expressing melanoma cell line is ECM-independent

To investigate how endogenous expression of the highly active Rac1-P29S mutant might be involved in the migration behavior in melanoma cells, phase-contrast microscopy was used to study the migration of UKE-Mel-55b cells over a period of 10 h. Individual cells were tracked using the manual tracking plugin from Fiji. The data were analyzed with IBIDI chemotaxis and migration tool to generate migration velocity and accumulated distance plots (Fig. 47B). Coating with poly-L-lysine and collagen I had no effect on the cell migration velocity (box plot in µ/min with 95% CI for glass: 0.34 ± 0.31-03.7 CI; collagen I: 0.33 ± 0.3-0.36 CI; PLL: 0.34 ± 0.3-0.38 CI, Fig. 47C) and distance (box plot in µm with 95% CI for glass: 196.1 ± 178-214 CI; collagen I: 192 ± 174.5-209.6 CI; PLL: 198.9 ± 175.9-221.8 CI, Fig. 47D) in Rac1-P29S expressing melanoma cells.

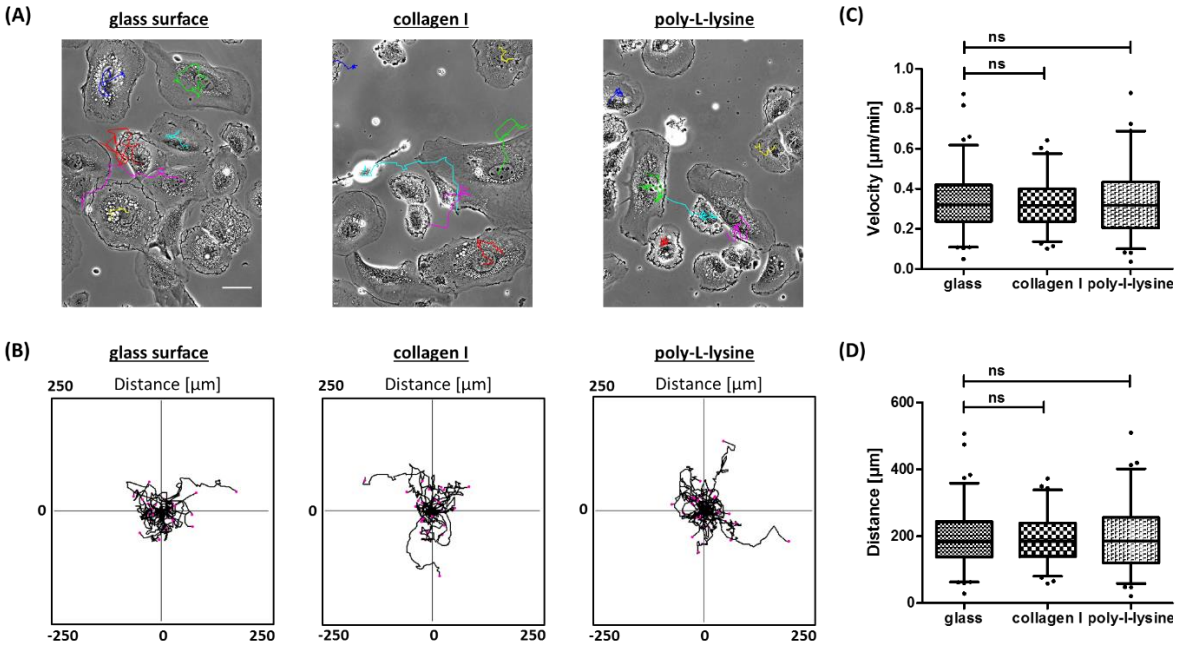

Figure 47: Cell migration of Rac1-P29S melanoma cells is not affect by extracellular matrix components. UKE-Mel-55b cells were seeded on 4-well IBIDI glass bottom dishes for phase-contrast microscopy. For coating, collagen I and poly-L-lysine were used and compared with glass as uncoated condition. Cells were incubated for 2 h after re-plating, followed by imaging. Cells were imaged in 20 minutes-intervals for a total timespan of 10 h. UKE-Mel-55b showed the same migratory behavior on all three substrates. **(A)** Representative images for cell migration are shown. Colored lines indicate migration trajectory of single cells. Scale bar 50 µm. **(B)** Representative migration plots of individual cells for all three conditions. **(C+D)** Graphs for migration velocity [µm/min] and accumulated distance [µm] are depicted. 73-88 cells from three individual experiments. Statistical analysis was performed with a One-Way-Anova test, post-test: Dunnett`s Multiple Comparison Test; ns=non-significant. Error bars indicate 95% confidence interval.

6.4 BRAF inhibition did not alter AKT signaling activity in Rac1-P29S melanoma cells

Rac1 depletion had only a minor effect on the AKT signal (n.t siRNA: 100 %; siRac1: 81.3 % ± 10.4 SEM) (Fig. 48A, C, D). Even after three days of drug treatment, AKT activity levels remained rather constant in all conditions (DMSO: n.t siRNA: 100 %; siRac1: 98.7 % ± 0.9 SEM) (PLX-4032: n.t siRNA: 92.2 % ± 4 SEM; siRac1: 100.5 % ± 5.6 SEM) (Fig. 48A, C). Changes in AKT activity were only observed after six days drug treatment (Fig. 48A, B). Notably, Rac1 depletion caused an enhanced AKT signaling. However, high fluctuations between individual experiments cause a high SEM around 35 %. (DMSO: n.t siRNA: 100 %; siRac1: 147.4 % ± 35.8 SEM) (PLX-4032: n.t siRNA: 111.8 % ± 38.2 SEM; siRac1: 147 % ± 36.9 SEM).

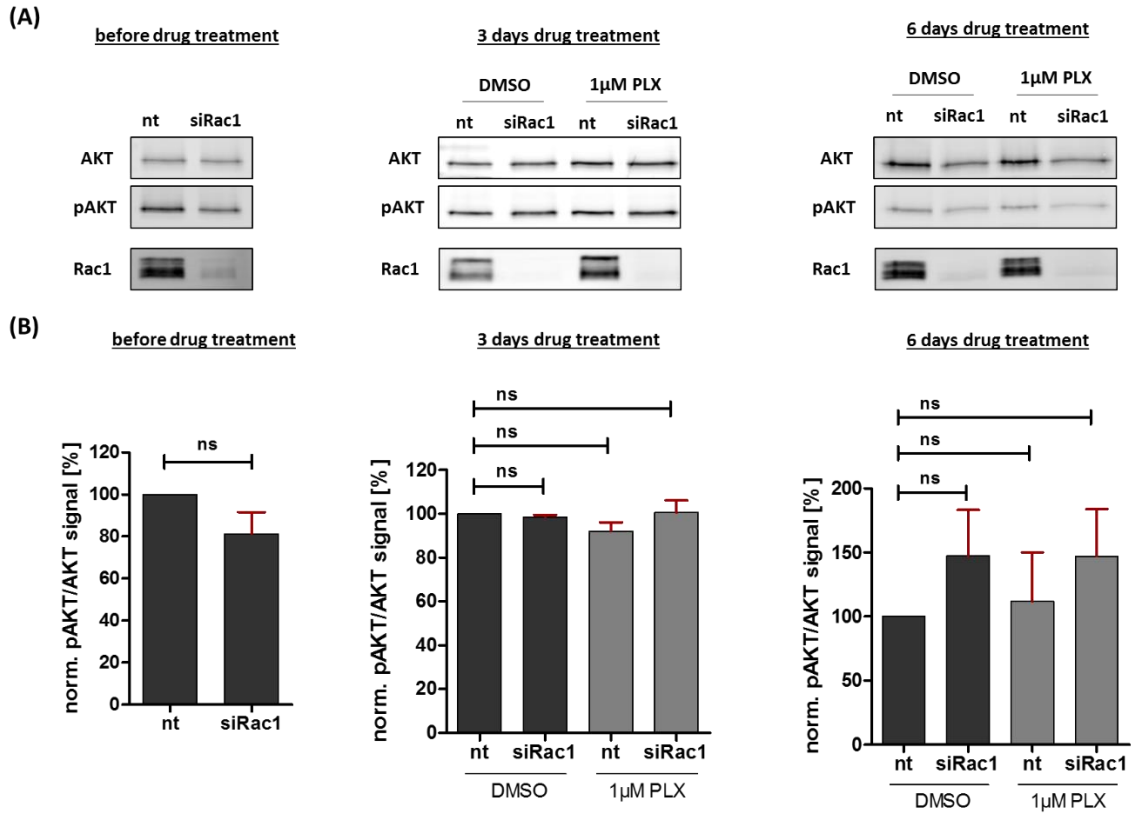

Figure 48: BRAF inhibition did not alter AKT activity in UKE-Mel-55b melanoma cells. The Rac1-P29S expressing melanoma cell line (UKE-Mel-55b) was first treated with n.t siRNA and siRac1 for 72h (before drug treatment). After three days, cells were re-plated and after additional 24 h, treatment with DMSO or 1 µM PLX-4032 was started (3 days vs. 6 days drug treatment). **(A)** Showing representative western blot images for all time points with protein signals for Rac1 and pAKT/AKT. **(B)**. Graphs for calculated pAKT/AKT signaling activity. Protein signals were normalised to total protein. Cells treated with n.t siRNA and DMSO were set to 100% protein expression. N=3 individual experiments. Statistical analysis was performed with two-tailed t-test, unpaired for condition – before drug treatment. Statistical analysis was performed with a One-Way-Anova test, post-test: Dunnett`s Multiple Comparison Test for three and six days drug treatment; P<0.05:*, p<0.001:**, p<0.0001:***, ns=non-significant. Error bars indicate SEM.

6.6 Western Blot studies for β-PIX, Nf-kß and PTEN expression in melanoma cell lines

To further investigate protein signaling pathways in melanoma cell lines western blot studies were performed to determine protein levels for PTEN, β-PIX and Nf-κβ (Fig. 49). UKE-Mel-55b cells did not show expression of PTEN, suggesting a loss of PTEN that might be involved in drug resistance and tumorigenesis. Furthermore, both melanoma cell lines express the Rac1 GEF β-PIX and the Nf-κβ, which regulate cell proliferation and cell survival.

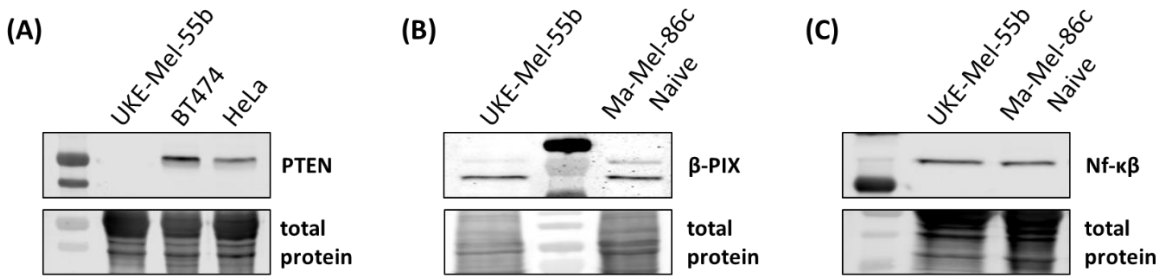

Figure 49: Western blot for PTEN, β-PIX and Nf-κβ in melanoma cell lines. Total protein staining was used as loading control. **(A)** Detection of PTEN in UKE-Mel-55b compared to BT474 and HeLa cells as positive control. **(B)** β-PIX expression in UKE-Mel-55b and Ma-Mel86c cells. **(C)** Detection of Nf-κβ protein levels in both melanoma cell lines.

6.7 Cdc42 is not involved in proliferation and survival signaling in UKE-Mel-55b cells

Based on data presented above, Cdc42 and RhoA were studied as possible candidates for such regulatory mechanisms contribute to proliferation and survival signaling in UKE-Mel-55b cells. First, Cdc42 was deleted using two different siRNAs. Western blot analysis validated the downregulation of Cdc42 protein levels. Interestingly, in contrast to depletion of Rac1-P29S, PAK1/2/3 protein levels were not altered after Cdc42 knock-down (Fig. 50A). Moreover, only slightly reduced pAKT levels were detected for siCdc42#6 (Fig. 50A). Furthermore, we analysed the hippo-Yap/Taz pathway using epi-fluorescence microscopy. Here, only for siRNA #5 a tendency to slightly decrease was observed (n.t siRNA 77 %; siCdc42#5: 63 %; siCdc42#6: 84 %) (Fig. 50B). The proliferation rate was determined using the ki-67 marker and showed no changes after Cdc42 depletion (n.t siRNA 74.4 5 %; siCdc42#5: 73 %; siCdc42#6: 78.8 %)(Fig. 50C).

Thus, these data suggest that Cdc42 does not play an important role in proliferation and survival signaling of UKE-Mel-55b cells.

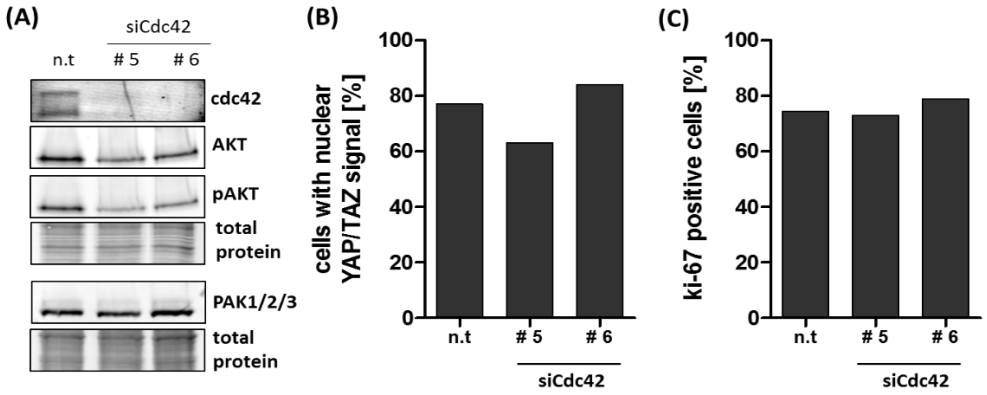

Figure 50: Cdc42 depletion did not regulate proliferation and survival signaling in Rac1-P29S expressing melanoma cells. UKE-Mel-55b cells were treated with n.t siRNA and tow different siRNAs for Cdc42 (siRNA #5, #6) for 72 h. **(A)** Western blot for AKT, pAKT and PAK1/2/3 signals and Cdc42 knock-down efficiency with total protein staining as loading control. **(B)** Graph with percentage of cells with nuclear Yap/Taz (mean value). **(C)** Shown percentage for ki-67 positive cells as indicator for proliferation rate (mean value). Five random imaging position/sample were analyzed. N=1 experiment.

6.8 Rho Inhibition reduce nuclear Yap/Taz localization in Ma-Mel-86c cells

After five hours of Rho inhibition, Ma-Mel-86c cells still exhibit actin stress fibers (Fig. 51A). Inhibition of RhoA, B and RhoC by using the C3 transferase reduced percentage of cells with nuclear Yap/Taz localization in the Rac1-wt expressing melanoma cell line Ma-Mel-86c (control: 21.2 % ± 3 SEM; Rho inhibitor: 10 % ± 1.5 SEM) (Fig. 51B).

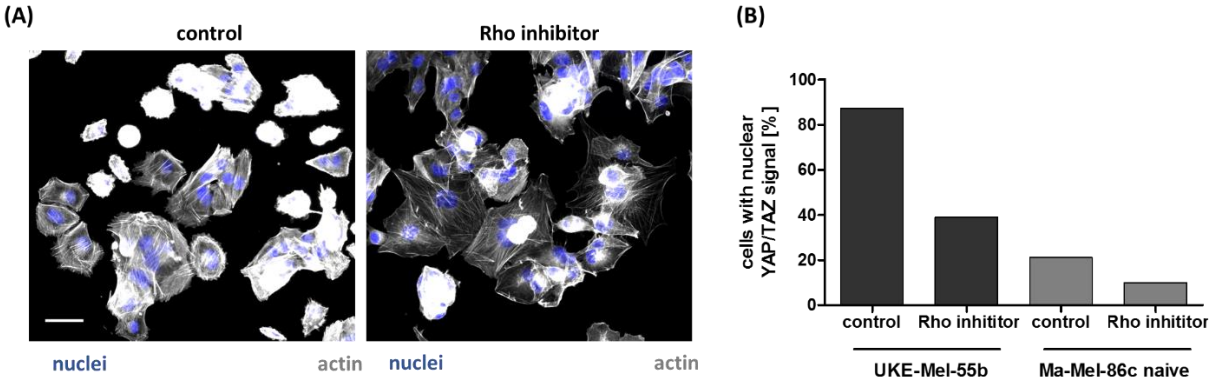

Figure 51: Rho inhibition reduce nuclear Yap/Taz localization in Ma-Mel-86c cells. (A) Representative wide-field microscope images of the actin (rhodamin-phalloidin) cytoskeleton and nuclei (Hoechst 33324) after H_2O (control) or Rho inhibition. Scale bar 50 µm. **(B)** Percentage of cells with nuclear Yap/Taz. N=1 experiment.

7. References

Abercrombie, M., J.E.M. Heaysman, and S.M. Pegrum. 1971. The locomotion of fibroblasts in culture. *Experimental Cell Research*. 67:359-367.

Abercrombie, M., E. Joan, M. Heaysman, and S.M. Pegrum. 1970. The locomotion of fibroblasts in culture. *Experimental Cell Research*. 60:437-444.

Arozarena, I., and C. Wellbrock. 2017. Overcoming resistance to BRAF inhibitors. *Ann Transl Med*. 5:387.

Ascierto, P.A., J.M. Kirkwood, J.J. Grob, E. Simeone, A.M. Grimaldi, M. Maio, G. Palmieri, A. Testori, F.M. Marincola, and N. Mozzillo. 2012. The role of BRAF V600 mutation in melanoma. *J Transl Med*. 10:85.

Balasenthil, S., A.A. Sahin, C.J. Barnes, R.A. Wang, R.G. Pestell, R.K. Vadlamudi, and R. Kumar. 2004. p21-activated kinase-1 signaling mediates cyclin D1 expression in mammary epithelial and cancer cells. *J Biol Chem*. 279:1422-1428.

Bamburg, J.R., and B.W. Bernstein. 2010. Roles of ADF/cofilin in actin polymerization and beyond. *F1000 Biol Rep*. 2:62.

Bid, H.K., R.D. Roberts, P.K. Manchanda, and P.J. Houghton. 2013. RAC1: an emerging therapeutic option for targeting cancer angiogenesis and metastasis. *Mol Cancer Ther*. 12:1925-1934.

Bishop, A.L., and A. Hall. 2000. Rho GTPases and their effector proteins. *Biochem J*. 348:241-255.

Boguski, M.S., and F. McCormick. 1993. Proteins regulating Ras and its relatives. *Nature*. 366:643-654.

Buccione, R., J.D. Orth, and M.A. McNiven. 2004. Foot and mouth: podosomes, invadopodia and circular dorsal ruffles. *Nat Rev Mol Cell Biol*. 5:647-657.

Cao, X., S.L. Pfaff, and F.H. Gage. 2008. YAP regulates neural progenitor cell number via the TEA domain transcription factor. *Genes Dev*. 22:3320-3334.

Carnero, A., C. Blanco-Aparicio, O. Renner, W. Link, and J.F. Leal. 2008. The PTEN/PI3K/AKT signalling pathway in cancer, therapeutic implications. *Curr Cancer Drug Targets*. 8:187-198.

Cernohorska, M., V. Sulimenko, Z. Hajkova, T. Sulimenko, V. Sladkova, S. Vinopal, E. Draberova, and P. Draber. 2016. GIT1/betaPIX signaling proteins and PAK1 kinase regulate microtubule nucleation. *Biochim Biophys Acta*. 1863:1282-1297.

Chambard, J.C., R. Lefloch, J. Pouyssegur, and P. Lenormand. 2007. ERK implication in cell cycle regulation. *Biochim Biophys Acta*. 1773:1299-1310.

Chang, F., C. Lemmon, D. Lietha, M. Eck, and L. Romer. 2011. Tyrosine phosphorylation of Rac1: a role in regulation of cell spreading. *PLoS One*. 6:e28587.

Chapman, P.B., A. Hauschild, C. Robert, J.B. Haanen, P. Ascierto, J. Larkin, R. Dummer, C. Garbe, A. Testori, M. Maio, D. Hogg, P. Lorigan, C. Lebbe, T. Jouary, D. Schadendorf, A. Ribas, S.J. O'Day, J.A. Sosman, J.M. Kirkwood, A.M. Eggermont, B. Dreno, K. Nolop, J. Li, B. Nelson, J. Hou, R.J. Lee, K.T. Flaherty, G.A. McArthur, and B.-S. Group. 2011. Improved survival with vemurafenib in melanoma with BRAF V600E mutation. *N Engl J Med*. 364:2507-2516.

Chen, B., H.T. Chou, C.A. Brautigam, W. Xing, S. Yang, L. Henry, L.K. Doolittle, T. Walz, and M.K. Rosen. 2017. Rac1 GTPase activates the WAVE regulatory complex through two distinct binding sites. *Elife*. 6.

Chhabra, E.S., and H.N. Higgs. 2007. The many faces of actin: matching assembly factors with cellular structures. *Nat Cell Biol*. 9:1110-1121.

Choi, C.K., M. Vicente-Manzanares, J. Zareno, L.A. Whitmore, A. Mogilner, and A.R. Horwitz. 2008. Actin and alpha-actinin orchestrate the assembly and maturation of nascent adhesions in a myosin II motor-independent manner. *Nat Cell Biol*. 10:1039-1050.

Clarke, S. 1992. Protein isoprenylation and methylation at carboxyl-terminal cysteine residues. *Annu Rev Biochem*. 61:355-386.

Clayton, N.S., and A.J. Ridley. 2020. Targeting Rho GTPase Signaling Networks in Cancer. *Front Cell Dev Biol*. 8:222.

Daum, G., I. Eisenmann-Tappe, H.-W. Fries, J. Troppmair, and U.R. Rapp. 1994. The ins and outs of Raf kinases. *Trends in Biochemical Sciences*. 19:474-480.

Davies, M.A. 2012. The role of the PI3K-AKT pathway in melanoma. *Cancer J*. 18:142-147.

Davis, M.J., B.H. Ha, E.C. Holman, R. Halaban, J. Schlessinger, and T.J. Boggon. 2013. RAC1P29S is a spontaneously activating cancer-associated GTPase. *Proc Natl Acad Sci U S A*. 110:912-917.

De, P., J.C. Aske, and N. Dey. 2019. RAC1 Takes the Lead in Solid Tumors. *Cells*. 8.

Deakin, N.O., and C.E. Turner. 2008. Paxillin comes of age. *J Cell Sci*. 121:2435-2444.

Delmas, A., J. Cherier, M. Pohorecka, C. Medale-Giamarchi, N. Meyer, A. Casanova, O. Sordet, L. Lamant, A. Savina, A. Pradines, and G. Favre. 2015. The c-Jun/RHOB/AKT pathway confers resistance of BRAF-mutant melanoma cells to MAPK inhibitors. *Oncotarget*. 6:15250-15264.

DerMardirossian, C., and G.M. Bokoch. 2005. GDIs: central regulatory molecules in Rho GTPase activation. *Trends Cell Biol*. 15:356-363.

Dhillon, A.S., S. Hagan, O. Rath, and W. Kolch. 2007. MAP kinase signalling pathways in cancer. *Oncogene*. 26:3279-3290.

Didsbury, J., R.F. Weber, G.M. Bokoch, T. Evans, and R. Snyderman. 1989. Rac, a Novel Ras-Related Family of Proteins That Are Botulinum Toxin Substrates. *Journal of Biological Chemistry*. 264:16378-16382.

Dowsett, M., T.O. Nielsen, R. A'Hern, J. Bartlett, R.C. Coombes, J. Cuzick, M. Ellis, N.L. Henry, J.C. Hugh, T. Lively, L. McShane, S. Paik, F. Penault-Llorca, L. Prudkin, M. Regan, J. Salter, C. Sotiriou, I.E. Smith, G. Viale, J.A. Zujewski, D.F. Hayes, and G. International Ki-67 in Breast Cancer Working. 2011. Assessment of Ki67 in breast cancer: recommendations from the International Ki67 in Breast Cancer working group. *J Natl Cancer Inst*. 103:1656-1664.

Dupont, S. 2016. Role of YAP/TAZ in cell-matrix adhesion-mediated signalling and mechanotransduction. *Exp Cell Res*. 343:42-53.

Dupont, S., L. Morsut, M. Aragona, E. Enzo, S. Giulitti, M. Cordenonsi, F. Zanconato, J. Le Digabel, M. Forcato, S. Bicciato, N. Elvassore, and S. Piccolo. 2011. Role of YAP/TAZ in mechanotransduction. *Nature*. 474:179-183.

Eblen, S.T., J.K. Slack, M.J. Weber, and A.D. Catling. 2002. Rac-PAK signaling stimulates extracellular signal-regulated kinase (ERK) activation by regulating formation of MEK1-ERK complexes. *Mol Cell Biol*. 22:6023-6033.

Ewen, M.E. 2000. Where the cell cycle and histones meet. *Genes Dev*. 14:2265-2270.

Fecher, L.A., R.K. Amaravadi, and K.T. Flaherty. 2008. The MAPK pathway in melanoma. *Curr Opin Oncol*. 20:183-189.

Feitelson, M.A., A. Arzumanyan, R.J. Kulathinal, S.W. Blain, R.F. Holcombe, J. Mahajna, M. Marino, M.L. Martinez-Chantar, R. Nawroth, I. Sanchez-Garcia, D. Sharma, N.K. Saxena, N. Singh, P.J. Vlachostergios, S. Guo, K. Honoki, H. Fujii, A.G. Georgakilas, A. Bilsland, A. Amedei, E. Niccolai, A. Amin, S.S. Ashraf, C.S. Boosani, G. Guha, M.R. Ciriolo, K. Aquilano, S. Chen, S.I. Mohammed, A.S. Azmi, D. Bhakta, D. Halicka, W.N. Keith, and S. Nowsheen. 2015. Sustained proliferation in cancer: Mechanisms and novel therapeutic targets. *Semin Cancer Biol*. 35 Suppl:S25-S54.

Feng, X., M.S. Degese, R. Iglesias-Bartolome, J.P. Vaque, A.A. Molinolo, M. Rodrigues, M.R. Zaidi, B.R. Ksander, G. Merlino, A. Sodhi, Q. Chen, and J.S. Gutkind. 2014. Hippo-independent activation of YAP by the GNAQ uveal melanoma oncogene through a trio-regulated rho GTPase signaling circuitry. *Cancer Cell*. 25:831-845.

Fisher, M.L., D. Grun, G. Adhikary, W. Xu, and R.L. Eckert. 2017. Inhibition of YAP function overcomes BRAF inhibitor resistance in melanoma cancer stem cells. *Oncotarget*. 8:110257-110272.

Flaherty, K.T., I. Puzanov, K.B. Kim, A. Ribas, G.A. McArthur, J.A. Sosman, P.J. O'Dwyer, R.J. Lee, J.F. Grippo, K. Nolop, and P.B. Chapman. 2010. Inhibition of mutated, activated BRAF in metastatic melanoma. *N Engl J Med*. 363:809-819.

Fournier, A.K., L.E. Campbell, P. Castagnino, W.F. Liu, B.M. Chung, V.M. Weaver, C.S. Chen, and R.K. Assoian. 2008. Rac-dependent cyclin D1 gene expression regulated by cadherin- and integrin-mediated adhesion. *J Cell Sci*. 121:226-233.

Frantz, C., K.M. Stewart, and V.M. Weaver. 2010. The extracellular matrix at a glance. *J Cell Sci*. 123:4195-4200.

Goicoechea, S.M., S. Awadia, and R. Garcia-Mata. 2014. I'm coming to GEF you: Regulation of RhoGEFs during cell migration. *Cell Adh Migr*. 8:535-549.

Goley, E.D., and M.D. Welch. 2006. The ARP2/3 complex: an actin nucleator comes of age. *Nat Rev Mol Cell Biol*. 7:713-726.

Gray-Schopfer, V., C. Wellbrock, and R. Marais. 2007. Melanoma biology and new targeted therapy. *Nature*. 445:851-857.

Griffin, M., D. Scotto, D.H. Josephs, S. Mele, S. Crescioli, H.J. Bax, G. Pellizzari, M.D. Wynne, M. Nakamura, R.M. Hoffmann, K.M. Ilieva, A. Cheung, J.F. Spicer, S. Papa, K.E. Lacy, and S.N. Karagiannis. 2017. BRAF inhibitors: resistance and the promise of combination treatments for melanoma. *Oncotarget*. 8:78174-78192.

Guilluy, C., R. Garcia-Mata, and K. Burridge. 2011. Rho protein crosstalk: another social network? *Trends Cell Biol*. 21:718-726.

Guo, F., J.A. Cancelas, D. Hildeman, D.A. Williams, and Y. Zheng. 2008. Rac GTPase isoforms Rac1 and Rac2 play a redundant and crucial role in T-cell development. *Blood*. 112:1767-1775.

Guo, F., M. Debidda, L. Yang, D.A. Williams, and Y. Zheng. 2006. Genetic deletion of Rac1 GTPase reveals its critical role in actin stress fiber formation and focal adhesion complex assembly. *J Biol Chem*. 281:18652-18659.

Haga, R.B., and A.J. Ridley. 2016. Rho GTPases: Regulation and roles in cancer cell biology. *Small GTPases*. 7:207-221.

Halaban, R. 2015. RAC1 and melanoma. *Clin Ther*. 37:682-685.

Hall, A. 1998. Rho GTPases and the actin cytoskeleton. *Science*. 279:509-514.

Hanahan, D., and R.A. Weinberg. 2011. Hallmarks of cancer: the next generation. *Cell*. 144:646-674.

Hawryluk, E.B., and H. Tsao. 2014. Melanoma: clinical features and genomic insights. *Cold Spring Harb Perspect Med*. 4:a015388.

Hein, A.L., C.M. Post, Y.M. Sheinin, I. Lakshmanan, A. Natarajan, C.A. Enke, S.K. Batra, M.M. Ouellette, and Y. Yan. 2016. RAC1 GTPase promotes the survival of breast cancer cells in response to hyper-fractionated radiation treatment. *Oncogene*. 35:6319-6329.

Heng, Y.W., and C.G. Koh. 2010. Actin cytoskeleton dynamics and the cell division cycle. *Int J Biochem Cell Biol*. 42:1622-1633.

Hennessy, B.T., D.L. Smith, P.T. Ram, Y. Lu, and G.B. Mills. 2005. Exploiting the PI3K/AKT pathway for cancer drug discovery. *Nat Rev Drug Discov*. 4:988-1004.

Hirata, E., M.R. Girotti, A. Viros, S. Hooper, B. Spencer-Dene, M. Matsuda, J. Larkin, R. Marais, and E. Sahai. 2015. Intravital imaging reveals how BRAF inhibition generates drug-tolerant microenvironments with high integrin beta1/FAK signaling. *Cancer Cell*. 27:574-588.

Hodge, R.G., and A.J. Ridley. 2016. Regulating Rho GTPases and their regulators. *Nat Rev Mol Cell Biol*. 17:496-510.

Hodis, E., I.R. Watson, G.V. Kryukov, S.T. Arold, M. Imielinski, J.P. Theurillat, E. Nickerson, D. Auclair, L. Li, C. Place, D. Dicara, A.H. Ramos, M.S. Lawrence, K. Cibulskis, A. Sivachenko, D. Voet, G. Saksena, N. Stransky, R.C. Onofrio, W. Winckler, K. Ardlie, N. Wagle, J. Wargo, K. Chong, D.L. Morton, K. Stemke-Hale, G. Chen, M. Noble, M. Meyerson, J.E. Ladbury, M.A. Davies, J.E. Gershenwald, S.N. Wagner, D.S. Hoon, D. Schadendorf, E.S. Lander, S.B. Gabriel, G. Getz, L.A. Garraway, and L. Chin. 2012. A landscape of driver mutations in melanoma. *Cell*. 150:251-263.

Holderfield, M., M.M. Deuker, F. McCormick, and M. McMahon. 2014. Targeting RAF kinases for cancer therapy: BRAF-mutated melanoma and beyond. *Nat Rev Cancer*. 14:455-467.

Hoogduijn, M.J., E. Cemeli, K. Ross, D. Anderson, A.J. Thody, and J.M. Wood. 2004. Melanin protects melanocytes and keratinocytes against H2O2-induced DNA strand breaks through its ability to bind Ca2+. *Exp Cell Res*. 294:60-67.

Huveneers, S., and E.H. Danen. 2009. Adhesion signaling - crosstalk between integrins, Src and Rho. *J Cell Sci*. 122:1059-1069.

Hynes, R.O. 2002. Integrins. *Cell*. 110:673-687.

Ishibe, S., D. Joly, Z.X. Liu, and L.G. Cantley. 2004. Paxillin serves as an ERK-regulated scaffold for coordinating FAK and Rac activation in epithelial morphogenesis. *Mol Cell*. 16:257-267.

Ivanov, V.N., and T.K. Hei. 2005. Combined treatment with EGFR inhibitors and arsenite upregulated apoptosis in human EGFR-positive melanomas: a role of suppression of the PI3K-AKT pathway. *Oncogene*. 24:616-626.

Jenkins, R.W., and D.E. Fisher. 2020. Treatment of Advanced Melanoma in 2020 and Beyond. *J Invest Dermatol*.

Kanai, F., P.A. Marignani, D. Sarbassova, R. Yagi, R.A. Hall, M. Donowitz, A. Hisaminato, T. Fujiwara, Y. Ito, L.C. Cantley, and M.B. Yaffe. 2000. TAZ: a novel transcriptional co-activator regulated by interactions with 14-3-3 and PDZ domain proteins. *EMBO J*. 19:6778-6791.

Karlsson, R., E.D. Pedersen, Z. Wang, and C. Brakebusch. 2009. Rho GTPase function in tumorigenesis. *Biochim Biophys Acta*. 1796:91-98.

Kim, J.E., G.J. Finlay, and B.C. Baguley. 2013. The role of the hippo pathway in melanocytes and melanoma. *Front Oncol*. 3:123.

Kim, M.H., J. Kim, H. Hong, S.H. Lee, J.K. Lee, E. Jung, and J. Kim. 2016. Actin remodeling confers BRAF inhibitor resistance to melanoma cells through YAP/TAZ activation. *EMBO J*. 35:462-478.

Kiyokawa, E., Y. Hashimoto, S. Kobayashi, H. Sugimura, T. Kurata, and M. Matsuda. 1998. Activation of Rac1 by a Crk SH3-binding protein, DOCK180. *Genes Dev*. 12:3331-3336.

Klein, R.M., and P.J. Higgins. 2011. A switch in RND3-RHOA signaling is critical for melanoma cell invasion following mutant-BRAF inhibition. *Mol Cancer*. 10:114.

Knaus, U.G., Y. Wang, A.M. Reilly, D. Warnock, and J.H. Jackson. 1998. Structural requirements for PAK activation by Rac GTPases. *J Biol Chem*. 273:21512-21518.

Koohestani, F., A.G. Braundmeier, A. Mahdian, J. Seo, J. Bi, and R.A. Nowak. 2013. Extracellular matrix collagen alters cell proliferation and cell cycle progression of human uterine leiomyoma smooth muscle cells. *PLoS One*. 8:e75844.

Kosoff, R. 2015. Signal Transduction in Mast Cells, Megakaryocytes and in Vivo Homeostasis. *University of Pennsylvania*.

Krauthammer, M., Y. Kong, B.H. Ha, P. Evans, A. Bacchiocchi, J.P. McCusker, E. Cheng, M.J. Davis, G. Goh, M. Choi, S. Ariyan, D. Narayan, K. Dutton-Regester, A. Capatana, E.C. Holman, M. Bosenberg, M. Sznol, H.M. Kluger, D.E. Brash, D.F. Stern, M.A. Materin, R.S. Lo, S. Mane, S. Ma, K.K. Kidd, N.K. Hayward, R.P. Lifton, J. Schlessinger, T.J. Boggon, and R. Halaban. 2012. Exome sequencing identifies recurrent somatic RAC1 mutations in melanoma. *Nat Genet*. 44:1006-1014.

Kumar, A., V. Rajendran, R. Sethumadhavan, and R. Purohit. 2013. Molecular dynamic simulation reveals damaging impact of RAC1 F28L mutation in the switch I region. *PLoS One*. 8:e77453.

Lavoie, J.N., G. L'Allemain, A. Brunet, R. Muller, and J. Pouyssegur. 1996. Cyclin D1 expression is regulated positively by the p42/p44MAPK and negatively by the p38/HOGMAPK pathway. *J Biol Chem*. 271:20608-20616.

Lawson, C.D., and K. Burridge. 2014. The on-off relationship of Rho and Rac during integrin-mediated adhesion and cell migration. *Small GTPases*. 5:e27958.

Lee, S., E.L. Heinrich, J. Lu, W. Lee, A.H. Choi, C. Luu, V. Chung, M. Fakih, and J. Kim. 2016. Epidermal Growth Factor Receptor Signaling to the Mitogen Activated Protein Kinase Pathway Bypasses Ras in Pancreatic Cancer Cells. *Pancreas*. 45:286-292.

Lee, S., J. Rauch, and W. Kolch. 2020. Targeting MAPK Signaling in Cancer: Mechanisms of Drug Resistance and Sensitivity. *Int J Mol Sci*. 21.

Letort, G., H. Ennomani, L. Gressin, M. Thery, and L. Blanchoin. 2015. Dynamic reorganization of the actin cytoskeleton. *F1000Res*. 4.

Li, A., and L.M. Machesky. 2013. Rac1 cycling fast in melanoma with P29S. *Pigment Cell Melanoma Res*.

Lionarons, D.A., D.C. Hancock, S. Rana, P. East, C. Moore, M.M. Murillo, J. Carvalho, B. Spencer-Dene, E. Herbert, G. Stamp, D. Damry, D.P. Calado, I. Rosewell, R. Fritsch, R.R. Neubig, M. Molina-Arcas, and J. Downward. 2019. RAC1(P29S) Induces a Mesenchymal Phenotypic Switch via Serum Response Factor to Promote Melanoma Development and Therapy Resistance. *Cancer Cell*. 36:68-83 e69.

Liu, F., X. Yang, M. Geng, and M. Huang. 2018. Targeting ERK, an Achilles' Heel of the MAPK pathway, in cancer therapy. *Acta Pharm Sin B*. 8:552-562.

Liu, L., H. Zhang, L. Shi, W. Zhang, J. Yuan, X. Chen, J. Liu, Y. Zhang, and Z. Wang. 2014. Inhibition of Rac1 activity induces G1/S phase arrest through the GSK3/cyclin D1 pathway in human cancer cells. *Oncol Rep*. 32:1395-1400.

Liu, Y., Y.J. Suzuki, R.M. Day, and B.L. Fanburg. 2004. Rho kinase-induced nuclear translocation of ERK1/ERK2 in smooth muscle cell mitogenesis caused by serotonin. *Circ Res*. 95:579-586.

Lopez-Colome, A.M., I. Lee-Rivera, R. Benavides-Hidalgo, and E. Lopez. 2017. Paxillin: a crossroad in pathological cell migration. *J Hematol Oncol*. 10:50.

Lu, H., S. Liu, G. Zhang, W. Bin, Y. Zhu, D.T. Frederick, Y. Hu, W. Zhong, S. Randell, N. Sadek, W. Zhang, G. Chen, C. Cheng, J. Zeng, L.W. Wu, J. Zhang, X. Liu, W. Xu, C. Krepler, K. Sproesser, M. Xiao, B. Miao, J. Liu, C.D. Song, J.Y. Liu, G.C. Karakousis, L.M. Schuchter, Y. Lu, G. Mills, Y. Cong, J. Chernoff, J. Guo, G.M. Boland, R.J. Sullivan, Z. Wei, J. Field, R.K. Amaravadi, K.T. Flaherty, M. Herlyn, X. Xu, and W. Guo. 2017. PAK signalling drives acquired drug resistance to MAPK inhibitors in BRAF-mutant melanomas. *Nature*. 550:133-136.

Maehama, T., and J.E. Dixon. 1998. The tumor suppressor, PTEN/MMAC1, dephosphorylates the lipid second messenger, phosphatidylinositol 3,4,5-trisphosphate. *J Biol Chem*. 273:13375-13378.

Mahajan-Thakur, S., S. Bien-Moller, S. Marx, H. Schroeder, and B.H. Rauch. 2017. Sphingosine 1-phosphate (S1P) signaling in glioblastoma multiforme-A systematic review. *Int J Mol Sci*. 18.

Manetti, F. 2012. LIM kinases are attractive targets with many macromolecular partners and only a few small molecule regulators. *Med Res Rev*. 32:968-998.

Manzano, J.L., L. Layos, C. Buges, M. de Los Llanos Gil, L. Vila, E. Martinez-Balibrea, and A. Martinez-Cardus. 2016. Resistant mechanisms to BRAF inhibitors in melanoma. *Ann Transl Med*. 4:237.

Marcoux, N., and K. Vuori. 2003. EGF receptor mediates adhesion-dependent activation of the Rac GTPase: a role for phosphatidylinositol 3-kinase and Vav2. *Oncogene*. 22:6100-6106.

Marei, H., and A. Malliri. 2017. Rac1 in human diseases: The therapeutic potential of targeting Rac1 signaling regulatory mechanisms. *Small GTPases*. 8:139-163.

Mazia, D., G. Schatten, and W. Sale. 1975. Adhesion of cells to surfaces coated with polylysine. Applications to electron microscopy. *J Cell Biol*. 66:198-200.

Michaelson, D., W. Abidi, D. Guardavaccaro, M. Zhou, I. Ahearn, M. Pagano, and M.R. Philips. 2008. Rac1 accumulates in the nucleus during the G2 phase of the cell cycle and promotes cell division. *J Cell Biol*. 181:485-496.

Miki, H., S. Suetsugu, and T. Takenawa. 1998. WAVE, a novel WASP-family protein involved in actin reorganization induced by Rac. *EMBO J*. 17:6932-6941.

Mohan, A.S., K.M. Dean, T. Isogai, S.Y. Kasitinon, V.S. Murali, P. Roudot, A. Groisman, D.K. Reed, E.S. Welf, S.J. Han, J. Noh, and G. Danuser. 2019. Enhanced Dendritic Actin Network Formation in Extended Lamellipodia Drives Proliferation in Growth-Challenged Rac1(P29S) Melanoma Cells. *Dev Cell*. 49:444-460 e449.

Molinie, N., S.N. Rubtsova, A. Fokin, S.P. Visweshwaran, N. Rocques, A. Polesskaya, A. Schnitzler, S. Vacher, E.V. Denisov, L.A. Tashireva, V.M. Perelmuter, N.V. Cherdyntseva, I. Bieche, and A.M. Gautreau. 2019. Cortical branched actin determines cell cycle progression. *Cell Res*. 29:432-445.

Moon, S. 2003. Rho GTPase-activating proteins in cell regulation. *Trends in Cell Biology*. 13:13-22.

Moore, K.A., R. Sethi, A.M. Doanes, T.M. Johnson, J.B. Pracyk, M. Kirby, K. Irani, P.J. Goldschmidt-Clermont, and T. Finkel. 1997. Rac1 is required for cell proliferation and G2/M progression. *Biochem J*. 326 (Pt 1):17-20.

Moroishi, T., C.G. Hansen, and K.L. Guan. 2015. The emerging roles of YAP and TAZ in cancer. *Nat Rev Cancer*. 15:73-79.

Moulding, D.A., M.P. Blundell, D.G. Spiller, M.R. White, G.O. Cory, Y. Calle, H. Kempski, J. Sinclair, P.J. Ancliff, C. Kinnon, G.E. Jones, and A.J. Thrasher. 2007. Unregulated actin polymerization by WASp causes defects of mitosis and cytokinesis in X-linked neutropenia. *J Exp Med*. 204:2213-2224.

Mrug, K. 2020. Role of Rac1 and RhoA in tumorigenesis and cell cycle. *Technische Universität Dortmund*.

Murga, C., M. Zohar, H. Teramoto, and J.S. Gutkind. 2002. Rac1 and RhoG promote cell survival by the activation of PI3K and Akt, independently of their ability to stimulate JNK and NF-kappaB. *Oncogene*. 21:207-216.

Nallet-Staub, F., V. Marsaud, L. Li, C. Gilbert, S. Dodier, V. Bataille, M. Sudol, M. Herlyn, and A. Mauviel. 2014. Pro-invasive activity of the Hippo pathway effectors YAP and TAZ in cutaneous melanoma. *J Invest Dermatol*. 134:123-132.

Narayanan, D.L., R.N. Saladi, and J.L. Fox. 2010. Ultraviolet radiation and skin cancer. *Int J Dermatol*. 49:978-986.

Narumiya, S., M. Tanji, and T. Ishizaki. 2009. Rho signaling, ROCK and mDia1, in transformation, metastasis and invasion. *Cancer Metastasis Rev*. 28:65-76.

Nayal, A., D.J. Webb, C.M. Brown, E.M. Schaefer, M. Vicente-Manzanares, and A.R. Horwitz. 2006. Paxillin phosphorylation at Ser273 localizes a GIT1-PIX-PAK complex and regulates adhesion and protrusion dynamics. *J Cell Biol*. 173:587-589.

Nguyen, C.D.K., and C. Yi. 2019. YAP/TAZ Signaling and Resistance to Cancer Therapy. *Trends Cancer*. 5:283-296.

Nheu, T., H. He, Y. Hirokawa, F. Walker, J. Wood, and H. Maruta. 2014. PAK Is Essential for RAS-Induced Upregulation of Cyclin D1 During the G1 to S Transition. *Cell Cycle*. 3:70-73.

Nimnual, A.S., L.J. Taylor, and D. Bar-Sagi. 2003. Redox-dependent downregulation of Rho by Rac. *Nat Cell Biol*. 5:236-241.

Nisenholz, N., K. Rajendran, Q. Dang, H. Chen, R. Kemkemer, R. Krishnan, and A. Zemel. 2014. Active mechanics and dynamics of cell spreading on elastic substrates. *Soft Matter*. 10:7234-7246.

Nobes, C.D., and A. Hall. 1995. Rho, Rac, and Cdc42 GTPases regulate the assembly of multimolecular focal complexes associated with actin stress fibers, lamellipodia, and filopodia. *Cell*. 81:53-62.

Ohta, Y., J.H. Hartwig, and T.P. Stossel. 2006. FilGAP, a Rho- and ROCK-regulated GAP for Rac binds filamin A to control actin remodelling. *Nat Cell Biol*. 8:803-814.

Oka, M., T. Kageshita, T. Ono, A. Goto, T. Kuroki, and M. Ichihashi. 2003. Protein kinase C alpha associates with phospholipase D1 and enhances basal phospholipase D activity in a protein phosphorylation-independent manner in human melanoma cells. *J Invest Dermatol*. 121:69-76.

Otomo, T., C. Otomo, D.R. Tomchick, M. Machius, and M.K. Rosen. 2005. Structural basis of Rho GTPase-mediated activation of the formin mDia1. *Mol Cell*. 18:273-281.

Paraiso, K.H., Y. Xiang, V.W. Rebecca, E.V. Abel, Y.A. Chen, A.C. Munko, E. Wood, I.V. Fedorenko, V.K. Sondak, A.R. Anderson, A. Ribas, M.D. Palma, K.L. Nathanson, J.M. Koomen, J.L. Messina, and K.S. Smalley. 2011. PTEN loss confers BRAF inhibitor resistance to melanoma cells through the suppression of BIM expression. *Cancer Res*. 71:2750-2760.

Parsons, J.T., A.R. Horwitz, and M.A. Schwartz. 2010. Cell adhesion: integrating cytoskeletal dynamics and cellular tension. *Nat Rev Mol Cell Biol*. 11:633-643.

Prudnikova, T.Y., S.J. Rawat, and J. Chernoff. 2015. Molecular pathways: targeting the kinase effectors of RHO-family GTPases. *Clin Cancer Res*. 21:24-29.

Ramminger, I. 2018. Role of the tumor-associated Rac1 P29S mutant in cancer-related cell behavior. *University of Duisburg-Essen*.

Ramos, J.W. 2008. The regulation of extracellular signal-regulated kinase (ERK) in mammalian cells. *Int J Biochem Cell Biol*. 40:2707-2719.

Reshetnikova, G., R. Barkan, B. Popov, N. Nikolsky, and L.S. Chang. 2000. Disruption of the actin cytoskeleton leads to inhibition of mitogen-induced cyclin E expression, Cdk2 phosphorylation, and nuclear accumulation of the retinoblastoma protein-related p107 protein. *Exp Cell Res*. 259:35-53.

Ridley, A.J. 2015. Rho GTPase signalling in cell migration. *Curr Opin Cell Biol*. 36:103-112.

Ridley, A.J., H.F. Paterson, C.L. Johnston, D. Diekmann, and A. Hall. 1992. The small GTP-binding protein rac regulates growth factor-induced membrane ruffling. *Cell*. 70:401-410.

Riebeling, C., C. Muller, and C.C. Geilen. 2003. Expression and regulation of phospholipase D isoenzymes in human melanoma cells and primary melanocytes. *Melanoma Res*. 13:555-562.

Roberts, P.J., N. Mitin, P.J. Keller, E.J. Chenette, J.P. Madigan, R.O. Currin, A.D. Cox, O. Wilson, P. Kirschmeier, and C.J. Der. 2008. Rho Family GTPase modification and dependence on CAAX motif-signaled posttranslational modification. *J Biol Chem*. 283:25150-25163.

Rossman, K.L., C.J. Der, and J. Sondek. 2005. GEF means go: turning on RHO GTPases with guanine nucleotide-exchange factors. *Nat Rev Mol Cell Biol*. 6:167-180.

Rottner, K., J. Faix, S. Bogdan, S. Linder, and E. Kerkhoff. 2017. Actin assembly mechanisms at a glance. *J Cell Sci*. 130:3427-3435.

Roy, P.S., and B.J. Saikia. 2016. Cancer and cure: A critical analysis. *Indian J Cancer*. 53:441-442.

Sabra, H., M. Brunner, V. Mandati, B. Wehrle-Haller, D. Lallemand, A.S. Ribba, G. Chevalier, P. Guardiola, M.R. Block, and D. Bouvard. 2017. beta1 integrin-dependent Rac/group I PAK signaling mediates YAP activation of Yes-associated protein 1 (YAP1) via NF2/merlin. *J Biol Chem*. 292:19179-19197.

Schaks, M., G. Giannone, and K. Rottner. 2019. Actin dynamics in cell migration. *Essays Biochem*. 63:483-495.

Schulze, N., M. Graessl, A. Blancke Soares, M. Geyer, L. Dehmelt, and P. Nalbant. 2014. FHOD1 regulates stress fiber organization by controlling the dynamics of transverse arcs and dorsal fibers. *J Cell Sci*. 127:1379-1393.

Seo, J., and J. Kim. 2018. Regulation of Hippo signaling by actin remodeling. *BMB Rep*. 51:151-156.

Shi, H., G. Moriceau, X. Kong, M.K. Lee, H. Lee, R.C. Koya, C. Ng, T. Chodon, R.A. Scolyer, K.B. Dahlman, J.A. Sosman, R.F. Kefford, G.V. Long, S.F. Nelson, A. Ribas, and R.S. Lo. 2012. Melanoma whole-exome sequencing identifies (V600E)B-RAF amplification-mediated acquired B-RAF inhibitor resistance. *Nat Commun*. 3:724.

Shtivelman, E., M.Q. Davies, P. Hwu, J. Yang, M. Lotem, M. Oren, K.T. Flaherty, and D.E. Fisher. 2014. Pathways and therapeutic targets in melanoma. *Oncotarget*. 5:1701-1752.

Small, J.V., T. Stradal, E. Vignal, and K. Rottner. 2002. The lamellipodium: where motility begins. *Trends in Cell Biology*. 12:112-120.

Smalley, K.S., M. Lioni, M. Dalla Palma, M. Xiao, B. Desai, S. Egyhazi, J. Hansson, H. Wu, A.J. King, P. Van Belle, D.E. Elder, K.T. Flaherty, M. Herlyn, and K.L. Nathanson. 2008. Increased cyclin D1 expression can mediate BRAF inhibitor resistance in BRAF V600E-mutated melanomas. *Mol Cancer Ther*. 7:2876-2883.

Stahl, J.M., M. Cheung, A. Sharma, N.R. Trivedi, S. Shanmugam, and G.P. Robertson. 2003. Loss of PTEN promotes tumor development in malignant melanoma. *Cancer Res*. 63:2881-2890.

Steffen, A., K. Rottner, J. Ehinger, M. Innocenti, G. Scita, J. Wehland, and T.E. Stradal. 2004. Sra-1 and Nap1 link Rac to actin assembly driving lamellipodia formation. *EMBO J*. 23:749-759.

Sudol, M., P. Bork, A. Einbond, K. Kastury, T. Druck, M. Negrini, K. Huebner, and D. Lehman. 1995. Characterization of the mammalian YAP (Yes-associated protein) gene and its role in defining a novel protein module, the WW domain. *J Biol Chem*. 270:14733-14741.

Suetsugu, S., D. Yamazaki, S. Kurisu, and T. Takenawa. 2003. Differential Roles of WAVE1 and WAVE2 in Dorsal and Peripheral Ruffle Formation for Fibroblast Cell Migration. *Developmental Cell*. 5:595-609.

Sun, C., L. Wang, S. Huang, G.J. Heynen, A. Prahallad, C. Robert, J. Haanen, C. Blank, J. Wesseling, S.M. Willems, D. Zecchin, S. Hobor, P.K. Bajpe, C. Lieftink, C. Mateus, S. Vagner, W. Grernrum, I. Hofland, A. Schlicker, L.F. Wessels, R.L. Beijersbergen, A. Bardelli, F. Di Nicolantonio, A.M. Eggermont, and R. Bernards. 2014. Reversible and adaptive resistance to BRAF(V600E) inhibition in melanoma. *Nature*. 508:118-122.

Sun, X., and P.D. Kaufman. 2018. Ki-67: more than a proliferation marker. *Chromosoma*. 127:175-186.

Takenawa, T., and H. Miki. 2001. WASP and WAVE family proteins: key molecules for rapid rearrangement of cortical actin filaments and cell movement. *J Cell Sci*. 114:1801-1809.

Tang, K., C.G. Boudreau, C.M. Brown, and A. Khadra. 2018. Paxillin phosphorylation at serine 273 and its effects on Rac, Rho and adhesion dynamics. *PLoS Comput Biol*. 14:e1006303.

Tapial Martinez, P., P. Lopez Navajas, and D. Lietha. 2020. FAK Structure and Regulation by Membrane Interactions and Force in Focal Adhesions. *Biomolecules*. 10.

Tomar, A., and D.D. Schlaepfer. 2009. Focal adhesion kinase: switching between GAPs and GEFs in the regulation of cell motility. *Curr Opin Cell Biol*. 21:676-683.

Tsai, J., J.T. Lee, W. Wang, J. Zhang, H. Cho, S. Mamo, R. Bremer, S. Gillette, J. Kong, N.K. Haass, K. Sproesser, L. Li, K.S. Smalley, D. Fong, Y.L. Zhu, A. Marimuthu, H. Nguyen, B. Lam, J. Liu, I. Cheung, J. Rice, Y. Suzuki, C. Luu, C. Settachatgul, R. Shellooe, J. Cantwell, S.H. Kim, J. Schlessinger, K.Y. Zhang, B.L. West, B. Powell, G. Habets, C. Zhang, P.N. Ibrahim, P. Hirth, D.R. Artis, M. Herlyn, and G. Bollag. 2008. Discovery of a selective inhibitor of oncogenic B-Raf kinase with potent antimelanoma activity. *Proc Natl Acad Sci U S A*. 105:3041-3046.

Tsubouchi, A., J. Sakakura, R. Yagi, Y. Mazaki, E. Schaefer, H. Yano, and H. Sabe. 2002. Localized suppression of RhoA activity by Tyr31/118-phosphorylated paxillin in cell adhesion and migration. *J Cell Biol*. 159:673-683.

Tybulewicz, V.L., and R.B. Henderson. 2009. Rho family GTPases and their regulators in lymphocytes. *Nat Rev Immunol*. 9:630-644.

Van Aelst, L., and C. D'Souza-Schorey. 1997. Rho GTPases and signaling networks. *Genes Dev*. 11:2295-2322.

Van Allen, E.M., N. Wagle, A. Sucker, D.J. Treacy, C.M. Johannessen, E.M. Goetz, C.S. Place, A. Taylor-Weiner, S. Whittaker, G.V. Kryukov, E. Hodis, M. Rosenberg, A. McKenna, K. Cibulskis, D. Farlow, L. Zimmer, U. Hillen, R. Gutzmer, S.M. Goldinger, S. Ugurel, H.J. Gogas, F. Egberts, C. Berking, U. Trefzer, C. Loquai, B. Weide, J.C. Hassel, S.B. Gabriel, S.L. Carter, G. Getz, L.A. Garraway, D. Schadendorf, and G. Dermatologic Cooperative Oncology Group of. 2014. The genetic landscape of clinical resistance to RAF inhibition in metastatic melanoma. *Cancer Discov*. 4:94-109.

Vicente-Manzanares, M., and A.R. Horwitz. 2011. Adhesion dynamics at a glance. *J Cell Sci*. 124:3923-3927.

Vidali, L., F. Chen, G. Cicchetti, Y. Ohta, and D.J. Kwiatkowski. 2006. Rac1-null mouse embryonic fibroblasts are motile and respond to platelet-derived growth factor. *Mol Biol Cell*. 17:2377-2390.

Villalonga, P., and A.J. Ridley. 2006. Rho GTPases and cell cycle control. *Growth Factors*. 24:159-164.

Villanueva, J., A. Vultur, and M. Herlyn. 2011. Resistance to BRAF inhibitors: unraveling mechanisms and future treatment options. *Cancer Res*. 71:7137-7140.

Wan, P.T.C., M.J. Garnett, S.M. Roe, S. Lee, D. Niculescu-Duvaz, V.M. Good, C.G. Project, C.M. Jones, C.J. Marshall, C.J. Springer, D. Barford, and R. Marais. 2004. Mechanism of Activation of the RAF-ERK Signaling Pathway by Oncogenic Mutations of B-RAF. *Cell*. 116:855-867.

Wang, Z., E. Pedersen, A. Basse, T. Lefever, K. Peyrollier, S. Kapoor, Q. Mei, R. Karlsson, A. Chrostek-Grashoff, and C. Brakebusch. 2010. Rac1 is crucial for Ras-dependent skin tumor formation by controlling Pak1-Mek-Erk hyperactivation and hyperproliferation in vivo. *Oncogene*. 29:3362-3373.

Watson, I.R., L. Li, P.K. Cabeceiras, M. Mahdavi, T. Gutschner, G. Genovese, G. Wang, Z. Fang, J.M. Tepper, K. Stemke-Hale, K.Y. Tsai, M.A. Davies, G.B. Mills, and L. Chin. 2014. The RAC1 P29S hotspot mutation in melanoma confers resistance to pharmacological inhibition of RAF. *Cancer Res*. 74:4845-4852.

Watts, K.L., E. Cottrell, P.R. Hoban, and M.A. Spiteri. 2006. RhoA signaling modulates cyclin D1 expression in human lung fibroblasts; implications for idiopathic pulmonary fibrosis. *Respir Res*. 7:88.

Webb, D.J., M.J. Schroeder, C.J. Brame, L. Whitmore, J. Shabanowitz, D.F. Hunt, and A.R. Horwitz. 2005. Paxillin phosphorylation sites mapped by mass spectrometry. *J Cell Sci*. 118:4925-4929.

Wellbrock, C., and A. Hurlstone. 2010. BRAF as therapeutic target in melanoma. *Biochem Pharmacol*. 80:561-567.

Whang, Y.E., X. Wu, H. Suzuki, R.E. Reiter, C. Tran, R.L. Vessella, J.W. Said, W.B. Isaacs, and C.L. Sawyers. 1998. Inactivation of the tumor suppressor PTEN/MMAC1 in advanced human prostate cancer through loss of expression. *Proc Natl Acad Sci U S A*. 95:5246-5250.

Winder, M., and A. Viros. 2018. Mechanisms of Drug Resistance in Melanoma. *Handb Exp Pharmacol*. 249:91-108.

Woodrow, M. 2003. Ras-induced serine phosphorylation of the focal adhesion protein paxillin is mediated by the Raf→MEK→ERK pathway. *Experimental Cell Research*. 287:325-338.

Woroniuk, A., A. Porter, G. White, D.T. Newman, Z. Diamantopoulou, T. Waring, C. Rooney, D. Strathdee, D.J. Marston, K.M. Hahn, O.J. Sansom, T. Zech, and A. Malliri. 2018. STEF/TIAM2-mediated Rac1 activity at the nuclear envelope regulates the perinuclear actin cap. *Nature Communications*. 9.

Wu, H., V. Goel, and F.G. Haluska. 2003. PTEN signaling pathways in melanoma. *Oncogene*. 22:3113-3122.

Yang, H., B. Higgins, K. Kolinsky, K. Packman, Z. Go, R. Iyer, S. Kolis, S. Zhao, R. Lee, J.F. Grippo, K. Schostack, M.E. Simcox, D. Heimbrook, G. Bollag, and F. Su. 2010. RG7204 (PLX4032), a selective BRAFV600E inhibitor, displays potent antitumor activity in preclinical melanoma models. *Cancer Res*. 70:5518-5527.

Yoshida, T., Y. Zhang, L.A. Rivera Rosado, J. Chen, T. Khan, S.Y. Moon, and B. Zhang. 2010. Blockade of Rac1 activity induces G1 cell cycle arrest or apoptosis in breast cancer cells through downregulation of cyclin D1, survivin, and X-linked inhibitor of apoptosis protein. *Mol Cancer Ther*. 9:1657-1668.

Zanconato, F., M. Cordenonsi, and S. Piccolo. 2016. YAP/TAZ at the Roots of Cancer. *Cancer Cell*. 29:783-803.

Zenke, F.T., M. Krendel, C. DerMardirossian, C.C. King, B.P. Bohl, and G.M. Bokoch. 2004. p21-activated kinase 1 phosphorylates and regulates 14-3-3 binding to GEF-H1, a microtubule-localized Rho exchange factor. *J Biol Chem*. 279:18392-18400.

Zhang, S., Q. Tang, F. Xu, Y. Xue, Z. Zhen, Y. Deng, M. Liu, J. Chen, S. Liu, M. Qiu, Z. Liao, Z. Li, D. Luo, F. Shi, Y. Zheng, and F. Bi. 2009. RhoA regulates G1-S progression of gastric cancer cells by modulation of multiple INK4 family tumor suppressors. *Mol Cancer Res*. 7:570-580.

Zhang, Y., and M.A. Frohman. 2014. Cellular and physiological roles for phospholipase D1 in cancer. *J Biol Chem*. 289:22567-22574.

Zhao, B., L. Li, Q. Lei, and K.L. Guan. 2010. The Hippo-YAP pathway in organ size control and tumorigenesis: an updated version. *Genes Dev*. 24:862-874.

Zhao, Z.S., J.P. Lim, Y.W. Ng, L. Lim, and E. Manser. 2005. The GIT-associated kinase PAK targets to the centrosome and regulates Aurora-A. *Mol Cell*. 20:237-249.

Zhu, G., Z. Fan, M. Ding, H. Zhang, L. Mu, Y. Ding, Y. Zhang, B. Jia, L. Chen, Z. Chang, and W. Wu. 2015. An EGFR/PI3K/AKT axis promotes accumulation of the Rac1-GEF Tiam1 that is critical in EGFR-driven tumorigenesis. *Oncogene*. 34:5971-5982.

Zins, K., T. Lucas, P. Reichl, D. Abraham, and S. Aharinejad. 2013. A Rac1/Cdc42 GTPase-specific small molecule inhibitor suppresses growth of primary human prostate cancer xenografts and prolongs survival in mice. *PLoS One*. 8:e74924.

8. Acknowledgment

An dieser Stelle möchte ich mich ganz herzlich bei allen bedanken, ohne die die Fertigstellung der Dissertation nicht möglich gewesen wäre.

Besonderer Dank gilt dabei Prof. Dr. Perihan Nalbant, die mir erst die Arbeit an diesem spannenden Projekt ermöglicht hat. Sie stand mir stets mit Rat und Tat zur Seite und ermöglichte mir zeitgleich eigene Idee zu entwickeln und umzusetzen.

Des Weiteren möchte ich mich bei Prof. Dr. Stefan Westermann für die Übernahme des Zweitgutachtens, sowie die tolle und lehrreiche Zeit bei diversen BIOME meetings bedanken.

Ein weiterer Dank gilt meinen Kolleginnen Dr. Manuela Kowalczyk, Dr. Rutuja Patwardhan, Jessica Wagner, Kristina Mrug, Imke Ramminger, Hildegard Eling und Claudia Wilmes die mich während der letzten Jahre begleitend haben. Zusammen mit Dr. Nina Schulze und Dr. Johannes Koch vom ICCE, möchte ich mich bei allen für die vielen lustigen aber auch lehrreichen Laborstunden, die kulinarischen Zusammenkünfte und die tolle Gemeinschaft bedanken.

Ebenfalls möchte ich mich bei unserem Kooperationspartner Prof. Dr. Annette Paschen für die Bereitstellung der verwendeten Zelllinien, sowie für die tollen Gespräche die uns einen Einblick in den klinischen Forschungsalltag ermöglicht haben, bedanken.

Ein großer Dank geht an meine Familie und Freunde die mich jederzeit unterstütz und motiviert haben. Ihr habt mir stets Halt gegeben und ohne diese Unterstützung wäre diese Arbeit so wahrscheinlich nicht zustande gekommen. Besonders möchte ich bei meinem Mann Dennis bedanken, der mir nicht nur mit fachlichen Rat zur Seite stand, sondern auch immer eine emotionale Unterstützung war, mich aufgebaut und ermutigt hat weiter zu machen.